University of Alberta

Geochronology and Trace Element Characteristics of Pyrite from Selected Carbonate Hosted Pb-Zn Ore Deposits

by

Danny Hnatyshin

A thesis submitted to the Faculty of Graduate Studies and Research
in partial fulfillment of the requirements for the degree of

Master of Science

Earth and Atmospheric Sciences

Fall 2012
Edmonton, Alberta

Abstract

Carbonate-hosted ore deposits, such as Mississippi Valley-type (MVT), and Irish-type deposits, are a major class of Pb-Zn ores. Due to the mineralogy of these deposits, numerical constraints on the timing of mineralization are few. This thesis investigates pyrite Re-Os geochronology for dating of ore formation, supplemented by a study of trace elements in pyrite. The two major deposits studied are the Lisheen deposit from Ireland, and the Nanisivik deposit from Nunavut. At Lisheen, different models of formation have been proposed, based upon ore formation ages of either ~ 345 Ma or ~ 280 Ma. The new Re-Os data show that Lisheen formed between 340 - 355 Ma in a primarily syngenetic/syndiagenetic fashion, and discount the significant of a ~ 280 Ma paleomagnetic age as a primary ore-forming event. The Re-Os pyrite geochronology from Nanisivik confirms it is a rare example of a Precambrian MVT deposit, forming at approximately 1100 Ma.

Acknowledgements

This thesis was completed under the supervision of Dr. Robert A. Creaser. Without his expertise and willingness to openly discuss the complexities of this research, this thesis would not have been possible. Additional thanks go out to Dr. Jamie J. Wilkinson and Dr. Elizabeth C. Turner for providing the necessary samples required for this thesis. Furthermore, Dr. Jamie J. Wilkinson, Dr. Elizabeth C. Turner, Dr. Daniel Kontak, and Dr. Sarah Gleason, all gave valuable insights throughout this research, which allowed me to have a comprehensive understanding of the results gathered for this thesis. On the technical/analytical side a number lab technicians were crucial guides for learning how to prepare, and analyze samples properly. In particular, I would like to thank Richard Shultz, Krystle Moore, Barbara Ziger, Guangcheng Chen, and Sergei Matveev, for their help with sample preparation, Re-Os chemistry, TIMS analysis, ICP-MS analysis, and electron microprobe analysis respectively. Additional funding for this thesis was generously provided by NSERC through a Alexander Graham Bell Canada Graduate Scholarship.

Table of Contents

List of Tables

List of Figures

List of Symbols/Abbreviations

A - Amps

~ - Approximately

As - Arsenic

$Ba(OH)_2$ - Barium Hydroxide

$Ba(NO_3)_2$ - Barium Nitrate

cm - Centimetre

ca. - Circa

Co - Cobalt

Cu - Copper

CrO_3 - Chromium Trioxide

deg - Degree

^{o}C - Degree Celsius

e^- - Electron

$\bar{\upsilon}_{e^-}$ - Electron Antineutrino

^{Y}X - Element X with Mass Y

g - Gram

Ga - Giga-annum or Gallium depending on context

HBr - Hydrobromic Acid

HCl - Hydrochloric Acid

ICP-MS - Inductively Coupled Plasma Mass Spectrometer

kV - kilovolt

Ma - Mega-annum

CH_2I_2 - Methylene Iodide

m - metre

μm - Micrometre

mbar - Millibar

mg - Milligram

mL - Millilitre

min - Minute

MVT - Mississippi Valley Type

N - Normality

N/A - Not Available

Ni - Nickel

Os - Osmium

ppm - Parts Per Million

ppb - Parts Per Billion

ppt - Parts Per Trillion

pg - Picogram

Re - Rhenium

λ - Rhenium Decay Constant

NaOH - Sodium Hydroxide

H_2SO_4 - Sulphuric Acid

σ - Standard Deviation

TIMS - Thermal Ionization Mass Spectrometer

wt % - Weight Percent

1.0 Introduction:

Age dating of geologic materials is a very important aspect of geology as it underpins much of our understanding about how different Earth system processes are related. This importance comes from the fact that age dating helps constrain our knowledge of how different geological processes are related to each other. Ore deposits are an example of a very complex and quite variable geologic system that requires a variety of tools to properly understand. Reliable geochronology simplifies many of the complexities associated with the origin of ore deposits, so that geologists have a much better base to work with when trying to test and evaluate formation mechanisms.

The focus of this research is to determine the age of formation of hydrothermal ore deposits that so far have proven very challenging to reliably date. In particular, this project will be focusing on carbonate-hosted Pb-Zn deposits that are generally thought to form by fluid flow in sedimentary basins (Wilkinson et al., 2005, Leach et al., 2010). The lack of reliable ages for these deposits has led to uncertainty as to which geologic processes are relevant for their origin. This study investigates the Lisheen deposit of Ireland, as well as the Nanisivik deposit and the Hawker Creek prospect from Nunavut.

The Lisheen deposit is a classical example of a Irish-Type Pb-Zn deposit, and epitomizes the problems surrounding the origin of these deposits. The Lisheen deposit and the related Irish-type deposits of Galmoy, Navan, and Silvermines all replace Carboniferous carbonate strata formed during a marine transgression in Ireland (Hitzman and Large, 1986; Hitzman and Beaty, 1996; Hitzman et al., 2002). These deposits show very similar mineralization styles, which suggest that they were formed at about the same time, and as a result of the same general processes. Stratigraphic and textural studies on some of these deposits provide evidence that mineralization occurred during basin deposition at approximately 340 Ma (Boyce et al., 1983; Anderson et al., 1998; Boyce et al., 2003; Wilkinson et al., 2003). At the time of writing, the Navan deposit is the most tied to this age as both stratigraphic studies (Anderson et al., 1998) and paleomagnetic studies (Symons et al., 2002) are indicative of ages of 330-345 Ma. However, for the other deposits, and in particular Lisheen, new paleomagnetic evidence suggests a much younger mineralization age of approximately 275 Ma (Pannalal et al., 2008). This age represents the time of metamorphism associated with the Variscan orogeny in Ireland

(Sevastopulo 1981; Coller, 1984; Hitzman, 1999). If this age is correct, then the formation of the Lisheen deposit is decoupled from that of Navan, and is of purely epigenetic origin.

The Nanisivik deposit is a Mississippi Valley-Type (MVT) deposit hosted in a relatively poorly understood region of ancient Proterozoic carbonate strata from northern Baffin Island. Current age constraints based on paleomagnetism of the host rocks, which is assumed to represent the hydrothermal activity associated with mineralization, suggest an age of 1090 ± 10 Ma (Symons et al., 2000). However, more recently a much younger age of 460Ma has been reported for the adularia alteration observed at Nansivik (Sherlock et al., 2004). Since ore deposits of this type are extremely rare in rocks older than 500 Ma, this research will give insight into the preservation potential of MVT style deposits associated with Precambrian basins.

To determine a reliable age for these deposits, geochronology based on the radioactive decay of ^{187}Re into ^{187}Os (Equation 1) is used. Rhenium and osmium are inherently chalcophile in nature and are therefore expected to be enriched in sulphide minerals. Early sulphide Re-Os work focused mainly on the mineral molybdenite due to its high Re content and lack of common Os. Unfortunately, molybdenite is restricted to relatively few geologic settings. To broaden the scope of Re-Os geochronology a variety of other minerals have been subsequently investigated. As techniques have improved, minerals such as pyrite have become more practical and useful for geochronology (Ootes et al., 2011; Morelli, 2008). Pyrite is the ideal mineral to investigate the Re-Os geochronology of carbonate hosted Pb-Zn deposits due to its widespread occurrence within the ore. The Re content of pyrite is typically at the parts per billion (ppb) level, whereas Os is typically present at the parts per trillion (ppt) level. At such low concentrations, in-situ measurements are impossible, therefore Re-Os geochronology is bulk sample method, analyzed using a thermal ionization mass spectrometer, using an isochron approach on multiple fractions of pyrite rich material (e.g. Ootes et al., 2011).

$$^{187}Re \rightarrow {}^{187}Os + e^{-} + \bar{\upsilon}_e \qquad (1)$$

1.1 References

Anderson, I.K., Ashton, J.H., Boyce, A.J., Fallick, A.E., and Russell, M.J., 1998, Ore depositional processes in the Navan Zn-Pb deposit, Ireland: Economic Geology, v. 93, p. 535–563.

Boyce, A.J., Coleman, M.L., and Russell, M.J., 1983, Formation of fossil hydrothermal chimneys and mounds from Silvermines, Ireland: Nature, v. 306, p. 545–550.

Boyce, A.J., Little, C.T.S., and Russell, M.J., 2003, A new fossil vent biota in the Ballynoe barite deposit, Silvermines, Ireland: Evidence for intracratonic seafloor hydrothermal activity about 352 Ma: Economic Geology and the Bulletin of the Society of Economic Geologists, v. 98, p. 649–656.

Coller, D.W., 1984, Variscan structures in the Upper Paleozoic rocks of west central Ireland: Geological Society of London Special Publication 14, p. 185–194.

Hitzman, M.W., 1999, Extensional faults that localize Irish syndiagenetic Zn-Pb deposits and their later compressional fate, in McCaffery, K., Lonergan, L, and Wilkinson, J., eds., Fractures, Fluid Flow and Mineralization: Geological Society of London Special Publication 155, p. 233–245.

Hitzman, M.W., and Beaty, D.W., 1996, The Irish Zn-Pb-(Ba) orefield, in Sangster, D. F., ed., Carbonate-Hosted Lead-Zinc Deposits: Society of Economic Geologists Special Publication 4, p. 112–143.

Hitzman, M. W. and Large, D., 1986, A review and classification of the Irish carbonate hosted base metal deposits, in Andrew, C. J., Crowe, R. W. A., Finlay, S., Pennell, W. M., and Pyne, J. F., eds., Geology and Genesis of Mineral Deposits in Ireland: Dublin, Irish Association for Economic Geology, p. 217-238.

Hitzman, M.W., Redmond, P.B., and Beaty, D.W., 2002, The carbonate hosted Lisheen Zn-Pb-Ag deposit, County Tipperary, Ireland: Economic Geology, v. 97, p. 1627–1655.

Leach, D.L., Taylor, R.D., Fey, D.L., Diehl, S.F., and Saltus, R.W., 2010, A deposit model for Mississippi Valley-Type lead-zinc ores, chap. A of Mineral deposit models for resource assessment: U.S. Geological Survey Scientific Investigations Report 2010–5070–A, 52 p.

Morelli, R., 2008, Rhenium-Osmium Geochronology of Low-Level Sulfide Minerals from Hydrothermal Ore Deposits - Applications, Limitations, and Implications: PhD thesis, University of Alberta.

Ootes, L., Morelli, R.M., Creaser, R.A., Lentz, D.R., Falck, F., William, D.J., 2011, The Timing of Yellowknife Gold Mineralization: A Temporal Relationship with Crustal Anatexis? : Economic Geology, v.1063, p. 713-720.

Pannalal, S.J., Symons, D.T.A., Sangster, D.F., 2008, Paleomagnetic Evidence for an Early Permian Age of the Lisheen Zn-Pb Deposit, Ireland: Economic Geology, v.103, p. 1641-1655.

Sevastopulo, G.D., 1981, Hercynian structures, *in* Holland, C.H., ed., A Geology of Ireland: Edinburgh, Scottish Academic Press, p. 147–172.

Sherlock, R.L., Lee, J.K.W. and Cousens, B.L., 2004, Geologic and geochronologic constraints on the timing of mineralization at the Nanisivik zinc-lead Mississippi Valley-type deposit, northern Baffin Island, Nunavut, Canada: Economic Geology, v. 99, p. 279–293.

Symons, D.T.A., Symons, T.B., and Sangster, D.F., 2000, Paleomagnetism of the Society Cliffs dolostone and the age of the Nanisivik zinc deposits, Baffin Island, Canada: Mineralium Deposita, v. 35, p. 672–682.

Symons, D.T.A., Smethurst, M.T., and Ashton, J.H., 2002, Paleomagnetism of the Navan Zn-Pb deposit, Ireland: Economic Geology, v. 97, p. 997–1012.

Wilkinson, J.J., Boyce, A.J., Everett, C.E., and Lee, M.J., 2003, Timing and depth of mineralization in the Irish Zn-Pb ore field, in Kelly, J.G., Andrew, C.J., Ashton, J.H., Boland, M.B., Earls, G., Fusciardi, L., and Stanley, G., eds., Europe's major base metal deposits: Dublin, Irish Association for Economic Geology, p. 483–497.

Wilkinson, J.J., Everett, C.E., Boyce, A.J., Gleeson, S.A., Rye, D.M. Rye, 2005, Intracratonic crustal seawater circulation and the genesis of subseafloor zinc-lead mineralization in the Irish orefield: Geology October, 2005 v. 33, no. 10, p. 805-808.

2.0 - Case Study 1: Re-Os age constraints for the Lisheen and Galmoy Irish-type ore deposits of South-Central Ireland

2.1 Introduction:

The Irish Midlands contain a number of carbonate-hosted Pb-Zn ore deposits. These range in size from small prospects, to the well known Irish-type deposits of Tynagh, Navan, Silvermines, Galmoy, and Lisheen (Figure 2.1). These ores are confined to the lowest clean carbonate units of their respective districts, the Navan Group in the North, and the Waulsortian Limestone in the South Central Irish Midlands (Wilkinson et al., 2005). Similarities in mineralization styles suggest that the same broad ore-forming process may be responsible for their origin. Whether the driving force behind mineralization in the Irish Midlands is syngenetic/syndiagenetic, or epigenetic in origin is still openly debated (Russell, 1978, 1983; Boast et al., 1981; Hitzman and Large, 1986; Lydon, 1986; Goodfellow et al., 1993; Hitzman and Beaty, 1996; Hitzman et al., 2002.; Everett et al., 2003.; Wilkinson et al., 2003, 2005; Pannalal 2008a' Wilkinson, 2010). Complicating the debate is the lack of consistent and accurate age dates for these deposits.

The Lisheen deposit, the focus of this study, was discovered in 1990 by the Ivemia West-Chevron Mineral Corporation of Ireland Joint Venture and started operation in 1999. With a preliminary resource of 17.9 Mt with a grade of 15.8wt% Zn and 2.6 wt% Pb (Guven et al., 2007) it is the second largest base metal deposit, after Navan, in Ireland. The Lisheen deposit and the nearby Galmoy deposit are hosted in the Waulsortian Limestone in the Rathdowney Trend in South Central Ireland (Johnston et al., 1996; Hitzman, 1999). Typically thought of as a Carboniferous-aged deposit potentially related to syngenetic/syndiagenetic processes occurring around 340 Ma (Hitzman et al., 2002; Wilkinson et al., 2005; Wilkinson 2010), recent paleomagnetic age data have suggested an alternative epigenetic origin for mineralization at ca. 277 Ma (Pannalal, 2008a). To help resolve this issue, a comprehensive study based on Re-Os geochronology was attempted on several sulphide-rich ore samples from the Lisheen deposit and the nearby Galmoy deposit.

This Re-Os study is complemented by a trace element study of the pyrite used for Re-Os geochronology. Recent studies on trace elements in pyrite have shown that different growth stages of pyrite can often be characterized by different trace element distributions (Large et al., 2009). Similar observations for the Lisheen and Galmoy ores are used to aid interpretation of the Re-Os data.

2.2 Stratigraphy

The studies of Hitzman (1992), Shearley et al. (1995), Hitzman and Beaty (1995), Hitzman (2002), and Fusciardi et al. (2003) provide a detailed description of the geology and geologic setting. Such a comprehensive description of the geology and mineralization of Lisheen is beyond the reach of this thesis, but the major geological features will be presented.

The immediate area around Lisheen is composed of a sedimentary succession of Carboniferous to Devonian age. The Lisheen stratigraphy is divided into a Carboniferous marine transgressive carbonate-dominated sequence, which conformably overlies the Devonian Old Red Sandstone, which in turn lies unconformably above metamorphosed Silurian rocks (Figure 2.2, Hitzman et al., 2002; Wilkinson et al., 2005). The carbonate sequences as described by Hitzman et al. (2002) are further divided into various basal carbonates and mudstones; the Ballysteen Group, the Waulsortian Limestone Formation, and the overlying Crosspatrick Formation, which is the highest stratigraphic unit around Lisheen. The main host for sulphide mineralization is the Waulsortian Limestone, which is composed of biomicrite, argillite, wavy laminated micrite, and stylonodular micrite (Hitzman et al., 2002; Wilkinson et al., 2005). The Lisduff Oolite Member of the Ballysteen Group contains a smaller, yet still significant, amount of massive sulphide mineralization.

The absolute ages of the Carboniferous strata near Lisheen are poorly defined, however, estimates have been provided by the work of George et al. (1976), Lippholt and Hess (1985), and Leeder and McMahon (1988). The stratigraphic descriptions of Hitzman et al. (2002) and a biostratigraphy summary presented in Waters et al. (2011) were used to update the stratigraphy for the Lisheen area (Figure 2.2). Based on the biostratigraphy of the Rathdowney trend and nearby locations in South Central Ireland,

the age constraints for strata associated with the Lisheen deposit can be determined. Direct biomarkers at Lisheen and the Rathdowney Trend are relatively rare, and are restricted to the Crosspatrick Formation or higher in the sequence. Current biostratigraphic controls (foraminifera) on the Crosspatrick Formation require that deposition occurred at about the Chadian-Courceyan boundary (Nagy 2003; Gatley et al., 2005), corresponding to an absolute age of ca. 347 Ma (Waters et al., 2011).

The age of units older than the Crosspatrick Formation, which host the mineralization at Lisheen, have been estimated by correlating similar units from other parts of South Central Ireland. The Ballysteen (Somerville and Jones, 1985; Sleeman and Pracht, 1999) and Ballymartin (Lewis, 1986) Formations yield ages in the middle Courceyan (ca. 353 Ma). The older Ringmoyan Shale Formation is assigned an age of early Courceyan (ca. 357 Ma) based on conodont fossils (Somerville and Jones, 1985). The Waulsortian Limestone itself is not dated using biostratigraphy but, based on the constraints given by the Crosspatrick and Ballysheen Formations, an age of middle Courceyan to late Courceyan is the most probable (~347 - 353 Ma). The biostratigraphy gives the general chronological correlations between the units, however, direct links between the biostratigraphy and radiometric ages still remain sparse in this area of Ireland. Therefore, the absolute ages associated with these formations should be interpreted as the current best estimates.

2.3 Major Structures and Tectonics

The hydrothermal activity and associated mineralization at Lisheen are controlled by four major east-west trending normal faults (Hitzman et al., 1992, 2002; Shearley et al., 1992, 1995). Three of these faults are associated with massive sulphide lenses at Lisheen. These faults, known as the Killoran, Derryville, and Bog Faults, are thought to feed the North/Main zone, Derryville zone, and Bog zone respectively. The fourth major fault is the Barnalisheen Fault and is only associated with minor mineralization. The fault system at Lisheen was probably sometime in the Courceyan and likely remained active into the Chadian based on an observed thickening of the Waulsortian Limestone proximal to these faults (Hitzman et al., 2002).

In the late Carboniferous and into the Permian, Ireland was subject to the Variscan orogeny associated with the formation of Pangaea between 260-315 Ma (Sevastopulo, 1981; Coller, 1984; Hitzman, 1999; Wartho et al. (2006). During this time, the Carboniferous strata of the Irish Midlands underwnt extensive reverse and wrench faulting and folding (Woodcock and Strachan, 2000; Graham, 2001), reactivating older normal fault systems (Chadwick et al., 1993). Reverse faulting has also occurred causing some deformation of the Lisheen ore (Fusciardi et al. 2003; Carboni et al., 2003). Hitzman et al. (2002) has also suggested that there was a strong possibility that substantial compression occurred at both Lisheen and Galmoy during the Variscan orogeny. Conodont alteration indexes and vitrinite reflectance values found throughout Ireland suggests that there was an episode of heating throughout to ore field perhaps associated with the Variscan orogeny (Clayton et al., 1980; Jones, 1992).

2.3 Dolomitization

Major hydrothermal activity at Lisheen was the cause of drastic changes to the surrounding host rock. Dolomitization is the prominent form of wall-rock alteration and is mainly found in the hanging walls of the major faults (Beaty et al., 1991; Hitzman et al., 1992, 2002; Shearley et al., 1995, 1996; Redmond, 1997; Fusciardi, 2003). Based on drill core observations, it is known that there is extensive dolomitization from the Silurian basement up through to the Crosspatrick Formation (Hitzman et al., 2002). The dolomitization at Lisheen is complex and is divided into several major phases, although the exact origins and timing of the different phases of dolomitization is still debated (Wilkinson, 2003;Wilkinson et al., 2005; Wilkinson, 2010)

Regional dolomite (D1 in Wilkinson et al. (2005) nomenclature) is the first major episode of dolomitization and is observed throughout the Waulsortian Limestone in the Lisheen area (Hitzman et al., 1998). At Lisheen, it is extensively developed around the Killoran and Derryville fault zones. It is composed of two separate dolomite textures, a fine-grained gray dolomite and a coarse-grained white dolomite (Hitzman et al. 2002). The exact nature of the Regional dolomite is contentious with Gregg et al. (2001) suggesting a purely diagenetic origin and Wilkinson (2003) suggesting that the coarse-grained white dolomite is of hydrothermal origin. Hitzman et al. (2002) suggested that

the regional dolomite was formed prior to ore mineralization, based on the crosscutting relationships observed. However, the possible diachronous manner in which diagenetic dolomite forms makes it of little use for a time marker(Wilkinson et al., 2005).

Besides the regional dolomite, two other major dolomitization styles also occur. The first is known as the black-matrix breccia (D2 in Wilkinson et al. (2005) nomenclature) and is characterized by brecciated clasts of previously dolomitized (D1) Waulsortian Limestone set in a matrix of black fine-grained dolomite. The black-matrix breccia is typically found in the hanging walls of the major fault zones near the base of the Waulsortian Limestone. This type of dolomitization is found as rough stratiform lenses that are often closely associated with, and replaced by, massive sulphides (Hitzman et al., 2002). Typically occurring above the black-matrix breccia is the white-matrix breccia (D3 in Wilkinson et al. (2005) nomenclature), which is characterized by clasts of previously dolomitized (D1) Waulsortian Limestone set in a matrix of coarse grained white dolomite. Beyond these major stages of dolomitization there are also later hydrothermal stages of dolomite and calcite, known as D4, D5, and C6 that occur, but these generally postdate main stage sulphide mineralization (Wilkinson et al., 2005).

2.4 Mineralization

Mineralization consists of three stratabound massive sulphide bodies associated with the Killoran, Derryville, and Bog Faults, and are divided into four ore zones; the Main, North, Derryville, and Bog zones (Figure 2.3). The dominant sulphides at Lisheen include sphalerite, galena, pyrite, and marcasite; although there are lesser amounts of bornite, chalcopyrite, tennantite, and other sulfo-salts present (Hitzman et al., 2002). The dominant gangue minerals at Lisheen are quartz, calcite, dolomite, and barite.

These sulphide bodies are hosted at the base of the Waulsortian Limestone on the hanging wall side of the faults, and are closely associated with the black-matrix breccia. The Lisduff Oolite Member is also the host for massive sulfides, in this case mineralization is found on both sides of the faults (Figure 2.2 B). Carbonate replacement is the main mechanism of mineralization at Lisheen, with the black-matrix breccia being the most pervasively replaced by sulphides (Hitzman et al., 2002).

The Main and Derryville Zones are both composed of several distinct sulphide lenses that have coalesced to form a large continuous ore body (Hitzman et al., 2002). The individual lenses are typically bounded by faults, across which strong variations in ore thickness and grade exist. As a result of these variations, there is a complicated distribution of sulphides, as is seen in Figures 13-16 of Hitzman et al. (2002). Hitzman et al. (2002) also noted that the areas of greatest fault movement appear to be associated with the largest sulphide lenses. The sulphide bodies as a whole gradually change from massive sulphides into a mix of disseminated sulphide and black-matrix breccia, however, there are locations where very sharp contacts with the black-matrix breccia do occur (Hitzman et al., 2002; Wilkinson et al., 2005). The Bog Zone mineralization is similar to that of the Main and Derryville Zones, however, it is simpler and occurs on a much smaller scale.

The complex textures associated with sulphide mineralization suggests a complicated paragenetic sequence, a generalized version of which is presented in Figure 2.4. Beyond this generalized trend there appear to be multiple events of mineralization, causing recrystallization, and overprinting throughout the Lisheen system (Wilkinson et al., 2005).

2.5 Previous Age Constraints

The majority of the previous age constraints for mineralization are based on the upper limits set by structural, textural, and stratigraphic observations. One such upper limit comes from the fact the mineralization must be synchronous with or post-date faulting, as these were the fluid conduits for the hydrothermal system at Lisheen (Hitzman et al., 1992, 2002, 2003; Shearley et al., 1992, 1995; Eyre, 1998). These faults were suggested to be first active during the Courceyan (347-358 Ma), based on observed sediment thickening near the major fault system (Sevastopulo and Redmond, 1999; Hitzman et al., 2002; Carboni et al., 2003; Fusciardi et al., 2003). Mineralization is inferred to have occurred during, or shortly after, fault movement. This constraint is a result of permeability being drastically decreased by precipitated minerals restricting fluid pathways (Wilkinson, 2003; Wilkinson et al., 2005). Wilkinson et al. (2005) supported this proposal with the observation that pre-ore sulphides have been

catacastically deformed and then overprinted by ore stage sulphides. Fault movement is known to have persisted at least into the Chadian (ca. 347 Ma) as synsedimentary faults are found within the Crosspatrick Formation (Fusciardi et al., 2003). Collectively, the relative timing of fault movement constrains the mineralization to occur from the Courceyan into the Chadian (344-358 Ma). Later stage reverse faulting has been observed at Lisheen, but no evidence exists to support that this faulting is associated with mineralization (Carboni et al., 2003; Fusciardi et al., 2003). However, no evidence exists to support that this episode of faulting is associated with mineralization.

Based on crosscutting relationships and replacement textures, it is also likely that the diagenetic and much of the hydrothermal dolomitization predate sulphide mineralization. If the regional dolomite formed prior to the ore it would provide another maximum age on mineralization (Hitzman et al., 2002; Wilkinson et al., 2005). Both regional and black-matrix dolomitization persist up to the Crosspatrick Formation, implying that both types of dolomitization lasted into the Chadian.

Sevastopulo and Redmond (1999) modeled the required time needed to bury sediments deep enough to produce the regional dolomite at Lisheen. Geologic observations from Lisheen by Hitzman et al. (1992), and Shearley et al. (1996), along with a saddle dolomite study from Radke and Mathis (1980, allowed them to calculate that the depth required to form dolomite, assuming a 70^{o}C formation, was only reached after the Arundian (< 342 Ma).

Dating of the hydrothermal activity at Lisheen was attempted by Hitzman et al. (1994) using ^{40}Ar-^{39}Ar step heating profiles of sericite from altered Old Red Sandstone beneath Lisheen. Based on these profiles it is apparent that argon loss had taken place between 315-350 Ma. The origin of the argon loss is unclear, however, Hitzman et al. (2002) suggested that the hydrothermal activity associated with Lisheen, or the effects related to the Variscan Orogeny, may be cause of the argon loss.

A paleomagnetic study by Pannalal (2008a) attempted to date the hydrothermal activity associated with ore formation. From this work they suggested a 277 ± 7 Ma age for mineralization associated with the formation of minute grains of magnetite found within the sulphides and carbonates. Complicating the interpretation of this date is the possibility of remagnetization. If the temperatures experienced by the rock are

sufficiently high, remagnetization of the rock can occur, either directly by bringing the temperature of the mineral above its Neel temperature, or indirectly by producing new magnetic minerals. Throughout the entire Irish midlands, high CAI indices and vitrinite reflectance values indicate elevated temperatures (Clayton et al., 1980; Jones, 1992). If sufficient temperatures were reached it is possible that pyrrhotite would be re-magnetized, pyrite will begin to oxidize to magnetite, and clay minerals may start to convert to magnetite (Pannalal, 2008a). As such, the magnetization at Lisheen may represent activity in the area during the Variscan orogeny. Pannalal (2008a) argues that this gives credence the idea that Lisheen was an epigenetic style deposit formed during the Variscan orogeny. However, these paleomagnetic results do not preclude a much older age for the deposit, and the Pannalal (2008a) age results are best interpreted as a minimum age for the formation of Lisheen.

Based on these previous studies, the age of the Lisheen is poorly constrained to an age range between ~355 Ma to ~277 Ma.

2.6 Methodology

Sulphide minerals from the Lisheen and Galmoy deposits were selected, prepared, and analyzed at the University of Alberta, from samples supplied by Dr. J.J. Wilkinson, Imperial College London.

2.61 Re-Os Sample Preparation

Below is a brief description of the sample preparation required for Re-Os analysis, for a full description of these processes and other supplemental techniques please refer to Appendix I-IV. For Re-Os analysis, samples were processed by a very specific procedure in order to obtain purified sulphide concentrates.

Initial preparation starts with crushing the starting material to approximately 100μm. A hammer is used as to prepare a sample for a shatterbox. To keep metallic contamination to a minimum the hammer is wrapped in plastic. The shatterbox is then used to crush the sample to the desired size (~100μm). To separate the unwanted quartz and carbonates from the crushed sample, a heavy liquid separation procedure is used. The dense material obtained from heavy liquid separation typically contains pyrite ±

sphalerite ± galena, which is subsequently divided and separated based on magnetic susceptibilities using a Frantz isodynamic separator. Galena and sphalerite were dissolved out in some fractions using concentrated hydrochloric acid, leaving behind a pyrite rich fraction.

2.62 Rhenium-Osmium Analytical Procedure

The Re-Os analyses were carried out by weighing up to 400mg of a sulphide sample and transferring it into a thick-walled Carius tube. The sample is then dissolved in inverse aqua regia (~2mL of 10N HCl and ~6mL 16N HNO_3) with a known amount of ^{185}Re + ^{190}Os spike and is immediately frozen in dry ice/ethanol and sealed with a glassblowing torch using natural gas and oxygen. To equilibrate the sample Re and Os with the spike Re and Os, the sealed Carius tube is heated at 220^{o}C for a minimum of 24 hours. After heating, the Carius tube is then frozen in a dry ice-ethanol slurry, prior to opening to prevent any loss of Os. Upon opening the Carius tube, 10.5mL chloroform is added to the acid solution in three aliquots of 3.5 mL, which provides a way to separate the Re from the Os. This creates a pair of immiscible liquids with the Os is preferentially partitioned in the chloroform, and the Re remains dissolved in the inverse aqua regia.

The chloroform portion containing Os is then transferred into a pre-cleaned 22ml glass scintillation vial containing 3mL of 9N HBr, then heated to ~80^{o}C for a minimum of 12 hours. This process transfers the Os from the chloroform into the HBr, via reduction. The HBr solution is then removed from the vial and dried down onto a Teflon cap prior to then next analytical step - micro distillations. To purify the Os, a 7N H_2SO_4 solution containing CrO_3 is added to the dried down HBr and is distilled at ~70^{o}C inside a Teflon conical vial (Savillex) in which the Os rich vapour is transferred to 20ul of clean 9N HBr held in the vial tip via surface tension. The process is repeated one more time; the sample is dried down, and is transferred onto a platinum filament. To ensure a strong signal the sample is activated using $Ba(OH)_2$, dissolved in 0.1N NaOH.

The remaining inverse aqua regia is transferred to a glass vial and dried down. To purify the Re, anion exchange chromatography is used. The dried sample residue is re-dissolved in 0.2N HNO_3 and is transferred into disposable anion column and is washed in the order specified in Figure 2.5. The final solution that contains the dissolved Re is then

dried down in a pre-cleaned PMP beaker. The sample is once again dissolved in 0.2N HNO_3. This solution is transferred into a 1mL centrifuge tube where a single ~20 mesh anion bead is used to extract the Re over a minimum of 6 hours. The anion bead is then washed and transferred into a clean 1mL centrifuge tube containing 6N HNO_3 in order to back-extract the Re from the bead. The purified Re sample is dried down and placed onto a Ni filament and is activated using $Ba(NO_3)_2$ dissolved in water.

These filaments are run on a thermal ionization mass spectrometer under specific conditions. The Re coated filament is heated to ~650-800^{o}C at a rate of ~200deg/min to create a stable beam of ReO_4^- for analysis by Faraday cup detectors. Both ^{185}Re and ^{187}Re are analyzed simultaneously 100 times at discrete time intervals to ensure good counting statistics. The Os coated filament is typically heated to between ~650^{o}C-735^{o}C at a rate of ~30deg/min under a pressure of ~2.00×10^{-7} mbar of O_2 to ensure a stable beam of OsO_3^- is obtained. Due to the low beam intensity associated with Os, a secondary electron multiplier is used for analysis. Each isotope is then measured independently 96 times to ensure good counting statistics.

Procedural blanks are also used to define the amount of impurities added through the chemical process. In particular, Os blank values (0.40 ± 0.20 pg) for non radiogenic isotopes of Os can be responsible for up to 25% of ^{188}Os, but values <5% are more typical. Blank values for both Re and Os can be used to correct raw data collected from the TIMS instrument. As a sample is run through the TIMS further corrections are made based on the oxygen isotope abundances, since it is the Re and Os oxides that are measured. Finally isotope fractionation corrections are spike unmixing corrections are applied before final analysis.

2.63 Trace Element Analysis

To obtain bulk trace element compositions of the separated mineral fractions, a Perkin Elmer Elan 6000 Quadrupole Inductively Coupled Plasma Mass Spectrometer at the University of Alberta was used. For analysis, acid digestion is performed on 200mg of sample and was subsequently run on the quadrupole ICP-MS using a DNC-1 standard for the calibration of trace elements. Appropriate dwell times and integration times were selected to optimize counting statistics for each element. For the majority of elements

20ms and 700ms integrations times were used, with the exception being Cu where the dwell and integration times were decreased to 10ms and 350ms respectively.

Spot analyses of all phases, back scattered images, and element maps were performed over numerous sessions on a Cameca SX100 electron microprobe. The following standards were used for all analyses, pyrite for S and Fe, nickel metal for Ni, cobalt metal for Co, sphalerite for Zn, arsenopyrite for As, and calcite for Ca. Data was then collected under beam conditions of 20kV and 20nA. Detection limits for trace elements were approximately 300 - 800ppm, depending on the element analyzed.

2.7 Sample Description

2.71 General Characteristics

Rock samples of sulphide material from the Main Zone, Derryville Zone, Bog Zone, and the K-Zone of Galmoy were used for Re-Os and trace element analysis (Table 2.1, Figures 2.7, 2.8, 2.9, 2.10). The naming convention for the prepared samples is shown in Table 2.2. These samples were all divided into different magnetic divisions using the procedure explained in Section 2.61, and have subsequently been analyzed for bulk trace element composition using quadrupole ICP-MS and in select samples with an SX100 electron microprobe.

These elemental analyses provide information on the major mineralogy present, and provide insight into trace element distribution within a sample. Figures 2.7, 2.8, 2.9, and 2.10 show that the general trace element distributions between the different sample divisions are very similar. On a relative scale, the sample divisions with higher magnetic susceptibility contain pyrite with the highest concentrations of Re, Os, As, and transition metals, regardless of sample morphology or bulk mineralogy. Sample divisions with low magnetic susceptibility sulphides or gangue minerals, have trace element concentrations that are much lower than their high magnetic susceptibility counterparts, often by up to an order of magnitude.

Microprobe analysis in general allows for the determination of the mineralogy of a rock, and in some cases, the individual magnetic divisions. Detection limitations on an electron microprobe usually restrict trace element measurements to As and rarely the Ni content of the minerals. However, since there is such a clear correlation between so many

elements it allows As and Ni to be used as proxies for other elements, perhaps even for Re and Os. Backscattered images and element maps of the processed material provide excellent information on how trace elements are distributed within minerals, and between sample divisions of differing magnetic susceptibilities. These images also allow for the accurate measurement of the modal abundances of the various minerals (Table 2.3). In short this is accomplished by counting the number of pixels associated with each mineral phase. This can be easily accomplished by associating each mineral with its intensity on a back scattered image or element map and then running a simple MATLAB code to calculate the area of the desired range of intensities. A full description of the calculation in presented in the Appendix V.

Table 2.1: Description and location of samples used for Re-Os analysis

Sample Name	Abbreviation	Deposit/Zone	Host Rock/Depth	Ore Minerals	Basic Description
121/194.01	LK 121	Lisheen/Main	Waulsortian Limestone /194.01m	Pyrite / Marcasite / Sphalerite / Galena	Intergrown ore minerals within a carbonate matrix
431/205.70	LK 431	Lisheen/Main	Waulsortian Limestone /205.7m	Pyrite / Sphalerite / Galena	Massive sulfides
8S08-FW	LK 8S08	Lisheen/Main	Lisduff Oolite (Foot Wall) / 176m	Pyrite	Massive Pyrite
325-146.20	LK 325	Lisheen/Derryville	Waulsortian Limestone / 146.2m	Pyrite / Sphalerite / Galena	Massive sulfides
359/143.60	LK 359	Lisheen/Derryville	Waulsortian Limestone / 143.6m	Pyrite / Sphalerite / Galena	Massive pyrite with integrown sphalerite
451/39.1	LK 451	Lisheen/Bog	Waulsortian Limestone / 139.1m	Pyrite / Sphalerite / Galena	Massive Sulfides
355/95.05	Gal 355	Galmoy/K-Zone	N/A / 95.05m	Pyrite / Sphalerite / Galena	Intergrown ore minerals within a carbonate matrix

Table 2.2: Naming convention for Re-Os analysis

Name	Comment
Sample A, B	A sample that has been partitioned into multiple fractions (e.g. A and B) before crushing
Sample Bulk	Bulk material that has been crushed but with no magnetic separation
Sample NM 2.0	Mineral separate was non-magnetic at a current of 2.0 amps
Sample M 2.0	Mineral separate was magnetic at a current of 2.0 amps
Sample rpt	A sample that has been analyzed more then once.
Sample Clean	Hydrochloric acid treatment
Sample 60min	Sample heated to 400^{o}C for 60 minutes
Sample HC	Hydrothermal carbonates (calcite/dolomite) and quartz

2.72 Lisheen Main Zone

Sample LK 121 is a mixture of early ore stage pyrite, marcasite, and sphalerite in a dolomite matrix (Figure 2.11). Pyrite crystals within this sample have a range of sizes from 1-2mm down to much finer grain material, mixed with the matrix of dolomite and quartz. The larger pyrite grains show extensive fracturing by veins containing elevated As contents. The sphalerite in this sample appears to have crystallized in the interstitial spaces between pyrite crystals. Few veins are observed crosscutting the sphalerite, in contrast to pyrite. Together, these observations suggest that sphalerite postdates pyrite in the paragenetic sequence. The latest stage mineral growth in this sample appears to be calcite veins that crosscut both the sphalerite and pyrite. Based on these crosscutting relationships, there appears to be several separate fluid events affecting this sample. These relate to pyrite growth, As-rich veins, sphalerite growth, and calcite veins.

Sample LK 8S08 is massive ore stage pyrite that has been crosscut by calcite veins (Figure 2.12). Trace element contents of the pyrite are enriched in areas within 0.5mm of the calcite veins (Figure 2.12C). These areas are likely associated with regions of highest magnetic susceptibility based on the relationships observed in the ICP-MS data.

Sample LK 431 is a complex mix of ore stage massive galena, sphalerite, and pyrite.

Table 2.3: Mineralogy of Sample Divisions

Sample	Fraction	Mineralogy (Modal Abundance)				
		Pyrite	Sphalerite	Galena	Quartz	Carbonate
LK 121 A	M1.3	x	x	Trace	Trace	Trace
LK 121 A	NM1.3	90.9	4.9	<0.1	2.3	3
LK 121 A	WR	Trace	Trace	Trace	x	x
LK 121 B	M1.0	x	x	Trace	Trace	Trace
LK 121 B	NM1.0	66.0%	29.1%	0.2%	4.4%	0.4%
LK 121 B	WR	Trace	Trace	Trace	x	x
LK 121 B	Bulk	x	x	x	x	x
LK 431	M1.6	x	x	x	Trace	Trace
LK 431	M2.0	x	x	x	Trace	Trace
LK 8S08	M0.8	x	x	Trace	Trace	x
LK 8S08	M1.0	83.2%	5.4%	0.1%	2.1%	9.1%
LK 8S08	M1.2	x	Trace	Trace	Trace	Trace
LK 8S08	NM 1.5	94.3%	0.4%	<0.1%	3%	2.3%
LK 8S08 B	M0.8	x	Trace	Trace	Trace	Trace
LK 8S08 B	NM1.0	x	Trace	Trace	Trace	Trace
LK 8S08 B	NM1.2	x	Trace	Trace	Trace	Trace
LK 8S08 B	WR	x	Trace	Trace	Trace	Trace
LK 325 A	NM 1.7	x	x	Trace	Trace	Trace
LK 325 A	NM 1.5	x	x	Trace	Trace	Trace
LK 325 A	NM 1.1	x	x	Trace	Trace	Trace
LK 325 B	NM 1.7	7.4%	82.5%	3.9%	6.2%	0.1%
LK 325 B	NM 1.5	x	x	Trace	Trace	Trace
LK 325 B	NM 1.1	85.4%	9.9%	1.5%	3%	0.2%
LK 359 A	NM 1.8	9%	69.1%	19%	2.5%	0.4%
LK 359 A	NM 1.6	x	x	Trace	Trace	Trace
LK 359 A	NM 1.4	x	x	Trace	Trace	Trace
LK 359 A	NM 1.2	x	x	Trace	Trace	Trace
LK 359 A	NM 1.0	39.6%	54.3%	0.3%	4.7%	1.2%
LK 359 A	NM 0.8	x	x	Trace	Trace	Trace
LK 359 A	M0.6	x	x	Trace	Trace	Trace
LK 359 B	NM 1.8	x	x	x	Trace	Trace
LK 359 B	NM 1.6	x	x	Trace	Trace	Trace
LK 359 B	NM 1.4	x	x	Trace	Trace	Trace
LK 359 B	NM 1.2	x	x	Trace	Trace	Trace
LK 359 B	M0.6	x	x	Trace	Trace	Trace
LK 451 A	M1.0	x	x	Trace	Trace	Trace
LK 451 A	NM1.0	x	x	Trace	Trace	Trace
LK 451 B	M1.0	x	x	Trace	Trace	Trace
LK 451 B	NM1.0	x	x	Trace	Trace	Trace
Gal 355	M0.8	x	x	x	Trace	Trace
Gal 355	M1.3	x	x	x	Trace	Trace
Gal 355	NM2.0	x	x	x	Trace	Trace
Gal 355	WR	Trace	Trace	Trace	x	x

All modal percentages were determined using MATLAB, refer to Appendix for more detail.
x = Proportion of mineral is likely greater than 5%
Trace = Proportion of mineral is likely less than 5%

2.73 Derryville Zone

Samples LK 359 and LK 325 are main stage massive sulphides containing inter-grown pyrite, sphalerite, and minor galena.

Sample LK 359 contains pyrite up to 5mm across and is the first ore mineral crystallized in the assemblage. Well defined growth zones are not observed within these pyrites, but the variation in the As content within these crystals suggests a complex growth and recrystallization history for these pyrites (Figure 2.13). Sphalerite crystallization takes on two distinct forms within LK 359. Colloform sphalerite often surrounds the cores of the larger pyrite grains and is also commonly associated with the replacement/recrystallization of pyrite. Interstitial sphalerite is also common and often crosscuts adjacent pyrite crystals. Minor carbonate and quartz are found throughout the sample, but are often spatially associated with areas of pyrite replacement/recrystallization.

Sample LK 325 is broadly similar to LK 359, as primary pyrite crystallization appears to have been replaced and crosscut by later stage sphalerite and galena. Areas of replacement are also associated with trace element enrichment within pyrite. The major difference between these two samples is that the pyrite crystals have better defined zoning patterns in LK 325 compared to LK 359 (Figure 2.14). Dolomite veins also occur within LK 325, however, much of the carbonate and quartz is associated with pyrite alteration, similar to that seen in LK 359

2.74 Bog Zone

Sample LK 451 has two major generations of pyrite, the first is represented as pyrite cores that contain relatively low abundances of trace elements (Figure 2.15). A second generation of fluid appears to have recrystallized the outer rims of the first generation pyrite, and is associated with higher trace element abundances and colloform sphalerite. Sphalerite is found as colloform grains about 10-20μm across and as interstitial masses between, and crosscutting, pyrite. The boundaries between the pyrite and interstitial sphalerite are often marked by replacement/dissolution and trace element enrichment of the pyrite. Calcite, dolomite, and quartz are found throughout the sample.

2.75 Galmoy

Sample Gal 355 is mineralogically similar to that of the Lisheen samples, but has differences in morphology. The sulphides in GAL 355 are found as intergrown masses inside a matrix of calcite. These sulfides contain galena and sphalerite that exist as millimetre size grains surrounded by interstitial pyrite (Figure 2.16). The pyrite has complex zoning in which over ten individual zones are observed, each with different trace element concentrations. Minor calcite veins crosscut pyrite and terminate against galena or sphalerite.

2.76 Paragenetic History

Complex zonation, crosscutting relationships, chemical, and textural changes throughout these samples indicate a complex paragenetic history. Although a complete paragenetic study of these samples and the deposit as a whole is beyond the scope of this thesis, several basic observations can be made. In general, the first sulphide formed is pyrite, which contains relatively low concentrations of trace elements. These original pyrite crystals are often fractured, replaced, or recrystallized, producing pyrite with an enriched trace element signature. This alteration of pyrite is often found in conjunction with the mineralization of sphalerite and galena. The only major exception is LK 8S08, which appears to have maintained much of its original pyrite without major changes.

2.8 Results

For Re-Os geochronology, analysis of 25 Main Zone, 32 Derryville Zone, 9 Bog Zone, and 8 Galmoy sample divisions were analyzed. The analytical results are presented in Tables 2.4, 2.5, 2.6 and 2.7. The data obtained from these sample divisions were used to construct isochron diagrams for the Main, Derryville, and Bog Zones. All isochron diagrams were constructed by plotting $\frac{^{187}\mathrm{Re}}{^{188}Os}$ vs. $\frac{^{187}Os}{^{188}Os}$ using Isoplot version 3.00 (Ludwig, 2001), with all uncertainties given to 2σ.

Table 2.4: Main Zone Re-Os Analytical Results

Sample	Sample Weight (g)	$^{185}Re/^{190}Os$ Spike Weight (g)	Total Re ppb	Total Os ppt	Total ^{192}Os ppt	^{187}Re / ^{188}Os	^{187}Os / ^{188}Os
121-194-01 A M1.3	0.20163	0.00670	20.21 ± 0.6	163.90 ± 1.16	35.34 ± 0.17	1137.54 ± 6.47	7.14 ± 0.04
121-194-01 A NM1.3	0.34861	0.00775	4.83 ± 0.02	42.60 ± 0.39	10.25 ± 0.10	936.64 ± 9.31	5.61 ± 0.06
121-194-01 B M1.0	0.29664	0.00769	45.57 ± 0.13	433.38 ± 2.17	105.55 ± 0.17	858.88 ± 2.90	5.46 ± 0.02
121-194-01 B NM1.0	0.29664	0.00769	14.97 ± 0.04	130.70 ± 0.78	30.50 ± 0.10	976.59 ± 4.18	6.02 ± 0.03
121-194-01 A HC	0.39923	0.00345	2.48 ± 0.01	48.69 ± 0.32	15.49 ± 0.09	318.87 ± 2.32	2.41 ± 0.02
121-194-01 B HC	0.39392	0.00355	5.67 ± 0.02	96.62 ± 0.49	29.62 ± 0.10	380.68 ± 1.73	2.78 ± 0.01
121-194-01 B Bulk	0.20948	0.01078	7.39 ± 003	102.53 ± 0.65	29.70 ± 0.16	495.27 ± 3.17	3.39 ± 0.02
LK431B-M16	0.33674	0.00500	4.93 ± 0.02	93.11 ± 0.53	31.73 ± 0.15	309.16 ± 1.78	1.75 ± 0.01
LK431B-M20	0.40019	0.00150	1.58 ± 0.01	39.65 ± 0.29	13.85 ± 0.11	226.37 ± 2.18	1.52 ± 0.02
8508FW M0.8	*0.21296*	*0.00432*	*7.01* ± 0.02	*47.91* ± 0.59	*10.16* ± 0.16	*1372.50* ± 21.60	*7.38* ± 0.12
8508FW M1.0	0.40373	0.00622	6.00 ± 0.02	46.64 ± 0.44	9.82 ± 0.09	1215.98 ± 11.12	7.50 ± 0.07
8508FW M1.2rpt	0.40424	0.00549	5.82 ± 0.02	46.41 ± 0.43	10.01 ± 0.09	1155.33 ± 10.47	7.13 ± 0.07
8508FW M1.2rpt RA	0.40424	0.00549	5.82 ± 0.02	47.86 ± 0.44	10.60 ± 0.09	1090.99 ± 9.50	6.75 ± 0.06
8508FW M1.2	0.40401	0.00531	5.62 ± 0.02	44.52 ± 0.46	9.52 ± 0.09	1173.92 ± 11.49	7.27 ± 0.08
8508FW NM1.5	0.40163	0.00377	2.63 ± 0.01	31.78 ± 0.28	8.88 ± 0.09	589.52 ± 6.06	3.79 ± 0.04
8508FW NM1.5 Clean	0.35166	0.00431	2.33 ± 0.01	27.37 ± 0.29	7.53 ± 0.10	615.68 ± 8.48	3.97 ± 0.06
8508FW NM1.5rpt Clean	0.35143	0.00436	2.30 ± 0.01	28.62 ± 0.65	8.09 ± 0.21	565.80 ± 14.72	3.65 ± 0.17
8508FW NM1.5rpt2 Clean	0.21937	0.00325	2.28 ± 0.02	25.53 ± 0.37	6.96 ± 0.15	652.56 ± 14.88	4.08 ± 0.10
8508FW NM1.5 45min	0.24359	0.00440	2.17 ± 0.01	26.76 ± 0.36	7.55 ± 0.14	571.60 ± 11.35	3.68 ± 0.08
8508FW NM1.5 60min	0.24240	0.00341	2.25 ± 0.01	26.48 ± 0.34	7.39 ± 0.14	604.53 ± 11.83	3.80 ± 0.08
8508FWB M0.8	0.24433	0.00824	7.77 ± 0.03	55.80 ± 0.68	10.69 ± 0.14	1445.99 ± 19.50	8.98 ± 0.13
8508FWB NM1.0	0.40948	0.00764	3.96 ± 0.01	39.10 ± 0.57	9.80 ± 0.13	803.36 ± 10.81	5.08 ± 0.11
8508FWB NM1.2	0.38125	0.00757	2.31 ± 0.01	38.30 ± 0.63	12.13 ± 0.22	378.36 ± 6.93	2.45 ± 0.09
8508FWB NM1.2 rpt	0.36776	0.00335	2.42 ± 0.01	31.29 ± 0.29	8.99 ± 0.09	536.75 ± 5.98	3.48 ± 0.04
8508FWB HC	0.14254	0.00231	4.46 ± 0.02	47.18 ± 0.60	12.91 ± 0.24	687.37 ± 12.99	4.03 ± 0.08

Table 2.5a: Derryville Zone LK 325 Re-Os Analytical Results

Sample	Sample Weight (g)	$^{185}Re/^{190}Os$ Spike Weight (g)	Total Re ppb	Total Os ppt	Total ^{192}Os ppt	^{187}Re / ^{188}Os	^{187}Os / ^{188}Os
325-146-20A NM1.7rpt	0.20416	0.01072	1.65 ± 0.02	15.03 ± 0.42	2.64 ± 0.17	1239.57 ± 76.98	10.44 ± 0.65
325-146-20A NM1.5	0.30137	0.01091	3.70 ± 0.01	30.54 ± 0.50	5.31 ± 0.12	1387.83 ± 30.32	10.67 ± 0.25
325-146-20A NM1.1	0.15109	0.02729	9.35 ± 0.03	73.67 ± 1.14	11.97 ± 0.23	1553.68 ± 29.92	11.95 ± 0.24
325-146-20B NM1.7	0.15180	0.02592	11.83 ± 0.04	63.03 ± 1.43	6.03 ± 0.23	3900.03 ± 142.79	25.54 ± 0.96
325-146-20B NM1.7rpt	0.20198	0.02193	11.74 ± 0.04	60.25 ± 1.25	5.73 ± 0.17	4077.62 ± 119.10	25.77 ± 0.78
325-146-20B NM1.7rpt2	0.30257	0.01611	11.99 ± 0.04	57.75 ± 0.98	5.19 ± 0.11	4597.83 ± 98.92	27.70 ± 0.61
325-146-20B NM1.5	0.20107	0.02015	20.81 ± 0.06	97.53 ± 1.80	8.32 ± 0.18	4973.32 ± 103.58	29.55 ± 0.67
325-146-20B NM1.5rpt	0.25532	0.02675	19.82 ± 0.06	95.78 ± 1.52	8.49 ± 0.14	4645.63 ± 75.29	28.17 ± 0.49
325-146-20B NM1.1	0.14825	0.02645	45.47 ± 0.13	221.41 ± 3.08	17.78 ± 0.23	5086.33 ± 67.22	31.87 ± 0.44
325-146-20B NM1.1rpt	0.19860	0.01933	45.09 ± 0.13	206.92 ± 3.25	17.40 ± 0.20	5156.33 ± 60.42	30.11 ± 0.45
325-146-20B NM1.1rpt2	0.20413	0.04369	44.82 ± 0.13	218.55 ± 3.25	18.14 ± 0.19	4915.85 ± 51.53	30.60 ± 0.41

Table 2.5b: Derryville Zone LK 359 Re-Os Analytical Results

Sample	Sample Weight (g)	$^{185}Re/^{190}Os$ Spike Weight (g)	Total Re ppb	Total Os ppt	Total ^{192}Os ppt	^{187}Re / ^{188}Os	^{187}Os / ^{188}Os
359-143-60A NM1.8	0.19767	0.02607	330.95 ± 0.96	1284.79 ± 10.52	58.75 ± 0.20	11206.10 ± 49.20	61.67 ± 0.28
359-143-60A NM1.6	0.15233	0.08105	508.91 ± 1.48	1937.69 ± 21.77	97.09 ± 0.40	10427.69 ± 52.59	55.63 ± 0.41
359-143-60A NM1.6rpt	0.10195	0.10850	540.18 ± 1.57	2047.37 ± 18.33	100.08 ± 0.38	10737.55 ± 50.96	57.21 ± 0.30
359-143-60A NM1.2	0.19662	0.02120	483.97 ± 1.41	1919.38 ± 13.44	112.15 ± 0.22	8584.80 ± 30.23	46.63 ± 0.16
359-143-60A NM1.2rpt	0.04809	0.07475	437.49 ± 1.27	1829.27 ± 42.37	111.67 ± 1.42	7794.07 ± 101.36	44.31 ± 0.98
359-143-60A NM1.0	0.05208	0.08246	1066.99 ± 3.10	4282.87 ± 40.37	214.69 ± 0.80	9887.18 ± 46.16	55.60 ± 0.31
359-143-60A NM0.8	0.05471	0.08763	2043.47 ± 5.94	7797.22 ± 60.38	361.49 ± 0.89	11245.79 ± 42.66	60.73 ± 0.24
359-143-60A NM0.8 rpt	0.05557	0.22126	1932.76 ± 5.62	7669.10 ± 54.37	355.77 ± 0.71	10807.65 ± 37.87	60.69 ± 0.21
359-143-60A M0.6	0.00860	0.10519	6096.14 ± 17.73	23593.30 ± 214.87	931.62 ± 4.21	13017.89 ± 69.10	72.62 ± 0.40
359-143-60B NM1.8	0.10208	0.10100	33.22 ± 0.10	206.50 ± 2.80	28.47 ± 0.37	2321.49 ± 30.23	15.42 ± 0.22
359-143-60B NM1.8rpt	0.19811	0.02061	39.08 ± 0.11	203.54 ± 2.31	27.26 ± 0.19	2851.66 ± 21.66	16.09 ± 0.16
359-143-60B NM1.6	0.09924	0.10405	65.03 ± 0.19	384.38 ± 3.92	52.20 ± 0.36	2478.26 ±18.47	15.77 ± 0.13
359-143-60B NM1.6rpt	0.09780	0.01859	69.21 ± 0.20	388.92 ± 3.81	51.45 ± 0.36	2676.16 ±19.98	16.39 ± 0.13
359-143-60B NM1.4	0.10026	0.10347	83.93 ± 0.25	468.11 ± 5.68	63.44 ± 0.45	2631.96 ± 20.06	15.82 ± 0.17
359-143-60B NM1.2	0.19715	0.02712	134.21 ± 0.39	709.19 ± 4.81	87.07 ± 0.20	3066.48 ±11.39	18.24 ± 0.07
359-143-60B M0.6	0.02042	0.08733	469.04 ± 1.37	2722.28 ± 23.55	362.70 ± 1.79	2572.73 ±14.39	16.22 ± 0.10
359-143-60A NM 0.8 Clean	0.01963	0.32975	3499.03 ± 10.17	14076.66 ± 122.03	621.51 ± 1.99	11200.03 ± 48.01	64.15 ± 0.31
359-143-60A M1.2 Clean	0.04111	0.07494	1187.30 ± 3.45	4747.78 ± 45.58	262.79 ± 1.00	8988.31 ± 42.76	49.65 ± 0.29
359-143-60A M1.2 Clean	0.02706	0.04679	1174.10 ± 3.42	4813.61 ± 50.31	263.03 ± 1.41	8880.12 ± 53.39	50.38 ± 0.36
359-143-60B NM1.4 Clean	0.09317	0.02848	73.60 ± 0.22	418.40 ± 5.26	55.86 ± 0.47	2621.32 ± 23.21	16.17 ± 0.19
359-143-60B NM1.6 Clean	0.07763	0.01515	60.36 ± 0.18	331.29 ± 4.15	45.93 ± 0.48	2614.28 ± 27.76	15.29 ± 0.19

Table 2.6: Bog Zone Re-Os Analytical Results

Sample	Sample Weight (g)	$^{185}Re/^{190}Os$ Spike Weight (g)	Total Re ppb	Total Os ppt	Total ^{192}Os ppt	^{187}Re / ^{188}Os	^{187}Os / ^{188}Os
LK451A-1	0.36526	0.02227	53.79 ± 0.21	237.11 ± 1.63	17.84 ± 0.10	5999.24 ± 40.65	34.54 ± 0.22
LK451A-2	0.41838	0.02217	54.99 ± 0.21	244.43 ± 2.02	17.84 ± 0.11	6131.48 ± 44.09	35.82 ± 0.28
LK451A-3	0.40639	0.02156	53.22 ± 0.18	234.41 ± 2.02	17.35 ± 0.11	6101.30 ± 45.22	35.22 ± 0.29
LK451B-1	0.39335	0.02204	45.19 ± 0.18	223.12 ± 1.29	24.02 ± 0.11	3742.90 ± 22.45	21.86 ± 0.14
LK451B-2	0.41456	0.02281	46.53 ± 0.18	224.89 ± 1.17	24.00 ± 0.10	3857.77 ± 22.18	22.13 ± 0.12
LK451A-2 reload Re	0.41838	0.02217	54.95 ± 0.21	244.43 ± 2.02	17.84 ± 0.11	6126.45 ± 44.06	35.82 ± 0.28
LK451B-1 reload Re	0.39335	0.02204	45.16 ± 0.18	223.12 ± 1.29	24.02 ± 0.11	3740.59 ± 22.45	21.86 ± 0.14
LK451B-2 reload Re	0.41456	0.02281	46.51 ± 0.18	224.89 ± 1.17	24.00 ± 0.10	3856.54 ± 22.17	22.13 ± 0.12
LK451-A M10	0.24753	0.02756	54.58 ± 0.21	278.53 ± 1.49	32.70 ± 0.15	3320.87 ± 20.29	19.42 ± 0.11
LK451-A NM10	0.11966	0.01681	40.16 ± 0.16	176.13 ± 4.52	13.32 ± 0.29	5998.92 ± 131.40	34.32 ± 0.77
LK451-B M10	0.24407	0.02740	46.98 ± 0.18	231.16 ± 1.94	24.92 ± 0.17	3751.10 ± 28.97	21.82 ± 0.20
LK451-B NM10	0.14831	0.01693	23.81 ± 0.10	123.38 ± 1.92	15.43 ± 0.23	3068.99 ± 47.67	17.76 ± 0.28

Table 2.7: Galmoy Re-Os Analytical Results

Sample	Sample Weight (g)	$^{185}Re/^{190}Os$ Spike Weight (g)	Total Re ppb	Total Os ppt	Total ^{192}Os ppt	^{187}Re / ^{188}Os	^{187}Os / ^{188}Os
355-195 Bulk	0.24490	0.01022	15.81 ± 0.05	96.65 ± 2.05	17.12 ± 0.31	1837.27 ± 33.22	10.33 ± 0.29
355-195 M0.8	0.29818	0.00732	53.70 ± 0.16	267.35 ± 2.02	31.89 ± 0.12	3350.20 ± 16.02	19.00 ± 0.09
355-195 M1.3	0.40195	0.00811	29.60 ± 0.09	174.89 ± 1.15	32.67 ± 0.10	1802.71 ± 7.60	9.40 ± 0.04
355-195 M1.3rpt	0.10619	0.01065	29.59 ± 0.09	173.72 ± 1.77	32.30 ± 0.32	1822.44 ± 18.63	9.48 ± 0.10
355-195 M2.0	0.30205	0.00774	16.22 ± 0.05	119.37 ± 0.88	24.17 ± 0.12	1334.79 ± 7.55	8.09 ± 0.05
355-195 NM2.0	0.40232	0.01056	2.65 ± 0.01	23.06 ± 0.27	5.57 ± 0.08	948.09 ± 14.57	5.57 ± 0.09
355-195 NM2.0rpt	0.40031	0.00676	2.64 ± 0.01	23.14 ± 0.29	5.58 ± 0.09	941.79 ± 14.92	5.59 ± 0.10
355-195 HC	0.40712	0.00243	13.52 ± 0.04	79.58 ± 0.73	11.89 ± 0.08	2261.08 ± 17.11	13.64 ± 0.10

2.81 Main Zone Samples

LK 8S08 has a variable Re content of ~2-7 ppb for pyrite rich material, whereas a single analysis of the associated calcite veins has a similar concentration of 5ppb. Thirteen of sixteen pyrite analyses produce a Model 3 isochron with an age of 356.7 ± 4.8 Ma (MSWD = 2.8) having an initial $\frac{^{187}Os}{^{188}Os}$ ratio of 0.253 ± 0.068 (Figure 2.17). The three sample divisions that were excluded from the regression were LK 8S08HC, LK 8S08 M0.8, and LK 8S08B M0.8, further details regarding these sample divisions are presented in Section 2.91.

Sample LK 121 has a slightly larger variation in pyrite Re content of ~2-20ppb whereas the associated gangue minerals contain 2-6ppb Re. A 5-point regression on the sulfide samples yields a Model 3 Re-Os age 340 ± 66 with a high degree of scatter (MSWD = 168) and a imprecise initial $\frac{^{187}Os}{^{188}Os}$ ratio of 0.5 ± 1.0. A 7-point regression containing an additional 2 data points from carbonate divisions yields a similar Model 3 Re-Os age of 334 ± 26 (MSWD = 108) with an initial $\frac{^{187}Os}{^{188}Os}$ ratio of 0.62 ± 0.34 (Figure 2.18).

2.82 Derryville Zone Samples

Sample LK 325 has an extremely variable Re content of 2 - 45ppb. A Model 3 isochron of 320 ± 20 Ma (MSWD = 42) with a very high initial $\frac{^{187}Os}{^{188}Os}$ ratio of 3.7 ± 1.4 (Figure 2.19) was created using 11 data points.

Sample LK 359 is similar to LK 325, having a large range of Re content from 30-6000ppb and yields a Model 3 age of 319.6 ± 8.0 Ma (MSWD = 134) and a high initial $\frac{^{187}Os}{^{188}Os}$ ratio of 2.0 ± 1.1 (Figure 2.20) based on 22 data points.

2.83 Bog Zone Samples

Compared to the other samples, LK 451 has a much smaller range of 20-45ppb Re. A 9-point Model 3 isochron yields an age of 343.0 ± 8.7 Ma (MSWD = 7.8) and a initial $\frac{^{187}Os}{^{188}Os}$ ratio of 0.26 ± 0.69 (Figure 2.21).

2.84 Galmoy Samples

Gal 355 contains sulfides that contain 2-50 ppb Re, whereas the associated carbonates contain 13ppb Re. The Model 3 isochron for Gal 355 gives an age of 336 ± 45 Ma (MSWD = 981) and an initial $\frac{^{187}Os}{^{188}Os}$ ratio of 0.1 ± 1.5 (Figure 2.22).

2.9 Discussion

2.91 Reliability of the Re-Os Data

The isochron diagrams produced using Isoplot 3.00 have a wide range of scatter with MSWD's ranging from of 2.8 to 981. Much of this uncertainly may be explained by considering the details of the sample divisions analyzed.

LK 8S08 produced a reasonably precise isochron with little scatter beyond analytical uncertainty (MSWD 2.8) with the caveat that three outliers were excluded. These exclusions are deemed appropriate based on the following criteria. LK 8S08HC is excluded due to it being composed of calcite, a mineral in which the Re-Os systematics are unknown. It is also evident from crosscutting relationships that it formed from a later fluid than that of the pyrite. This could lead to the observed scatter, especially if the later fluid contained a different initial $\frac{^{187}Os}{^{188}Os}$ ratio (Figure 2.12). The two divisions with the highest magnetic susceptibly, LK 8S08 M0.8 and LK 8S08B M0.8, are also excluded. Exclusion of these divisions is based on the observation that they contain the highest carbonate content, and trace element concentration. Calcite can potentially cause scatter in these divisions as it is a mineral known to plot off the isochron (Table 2.3). Additionally, the positive correlation between trace element concentrations and magnetic susceptibility (Figures 2.7-2.10) suggests that these sample divisions contain pyrite with the highest trace element abundances. According to Figure 2.12 these sample divisions

would be associated with the chemically overprinted regions near the calcite veins. As such, the data from LK8S08 HC, LK 8S08 M0.8 and LK 8S08B M0.8 were excluded based on the strong likelihood that they contain Re-Os that is not associated with the primary pyrite mineralizing event.

Compared to LK 8S08, the other samples studied at Lisheen and Galmoy have very complex Re-Os isotopic characteristic (Figure 2.11, 2.13, 2.14, 2.15, 2.16), and as such, it is much harder to pin down the exact cause of the uncertainty observed in the isochron diagrams. To some extent, each sample contains multiple generations of sulfides, as well as subsequent alteration, and recrystallization, which are all due to changes in the fluid components through time. It is not unreasonable to suspect that the multiple fluids that formed Lisheen and Galmoy would contain variable initial $\frac{^{187}Os}{^{188}Os}$ ratios. These would in turn depend on the particular history of fluid/rock interaction prior to mineral precipitation. If that is the case, each sample, and the various magnetic divisions associated with them, would have slightly different initial $\frac{^{187}Os}{^{188}Os}$ ratios. When an isochron is constructed from data that contains variable initial $\frac{^{187}Os}{^{188}Os}$ ratios the data points will produce scatter, even if they are formed at approximately the same time.

The limit to which the scatter might be explained by variations in the initial $\frac{^{187}Os}{^{188}Os}$ ratio can be tested for each mineral division. This is investigated under two circumstances, one in which the isochron age is the age of every sample, and a second in which the age of the divisions are allowed to vary.

If it is assumed that each data point represents the same age then there is some range of initial $\frac{^{187}Os}{^{188}Os}$ ratios that would be needed to explain the scatter observed in the isochron (Figure 2.23A). In order for the initial $\frac{^{187}Os}{^{188}Os}$ ratio variations to be an acceptable explanation for the scatter, this range cannot include unrealistic values, such as values below that of the mantle value of 0.1296 (Meisel et al., 2001).

Since a range of ages are possible for any one sample division it is also important to calculate what ranges of ages can be supported by varying the initial $\frac{^{187}Os}{^{188}Os}$ ratio. This is tested by using the mantle $\frac{^{187}Os}{^{188}Os}$ ratio of 0.1296 (Meisel et al., 2001) as the lower limit for the initial $\frac{^{187}Os}{^{188}Os}$ ratio for each sample division. From this, a theoretical maximum age is calculated for each division, with the constraint that all sample divisions formed with an initial ratio above 0.1296. For a sample to maintain a realistic initial ratio, the error ellipse associated with each fraction must not lie entirely below the Os evolution line defined by the initial $\frac{^{187}Os}{^{188}Os}$ ratio of 0.1296 (Figure 2.23B). If the maximum age is larger than the value calculated from the isochron, then initial $\frac{^{187}Os}{^{188}Os}$ fluctuation cannot be ruled out as the cause of the scatter. The calculation for each isochron is compiled in Table 2.8 and demonstrates that for LK 121 and LK 8S08, the observed scatter may be due to variations in initial $\frac{^{187}Os}{^{188}Os}$ ratio. For LK 455, variations in initial $\frac{^{187}Os}{^{188}Os}$ ratio can not been ruled as a possible cause of a scatter based on the these calculations, due to the uncertainties inherent in the data. Gal 355 has one point (Gal 355 M1.3) that cannot be explained by variations of initial $\frac{^{187}Os}{^{188}Os}$ ratio, which suggests that either this division has been reset, or that recrystallization/secondary mineralization occurred prior to 299 Ma.

Beyond variable initial $\frac{^{187}Os}{^{188}Os}$ ratios, a second possibility to consider is the effect of mineralogy on the Re-Os results. Ideally, pyrite is extracted as a pure separate, however, complex intergrowth within a sample can cause substantial mineral impurities to be present (Table 2.3). The two major impurities found are sphalerite and galena. Galena impurities are only really considered a major issue in the divisions with the lowest magnetic susceptibility, as galena is nearly absent in all other sample divisions (Table 2.3). The Re-Os systematics of galena is not well understood, but the sample divisions associated with high galena content do not qualitatively appear to have more scatter than

divisions that contain no galena. Sphalerite impurities are almost ubiquitous, excluding LK 8S08 (Table 2.3), with some divisions containing upwards of 80% sphalerite. This is particularly problematic, as the Re-Os system in sphalerite is more easily disturbed than pyrite (Morelli et al., 2004). Selective dissolution experiments of sphalerite (and galena) were undertaken to determine the effect of sphalerite (and galena) on the isochron quality of LK 359, and possibly by extension LK 325 (see Appendix III for details). These experiments consisted of reacting a sample in concentrated hydrochloric acid to selectively removes galena, sphalerite, and carbonate, leaving behind a sample that is enriched in pyrite. From these experiments, no major changes in Re-Os regressions were observed between the untreated and acid treated samples. Whereas impurities are obviously present in the majority of sample divisions, they are therefore unlikely to be the root cause of the scatter observed in the isochron diagrams (Figure 2.24).

The Re-Os characteristics of the Derryville samples differ from the Main and Bog Zones. The high initial $\frac{^{187}Os}{^{188}Os}$ ratios and younger ages observed in Derryville samples, compared to the Main and Bog Zones, is broadly indicative of a system undergoing resetting (Figure 2.25), producing an effective "rotation" of an isochron to a younger age. The timing of this resetting is unclear because the 320 Ma age is not associated with any known event in the Lisheen area. However, partial resetting during the Variscan orogeny may be the cause. It is possible that LK 359 and LK 325 contain Re-Os from both the ore formation event (~340-360 Ma), and that of resetting during the Variscan orogeny (~280 Ma). This would exacerbate any scatter seen in the associated isochron diagrams as well as producing spurious ages.

From these results three main groups of ages are seen within the data set (Figure 2.24). The oldest and most precise age of these is provided by LK 8S08 at 356.5 Ma. The second group that contains LK 121, LK 451, Gal 355 represents a later group at around 341.9 ± 6.0 Ma based on a combined isochron from these samples (Figure 2.26). The MSWD of this particular isochron is high, at 434, which is to be expected as different generations of sulphides are contained within the isochron. Even with the scatter present these samples still indicate that formation occurred around 340 Ma. The Bog Zone

sample LK451 produces the lowest-scatter regression for these samples, corresponding to an age of 343.0 ± 8.7 Ma.

A consistency check on these ages can be done by calculating Model Ages of a single sample division. For divisions that contain high $\frac{^{187}\mathrm{Re}}{^{188}Os}$ ratios of >5000, Model Ages can be calculated. For such high ratios the effect of any variation in the initial $\frac{^{187}Os}{^{188}Os}$ ratio is nearly negligible for age calculations, as the vast majority of Os is radiogenically derived. At Lisheen, the only sample divisions that have $\frac{^{187}\mathrm{Re}}{^{188}Os}$ ratios of 5000 or higher are LK 451A-1, LK 451A-2, LK 451A-3, and LK 451A NM10, all of which come from the Bog Zone. For these sample divisions Model Ages were calculated based on an initial $\frac{^{187}Os}{^{188}Os}$ ratio of 0.26±0.68 from the Bog Zone isochron (Figure 2.21). Averaging the Model Ages from these sample divisions gives an age of 343.0 ± 6.9 Ma for LK 451, an age which correlates well with the isochron age.

These two groups have similar, albeit poorly defined, initial $\frac{^{187}Os}{^{188}Os}$ ratios which approximately lay in the range of 0.1-0.6. The Derryville Zone samples have much higher initial ratios and a younger age of ~320 Ma, likely caused by resetting of the isotope system, and as such this data cannot be used to constrain the age of primary ore mineralization.

Table 2.8: Maximum age of a sample such that scatter can be attributed to variations in initial $\frac{^{187}Os}{^{188}Os}$ ratios

Isochron	Isochron Age (Ma)	Isochron Initial Ratio	Initial Ratio Range*	Maximum Age (Ma)**	Initial ratio variations responsible for scatter?
LK 8S08	356.7	0.253±0.068	0.13-0.50	365.0	Possible
LK 121 Sulfides	340	0.5±1.0	0.29-0.73	354.3	Possible
LK 121 All Data	334	0.62±0.34	0.35-0.83	354.3	Possible
LK 455	343.0	0.26±0.69	-0.28-1.10	343.5	Indeterminate
Gal 355	336	0.1±1.5	-0.75-1.10	299.2	Impossible

* Range from the method shown in Figure 2.23, ** Maximum ages assumed the minimum initial $\frac{^{187}Os}{^{188}Os}$ ratio is 0.1296.

2.92 Re-Os Constraints on Ore Formation

The Re-Os isotope system constrains mineralization at Lisheen to the Early Carboniferous between 340-360 Ma. Subsequent events have also been recorded at Lisheen via the resetting of the Derryville Re-Os system, as well as the imparted magnetization reported in Pannalal (2008a).

The oldest age related to Lisheen mineralization is from the Main Zone massive pyrite sample LK 8S08, which gives an age of 356.7 ± 4.8 Ma. This age is within the expected bounds of the host Lisduff Oolite Member of the Ballysheen Group. This age is older than the ages typically ascribed to the Waulsortian Limestone, such as the value of 346 ± 4 Ma used by Pannalal et al. (2008a). However, this age also overlaps within the uncertainty of the most recent age estimates for the depositional age of the Waulsortian Limestone, which must lie between the ages of the overlying Crosspatrick Formation (347 Ma), and underlying Ballysteen Group (353-356 Ma). The absolute age constraints for the biostratigraphic markers in Ireland in the Early Carboniferous in general are weak according to the summary provided in Waters el al. (2011). Thus, the true depositional age of the Waulsortian Limestone and Ballysheen Formation remains poorly defined, and given the fairly precise nature of the LK 8S08 isochron, no reason exists to disregard this age.

The Bog Zone isochron yields an age of mineralization at 343.0 ± 8.7 Ma, and is similar to that of LK 121, LK 451, Gal 355 isochron of 341.9 ± 6.0 Ma.

Thus, the Re-Os data constrains the mineralization of Lisheen to the period between 340-356 Ma, which has significant impact on our understanding of the major processes that have taken place at Lisheen. First, the suite of Re-Os ages obtained debunks the argument that Lisheen is the result of epigenetic fluid flow associated with the Variscan orogeny (Pannalal et al., 2008a). Secondly, due to the fact the dolomitization persists into the Crosspatrick Formation, the dolomitization at Lisheen must have formed diachronously because it is a precursor to sulphide mineralization. Furthermore, the model provided by Sevastopulo and Redmond (1999) cannot explain the results of LK 8S08 and may indicate that the formation of regional dolomite is more complex than the simple diagenetic model they used. The ^{40}Ar-^{39}Ar data from Hitzman et

al. (1994) is also largely disconnected from the Re-Os data. The upper range of 350 Ma falls within the time of hydrothermal activity associated with Lisheen based on the Re-Os results. The younger Ar losses around 315 Ma are harder to explain although these ages are close to the initiation of the Variscan orogeny. It is unclear, at least based on the Re-Os data, what could have been responsible for ^{40}Ar-^{39}Ar losses that are younger than about 340 Ma. The timeline of these major events are summarized in Figure 2.27.

Within the Re-Os dataset there are two apparently disconnected ages. The ages given by the Bog Zone and the combined data of LK 121, LK 451, and Gal 355 are younger than the 356 ± 5 Ma age of LK 8S08, perhaps by as much as 15 million years. These two sets of data require two completely separate fluid events to have caused mineralization at Lisheen, this would then imply that the sulphide mineralization at Lisheen was formed over an extended period of time.

The duration of hydrothermal activity associated with carbonate-hosted Pb-Zn deposits in general is not well constrained. Depending on the dating method used, and district studied, the duration of mineralization may be anywhere from a few tens of thousands of years, to over ten million years (Leach et al., 2001). The hydrothermal and structural systems present at Lisheen are required to have been active, at least intermittently, over a long period of time between 340-356 Ma. This duration is at the upper range of what has been previously reported for carbonate-hosted Pb-Zn deposits.

2.93 Chemistry of Mineralization Fluids

A recent review of fluid chemistry on Lisheen by Wilkinson (2010), which was based off previous studies of Thomson et al, (1992), Erye et al. 1996, Erye et al. 1998, and Wilkinson et al. (2005), is briefly described below, and provides additional support for Early Carboniferous mineralization. Early dolomitization at Lisheen was likely related to evaporation of seawater based on fluid chemistry and would require a near surface source of fluids. Seawater-based brines are then thought to have been transported to depth where they became metalliferous. These fluids were subsequently channelled up through normal faults where they mixed with near surface sulphur rich brines to create the mineralization observed at Lisheen. This requires a near surface fluid flow

mechanism with strong ties to seawater, much different then what would be expected for an epigenetic dominated deposit based on halite dissolution.

The source of the Pb for Lisheen is likely to have came from the lower Palaeozoic sediments that underlie the Old Red Sandstone (Everett et al., 2003), whereas the elements such as Ni and Co are likely from alteration of the Old Red Sandstone (Wilkinson et al., 2005). Based on the trace element analyses of this study it also appears that Cu, As, Re and Os may have also been mainly derived from the Old Red Sandstone due to the general association between these elements, Ni, and Co. The relatively precise initial $\frac{^{187}Os}{^{188}Os}$ ratio given for LK 8S08 (0.253 ± 0.068) can put constraints on the nature of the source rocks by running the Re-Os decay scheme backwards (equation 2.1), using 0.253±0.068 as the "present" day value, a hypothetical mantle source value of 0.1296 ± 0.0008 (Meisel et al., 2001) for the initial $\frac{^{187}Os}{^{188}Os}$ ratio, and an average crustal value for $\left(\frac{^{187}\mathrm{Re}}{^{188}Os}\right)$. Average crustal values for $\frac{^{187}\mathrm{Re}}{^{188}Os}$ are very poorly constrained but a very broad range of estimates exist. Direct measurements on loess samples have been reported by Peucker-Ehrenbrink and Jahn (2001), which give a low estimate of 34.5 for crustal $\frac{^{187}\mathrm{Re}}{^{188}Os}$, that results in a maximum age of 567 ± 120 Ma for the Os source rock(s) at Lisheen. A much higher $\frac{^{187}\mathrm{Re}}{^{188}Os}$ ratio of 450 can be obtained using Os measurements from Peucker-Ehrenbrink and Jahn (2001) and Re concentrations calculated in Sun et al. (2003). This $\frac{^{187}\mathrm{Re}}{^{188}Os}$ ratio may be more appropriate if it assumed that Re loss during magma degassing has a large impact on calculating the Re content of the crust based on the composition of arc magmas. In this case, a maximum age 373.1 ± 9.2 Ma is produced. While these estimates are relatively imprecise, they do not exclude the Devonian Old Red Sandstone from being the source of the Os in the Lisheen hydrothermal system.

$$\left(\frac{^{187}Os}{^{188}Os}\right)_{present} = \left(\frac{^{187}Os}{^{188}Os}\right)_{initial} + \left(\frac{^{187}\mathrm{Re}}{^{188}Os}\right)\left(e^{\lambda t} - 1\right) \qquad (2.1)$$

The sulphate component of the Lisheen fluids are derived from two broad sources based on the isotope data presented in Wilkinson et al. (2005), a brief summary of their findings are described below. The main component of ore stage mineralization comes from bacteriogenic derived sulphur, with a subsidiary component containing a higher $\delta^{34}S$, possibly coming from somewhere deeper in the system. A general trend of progressively lower $\delta^{34}S$ going from the Main Zone, Derryville Zone, through to the Bog Zone is also observed at Lisheen. Within individual zones there are also very large heterogeneities (Figure 11 of Wilkinson et al., 2005). Another important variation seen is the increase of $\delta^{34}S$ deeper into the mineralizing system, likely as a result increasing input from the deep $\delta^{34}S$ source region.

This complex relationship is the result of fluids that were heterogeneous in both time and spatial extent. By extension it is not hard to envision that the initial $\frac{^{187}Os}{^{188}Os}$ ratio would also be changing as the composition of the fluids varied, causing scatter in the isochron diagrams. Additionally, since the Bog Zone is a much simpler ore body, with a lower $\delta^{34}S$ content, it is likely there was less input from the second, high $\delta^{34}S$ source, compared to the other zones. This may explain the why much higher precision is associated with the Bog Zone isochron, as it is formed by a much narrower range of fluid sources then those of the Main and Derryville Zones.

2.94 Implications for other Irish Pb-Zn deposits

A Carboniferous age for the Lisheen deposit has implications for the age of the Irish Pb-Zn ore field in general. Most of the previous age constraints for the Irish deposits are based on paleomagnetism of the ore body and associated host rocks, although some studies using radioactive isotopes do exist.

The large disparity between the Re-Os ages and the paleomagnetic ages at Lisheen cast doubt on the validity of the previous paleomagnetic studies undertaken throughout the Irish ore field. Since the ore field in general has high conodont alteration indexes (Figure 1 from Pannalal, 2008a), it is likely much of the area has been remagnetized in response to the orogenic heating, causing a disconnect in the ages between isotopic and paleomagnetic systems. In particular, Lisheen, Galmoy,

Silvermines, and Tynaugh are in areas associated with particularly high CAI values. Previous paleomagnetic work on Silvermines (Symons et al., 2007), Galmoy (Pannalal 2008b), and Lisheen (Pannalal 2008a) produced ages of 269 ± 4, 290 ± 9 Ma, and 277 ± 7 Ma, respectively, which all fall within the ages associated with the Variscan orogeny (Figure 2.25). This observation, coupled with the Re-Os ages from Lisheen and Galmoy (this study), and a 360 ± 5.2 Ma Rb-Sr age from Silvermines (Schneider et al., 2003), strongly suggests that mineralization occurred during the Early Carboniferous, whereas the paleomagnetic ages are associated with remagnetization during the Variscan orogeny. Navan on the other hand was in a slightly cooler thermal regime during Variscan orogeny, and has a much older paleomagnetic age of 333 ± 4 Ma (Symons et al., 2002). This can be explained if much of the primary magnetism has remained stable due to this cooler thermal regime, and as a result provides a much more accurate timing of mineralization compared to the other deposits.

In summary, the radiogenic, paleomagnetic, and thermal regime data indicate that Pb-Zn mineralization in the Irish ore field was the result of fluid flow in the Early Carboniferous time, and was not related to the Variscan orogeny.

2.10 Conclusions

The Re-Os data provide a firm age constraint on the timing of the Lisheen Pb-Zn ore deposit, and the general timeline for mineralization at the other Irish-type deposits. The Lisheen system was active from 340-356 Ma and was likely associated with syngenetic/syndiagenetic processes caused by near surface fluid mixing. The most robust isochron diagrams are in areas of simplified fluid flow (Bog Zone), or single generation pyrites (LK 8S08). This observation provides valuable insight into the kind of samples required to obtain precise Re-Os data. This data also indicates that the mineralization at Lisheen was not a single-stage event, but possibly occurred over a period of up to 15 Myr. The scatter seen in the other isochron diagrams is most likely due to the large ranges in fluid chemistry associated with mineralization.

The data also supports a similar age for Galmoy due to the fact that the Gal 355 Re-Os data is quite similar to that of Lisheen. The other Irish deposits are suspected have formed at a similar time to that of Lisheen as well, since previous paleomagnetic dates

have been put into question. Follow up investigation on some of the other Irish deposits would be required to confirm these suspicions.

2.11 References

Beaty, D.W., Allan, J.R., and Hitzman, M.W., 1991, The relationship of dolomitization and mineralization at the Lisheen deposit, south central Ireland [abs.]: Geological Society of America Abstracts with Programs, v. 23, p. A172.

Boast, A.M., Coleman, M.L., and Halls, C., 1981, Textural and stable isotopic evidence for the genesis of the Tynagh base metal deposit, Ireland: Economic Geology, v. 76, p. 27–55.

Carboni, V., Walsh, J.J., Stewart, D.R.A., and Güven, J.F., 2003, Timing and geometry of normal faults and associated structures at the Lisheen Zn/Pb deposit, Ireland—investigating their role in the transport and trapping of: Society for Geology Applied to Mineral Deposits Meeting, 7th biennial, Athens, Greece, Proceedings, p. 665–668.

Chadwick, R.A., Evans, D.J., and Halliday, D.W., 1993, The Maryport fault: The post-Caledonian tectonic history of southern Britain in microcosm: Geological Society of London Journal, v. 150, p. 247–250.

Clayton, G., Haughey, N., Sevastopulo, G.D., and Burnett, R.D., 1989, Thermal maturation levels in the Devonian and Carboniferous rocks in Ireland (1:750,000): Geological Survey of Ireland Special Publication, 36 p.

Coller, D.W., 1984, Variscan structures in the Upper Paleozoic rocks of west central Ireland: Geological Society of London Special Publication 14, p. 185–194.

Everett, C.E., Rye, D.M., and Ellam, R.M., 2003, Source or sink? An assessment of the role of the Old Red Sandstone in the genesis of the Irish Zn-Pb deposits: Economic Geology, v. 98, p. 31–50.

Eyre, S.L., 1998, Geochemistry of dolomitization and Zn-Pb mineralization in the Rathdowney trend, Ireland: Unpublished Ph.D. thesis, University of London, p. 414

Eyre, S.L., Wilkinson, J.J., Stanley, C.J., and Boyce, A.J., 1996, Geochemistry of dolomitisation and zinc-lead mineralisation in the Rathdowney trend, Ireland [abs.]: Geological Society of America Abstracts with Programs, v. 28, p. A210−A211.

Fusciardi, L.P., Guven, J.F., Stewart, D.R.A., Carboni, V., and Walshe, J.J., 2003, The geology and genesis of the Lisheen Zn-Pb deposit, Co. Tipperary, Ireland, *in* Kelly, J.G., Andrew, C.J., Ashton, J.H., Boland, M.B., Earls, G., Fusciardi, L., and Stanley, G., eds., Europe's major base metal deposits: Dublin, Irish Association for Economic Geology, p. 455–481.

Gatley, S., Sleeman, A.G., Somerville, I.D., Morris, J. and Emo, G., 2005, A Geological description of Galway and Offaly, and adjacent parts of Westmeath, Tipperary, Laois, Clare and Roscommon to accompany the Bedrock Geology 1:100, 000 Scale Map Series Sheet 15, Galway and Offaly, with contributions by W. Cox, T. Hunter=Williams, R. van den Berg and E. Sweeny. Geological Survey of Ireland, Dublin.

George, T.N., Johnson, G.A.L., Mitchell, M., Prentice, J.E., Ramsbottom, W.H.C., Sevastopulo, G.D., and Wilson, R.B., 1976, A correlation of Dinantian rocks in the British Isles: Geological Society of London Special Reports 7, 87 p.

Goodfellow, W.D., Lydon, J.W., and Turner, R.J.W., 1993, Geology and genesis of stratiform sediment-hosted (SEDEX) zinc-lead-silver sulphide deposits, *in* Kirkham, R.V., Sinclair, W.D., Thorpe, R.I., and Duke, J.M., eds., Mineral Deposit Modeling: Geological Association of Canada Special Paper 40, p. 201–252.

Graham, J.R., 2001, Variscan structures, *in* Holland, C.H., ed., The geology of Ireland: Edinburgh, Dunedin Academic Press, p. 312–330.

Gregg, J.M., Shelton, K.L., Johnson, A.W., Somerville, I.D., and Wright, W.R., 2001, Dolomitization of the Waulsortian Limestone (Lower Carboniferous) in the Irish Midlands: Sedimentology, v. 48, p. 745–766.

Güven, J.F., Passmore, M.J., and Harney, D.M.W., 2007, Updates on the geology and metallogenesis of the Lisheen Zn-Pb deposit in Ireland, *in* Andrew, C.J., et al., eds., Digging deeper: Proceedings of Ninth Biennial SGA meeting: Dublin, Ireland, Irish Association for Economic Geology, p. 295–298.

Hitzman, M.W., 1992, Discovery of the Lisheen Zn-Pb-Ag deposit, Ireland: Society of Economic Geology Newsletter, April, 1992, v. 9, p. 1, 12–15.

Hitzman, M.W., 1999, Extensional faults that localize Irish syndiagenetic Zn-Pb deposits and their later compressional fate, *in* McCaffery, K., Lonergan, L, and Wilkinson, J., eds., Fractures, Fluid Flow and Mineralization: Geological Society of London Special Publication 155, p. 233–245.

Hitzman, M.W., and Beaty, D.W., 1996, The Irish Zn-Pb-(Ba) orefield, *in* Sangster, D. F., ed., Carbonate-Hosted Lead-Zinc Deposits: Society of Economic Geologists Special Publication 4, p. 112–143.

Hitzman, M. W. and Large, D., 1986, A review and classification of the Irish carbonate-hosted base metal deposits, *in* Andrew, C. J., Crowe, R. W. A., Finlay, S., Pennell, W. M., and Pyne, J. F., eds., Geology and Genesis of Mineral Deposits in Ireland: Dublin, Irish Association for Economic Geology, p. 217-238.

Hitzman, M.W., Layer, P. W., and Newberry, R.J., 1994, Argon-argon step heating studies of muscovite in the Upper Devonian Old Red Sandstone: the first absolute dates for the age of the Irish zinc-lead mineralization [abs.]: Geological Society of America Abstract with Programs, v. 26, p. A381.

Hitzman, M.W., Allan, J.R., and Beaty, D.W., 1998, Regional dolomitization of the Waulsortian Limestone in southeastern Ireland: Evidence of largescale fluid flow driven by the Hercynian orogeny: Geology, v. 26, p. 547–550.

Hitzman, M.W., Redmond, P.B., and Beaty, D.W., 2002, The carbonate hosted Lisheen Zn-Pb-Ag deposit, County Tipperary, Ireland: Economic Geology, v. 97, p. 1627–1655.

Hitzman MW, Redmond PB, Beaty DW (2003) The carbonate hosted Lisheen Zn-Pb-Ag deposit, County Tipperary, Ireland. Econ Geol 97:1627–1655

Johnston, J.D., Coller, D., Millar, G., and Critchley, M. F., 1996, Basement structural controls on Carboniferous-hosted base metal mineral deposits in Ireland, *in* Strongmen, P., Somerville, I.D., and Jones, G.L., eds., Recent Advances in Lower Carboniferous Geology: Geological Society of London Special Publication 107, p. 2–21.

Jones, G.L., 1992, Irish Carboniferous conodonts record maturation levels and the influence of tectonism, igneous activity and mineralization: Terra Nova, v. 4, p. 238–244.

Large, R.R., Danyushevsky, L., Hollit, C., Maslennikov, V., Meffre, S., Gilbert, S., Bull, S., Scott, R., Emsbo, P., Thomas, H., Singh, B. and Foster, J. (2009) Gold and trace element zonation in pyrite using a laser imaging technique: implications for the timing of gold in orogenic and Carlin-style sediment-hosted deposits. Economic Geology, v. 104, p. 635-668.

Leach, D.L., Bradley, D., Lewchuk, M.T., Symons, D.T.A., de Marsily, G., and Brannon, J., 2001, Mississippi Valley-type lead-zinc deposits through geological time – Implications from recent age-dating research: Mineralium Deposita, v. 36, p. 711-740.

Leeder, M.R., and McMahon, A.H., 1988, Upper Carboniferous (Silesian) basin subsidence in northern Britain, *in* Besley, B.M., and Kelling, G., eds., Sedimentation in a

synorogenic basin complex: The Upper Carboniferous of NW Europe: Glasgow, Blackie, p. 43–52.

Lewis, D. 1986. The Carboniferous Geology of the East Clare Syncline. Unpublished PhD thesis, University of Dublin.

Lippholt, H.J., and Hess, J.C., 1985, Ar40/Ar39 dating of sanidines from Upper Carboniferous tonsteins: Compte Rendu 10eme Congres International de Stratigraphie et de Geologie du Carbonifere, Madrid, v. 4, p. 174–181.

Ludwig, K.R., 2001, Isoplot 3.0—A geochronological toolkit for Microsoft Excel: Special publication No. 4, Berkeley Geochronology Center, Berkeley, Calif., 71 p.

Lydon, J.W., 1986, Models for the generation of metalliferous hydrothermal systems within sedimentary rocks and their applicability to the Irish Carboniferous Zn-Pb deposits, *in* Andrew, C.J., Crowe, R.W.A., Finlay, S., Pennell, W.M., and Pyne, J.F., eds., Geology and Genesis of Mineral Deposits in Ireland: Dublin, Irish Association for Economic Geology, p. 555–577.

Meisel T., Walker R.J., Irving A.J., and Lorand J.-P. (2001) Osmium isotopic compositions of mantle xenoliths: a global perspective. Geochim. Cosmochim Acta . **65**, 1311-1323.

Morelli, R.M., Creaser, R.A., Selby, D., Kelley, K.D., Leach, D.L., and King, A.R., 2004, Re-Os sulfide geochronology of the Red Dog sediment-hosted Zn-Pb-Ag deposits, Brooks Range, Alaska: Economic Geology, v. 99, p. 1569–1576.

Nagy, Z.R., 2003, The lower Carboniferous (Chadian-Brigantian) geology of shallow marine carbonate rocks in the central and southeast Irish Midlands and the Wexford Outlier. Unpublished PhD thesis, University of Missouri-Rolla, USA.

Pannalal, S.J., Symons, D.T.A., Sangster, D.F., 2008a, Paleomagnetic Evidence for an Early Permian Age of the Lisheen Zn-Pb Deposit, Ireland: Economic Geology, v.103, p. 1641-1655.

Pannalal, S.J., Symons, D.T.A., and Sangster, D.F, 2008b, Paleomagnetic evidence of a Variscan age for the epigenetic Galmoy zinc-lead deposit, Ireland: Terra Nova, v. 20, p. 385–393.

Peucker-Ehrenbrink B. and Jahn B. M. 2001. Rhenium-Osmium isotope systematics and platinum group element concentrations: Loess and the upper continental crust. Geochemistry, Geophysics, Geosystems 2, paper number 2001GC000172.

Radke, B. M., and Mathis, R. l., 1980, On the formation and occurrence of saddle dolomites: Journal of Sedimentary Petrology, v. 50, p. 1149-1168.

Russell, M.J., 1978, Downward-excavating hydrothermal cells and Irish-type ore deposits: Importance of an underlying thick Caledonian prism: Transactions of the Institution of Mining and Metallurgy (England), Section B, v. 87, p. 168–171.

Russell, M.J., 1983, Major sediment-hosted exhalative zinc + lead deposits: Formation from hydrothermal convection cells that deepen during crustal extension, *in* Sangster, D.F., ed., Sediment-Hosted Stratiform Lead-Zinc Deposits: Mineralogical Association of Canada Short Course Handbook 8, p. 251–282.

Schneider, J., Quadt, A.V. , Wilkinson, J.J., and Boyce, A.J., 2007, Age of Silvermines Irish-type Zn-Pb deposit from direct Rb-Sr dating of sphalerite, *in* Andrew, C.J., et al., eds., Digging deeper: Proceedings of the Ninth Biennial SGA meeting: Dublin, Ireland, Irish Association for Economic Geology, p. 373–376.

Sevastopulo, G.D., 1981, Hercynian structures, *in* Holland, C.H., ed., A Geology of Ireland: Edinburgh, Scottish Academic Press, p. 147–172.

Sevastopulo, G.D., and Redmond, P., 1999, Age of mineralization of carbonate- hosted base metal deposits in the Rathdowney Trend, Ireland, *in* McCaffrey, K.W., Lonergan, L., and Wilkinson, J.J., eds., Fractures, Fluid Flow and Mineralization: Geological Society of London Special Publication 151, p. 303–311.

Shearley, E., Hitzman, M.W., Walton, G., Redmond, P., Davis, R., King, M., Duffy, L., and Goodman, R., 1992, Structural controls of mineralization, Lisheen Zn-Pb-Ag deposit, Co. Tipperary, Ireland [abs.]: Geological Society of America Abstracts with Programs, v. 24, p. A354.

Shearley, E., Redmond, P., Goodman, R., and King, M., 1995, Guide to the Lisheen Zn-Pb-deposit, *in* Anderson, K., Ashton, J. Earls, G., Hitzman, M., and Tear, S., eds., Irish Carbonate-hosted Zn-Pb Deposits: Society of Economic Geologists Guidebook Series, v. 21, p. 123–138.

Sleeman, A. G., and Pracht, M., 1999, Geology of the Shannon Estuary. A geological description of the Shannon Estuary regions including parts of Clare, Limerick, and Kerry, to accompany the Bedrock Geology 1:100000 Scale Map Series, Sheet 17, Shannon estuary. Geological Survey of Ireland.

Somerville, I.D. and Jones, G.L 1985. The Courceyan stratigraphy of the Pallaskenry Borehole, County Limerick, Ireland. Geological Journal, 20, 377-400.

Sun, W., Bennett, V.C., Eggins, S.M., Kamenetsky, V.S., and Arculus, R.J., 2003, Enhanced mantle-to-crust rhenium transfer in undegassed arc magmas: Nature, v. 422, p. 94–297.

Symons, D.T.A., Smethurst, M.T., and Ashton, J.H., 2002, Paleomagnetism of the Navan Zn-Pb deposit, Ireland: Economic Geology, v. 97, p. 997–1012.

Symons, D.T.A., Pannalal, S.J., Kawasaki, K., Sangster, D.F., and Stanley, G.A., 2007, Paleomagnetic age of the Magcobar Ba deposit, Silvermines, Ireland, *in* Andrew, C.J., et al., eds., Mineral exploration and research: Digging deeper: Dublin, Irish Association for Economic Geology, p. 377–380.

Thompson, T.B., Hitzman, M.W., and Beaty, D.W., 1992, Paragenesis and fluid inclusions of the Lisheen Zn-Pb-Ag deposit, Co. Tipperary, Ireland [abs.]: Geological Society of America Abstracts with Programs, v. 24, p. A354.

Waters, C.N., Somerville, I.D., Jones, N.S., Cleal. C.K., Collinson, J.D., Waters, R.A., Besly, B.M., Dean, M.T., Stephenson, M.H., Davies, J.R., Freshney, E.C., Jackson, D.I., Mitchell, W.I., Powell, J.H., Barclay, W.J., Browne, M.A.E, Leveridge, B.E., Long, S.L., and Maclean, D., 2011, A Revised Correlation of Carboniferous Rocks in the British Isles: The Geological Society of London.

Wartho, J.-A., Quinn, D. and Meere, P.A. 2006. The timing of Variscan deformation: UV laser 40Ar/39Ar dating of synnlate-orogenic intrusions from SW Ireland. Geochim et Cosmochim Acta v. 70, Supplement 1, p. A690.

Wilkinson, J.J., 2003, On diagenesis, dolomitisation and mineralisation in the Irish Zn-Pb orefield: Mineralium Deposita, v. 38, p. 968–983.

Wilkinson, J.J., Boyce, A.J., Everett, C.E., and Lee, M.J., 2003, Timing and depth of mineralization in the Irish Zn-Pb ore field, *in* Kelly, J.G., Andrew, C.J., Ashton, J.H., Boland, M.B., Earls, G., Fusciardi, L., and Stanley, G., eds., Europe's major base metal deposits: Dublin, Irish Association for Economic Geology, p. 483–497.

Wilkinson, J.J., Eyre, S.L., and Boyce, A.J., 2005, Ore-forming processes in Irish-type carbonate-hosted Zn-Pb deposits: Evidence from mineralogy, chemistry, and isotopic composition of sulfides at the Lisheen mine: Economic Geology , v. 100, p. 63–86.

Wilkinson, J.J., 2010, A Review of Fluid Inclusion Constraints on Mineralization in the Irish Ore Field and Implications for the Genesis of Sediment-Hosted Zn-Pb Deposits: Economic Geology, v.105, pp. 417-442.

Woodcock, N., and Strachan, R., 2000, Geological history of Britain and Ireland: Oxford, Blackwell Science, 423 p.

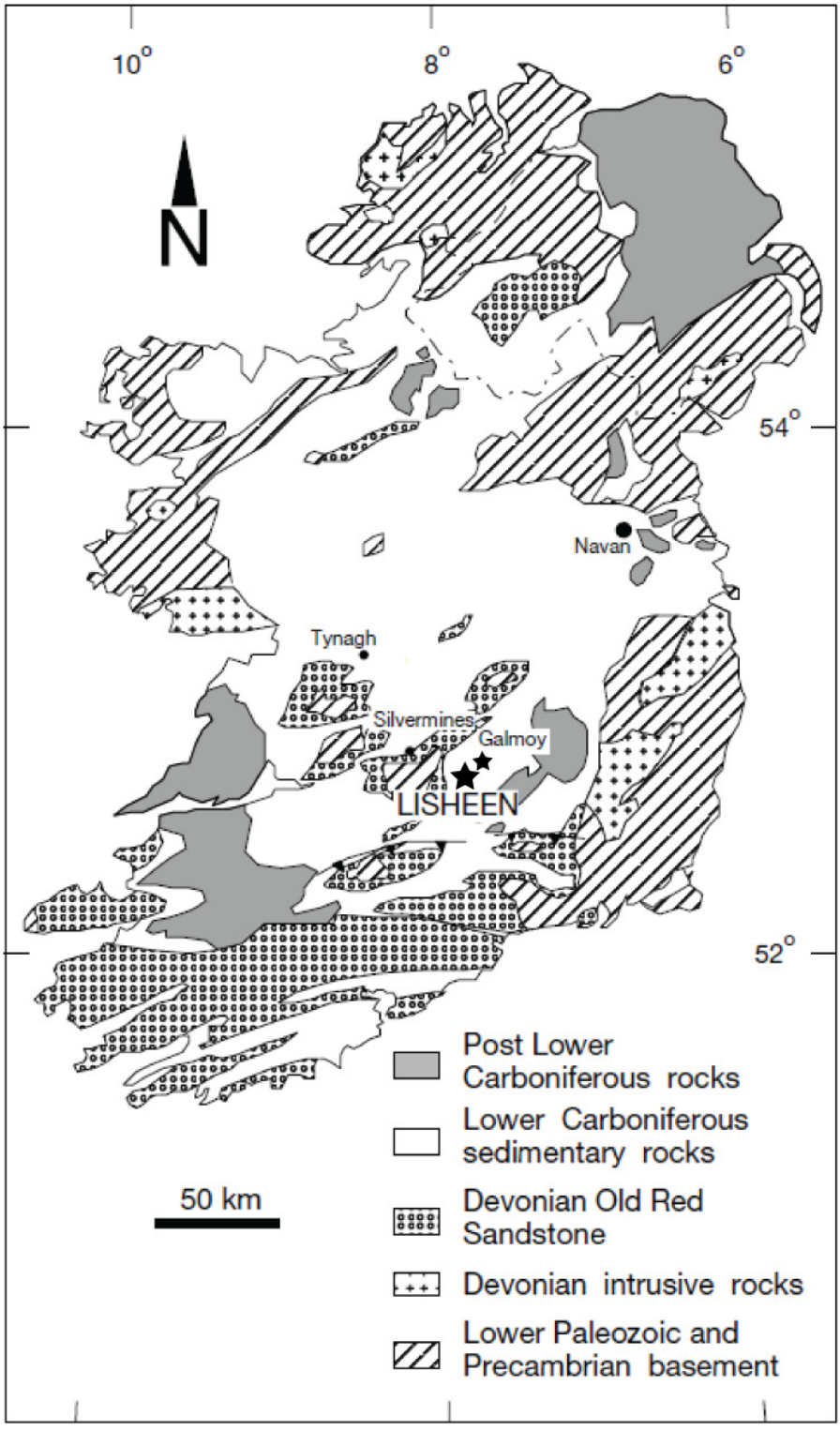

Figure 2.1: Basic geologic map of Ireland with select ore deposits shown (modified from Hitzman et al., 2002).

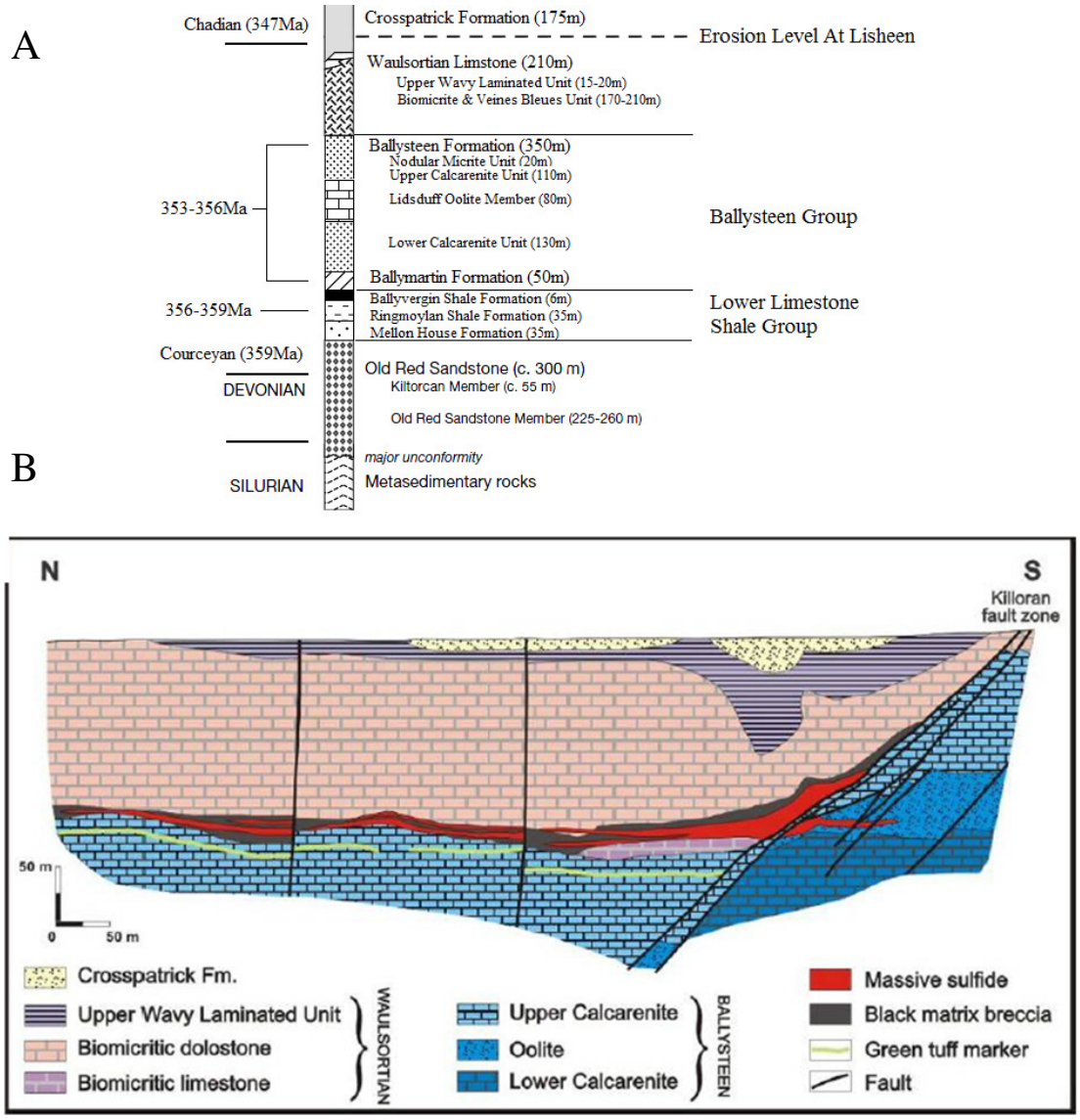

Figure 2.2: (A) The stratigraphy near Lisheen (modified from Hitzman et al. 2002 using data from Waters et al. 2011). (B) Cross-section of the Main zone of Lisheen (Shearley et al., 1995).

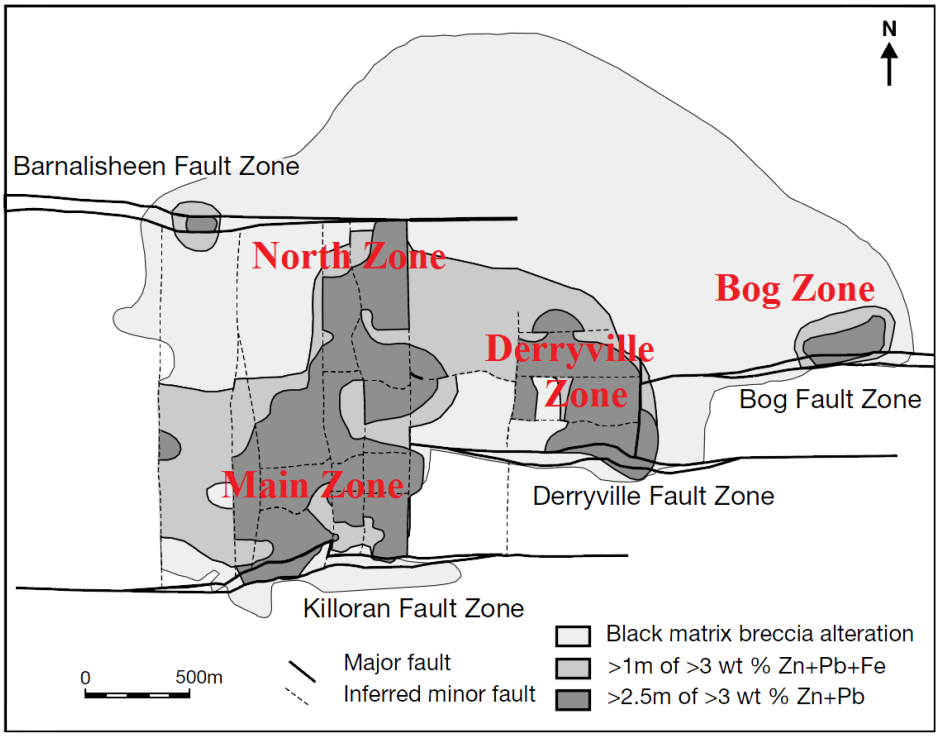

Figure 2.3: Extent of mineralization at Lisheen (modified from Hitzman et al., 2002).

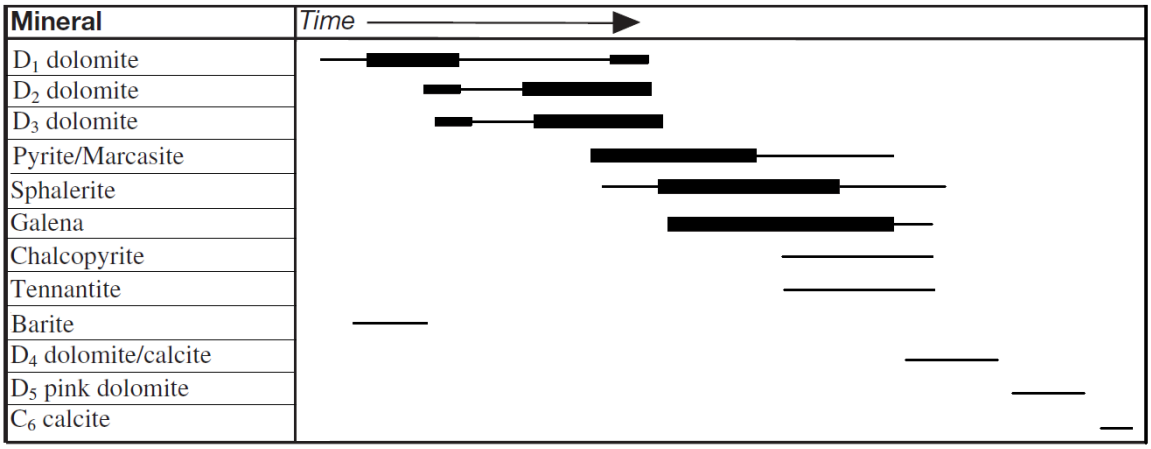

Figure 2.4: Generalized paragenesis of major mineralization styles at Lisheen (modified from Wilkinson et al. (2005) with data from Wilkinson (2010)).

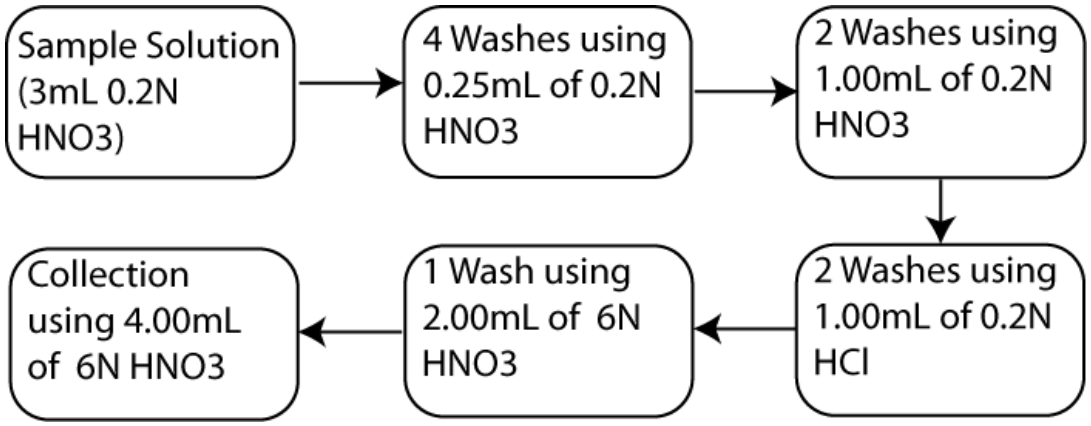

Figure 2.5: Rhenium column chromatography procedure.

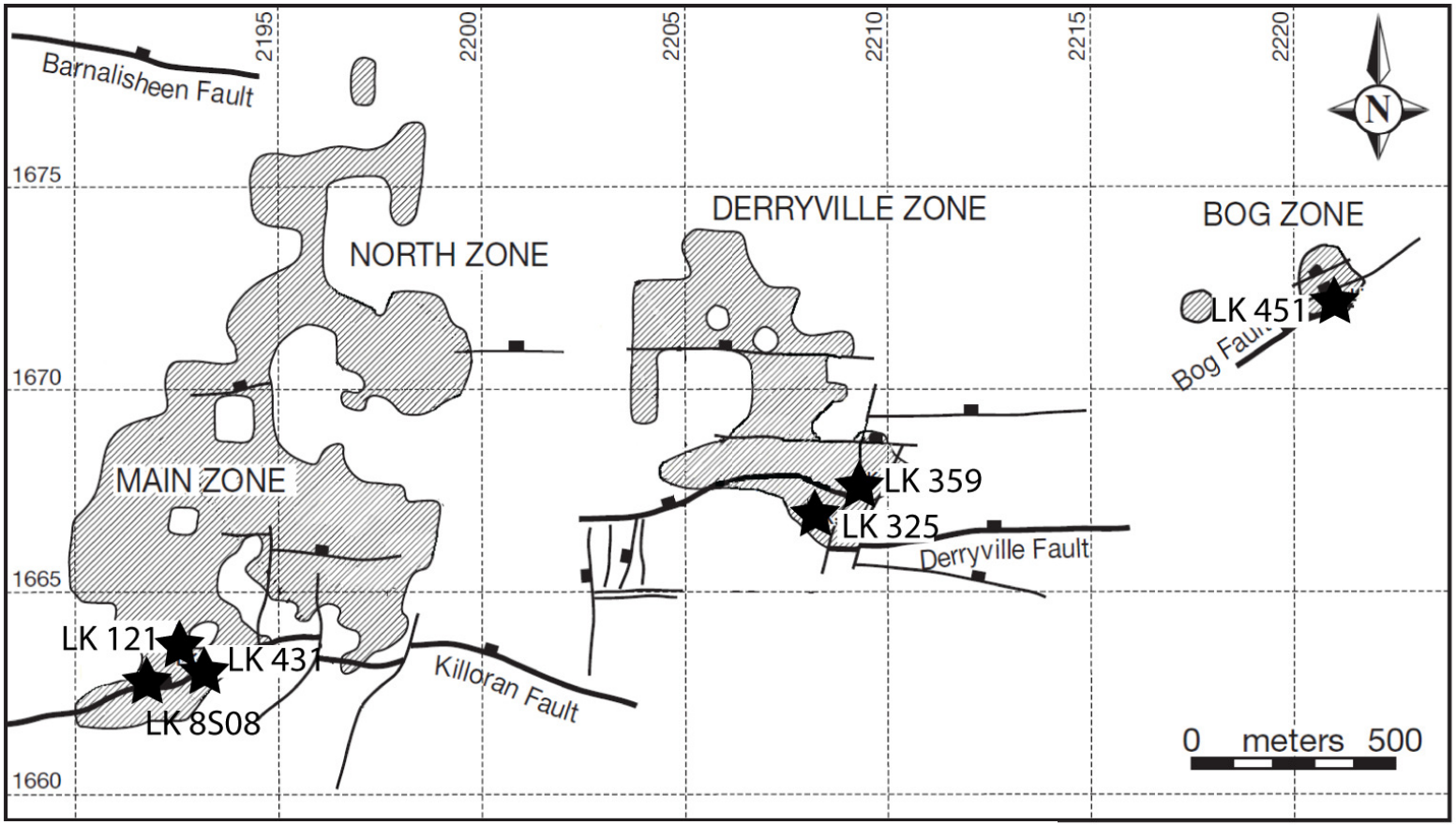

Figure 2.6: Sample Collection Sites at Lisheen (Modified from Wilkinson et al. 2005)

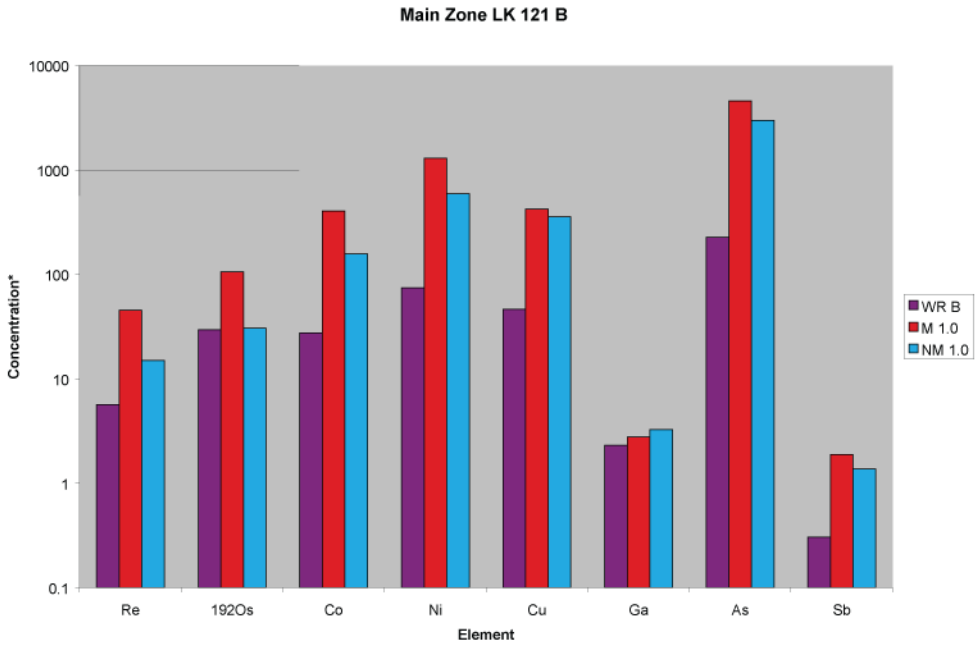

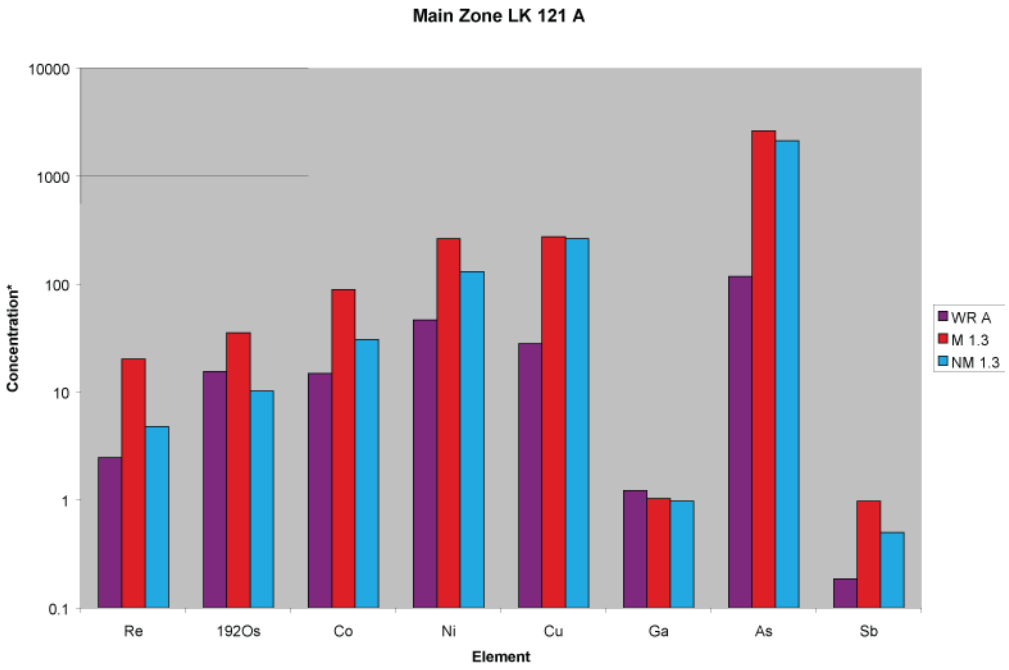

Figure 2.7: Trace element distribution for LK 121.
*Re concentration is in ppb, Os concentration is in ppt, and Ni, Co, Cu, Ga, As, and Sb are in ppm.
** These bulk analyses do not independently indentify which minerals show the trace element variations.

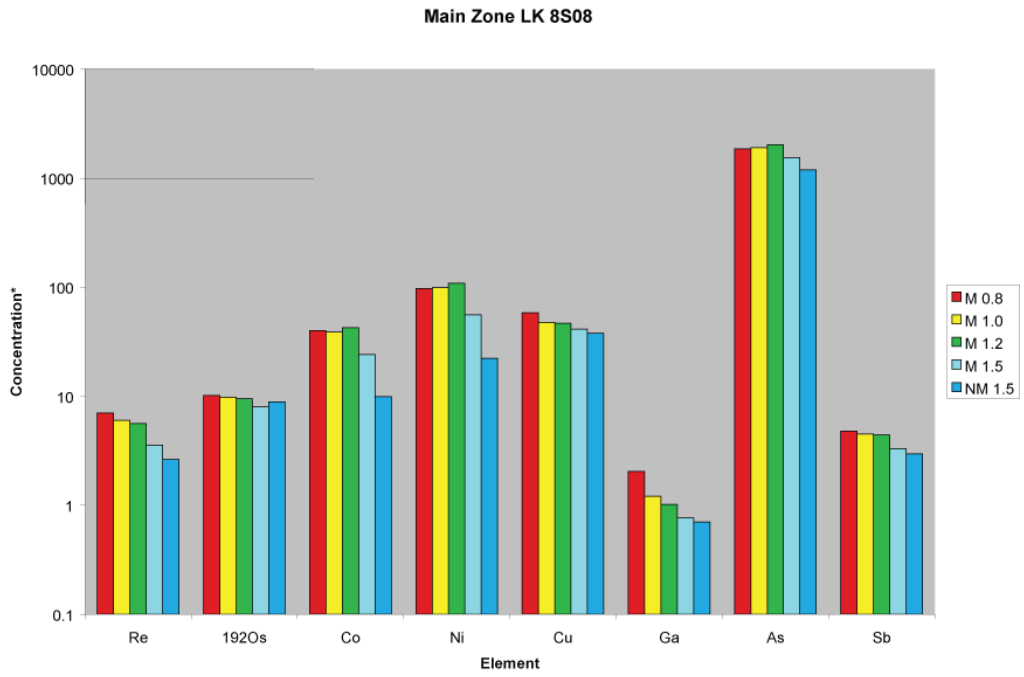

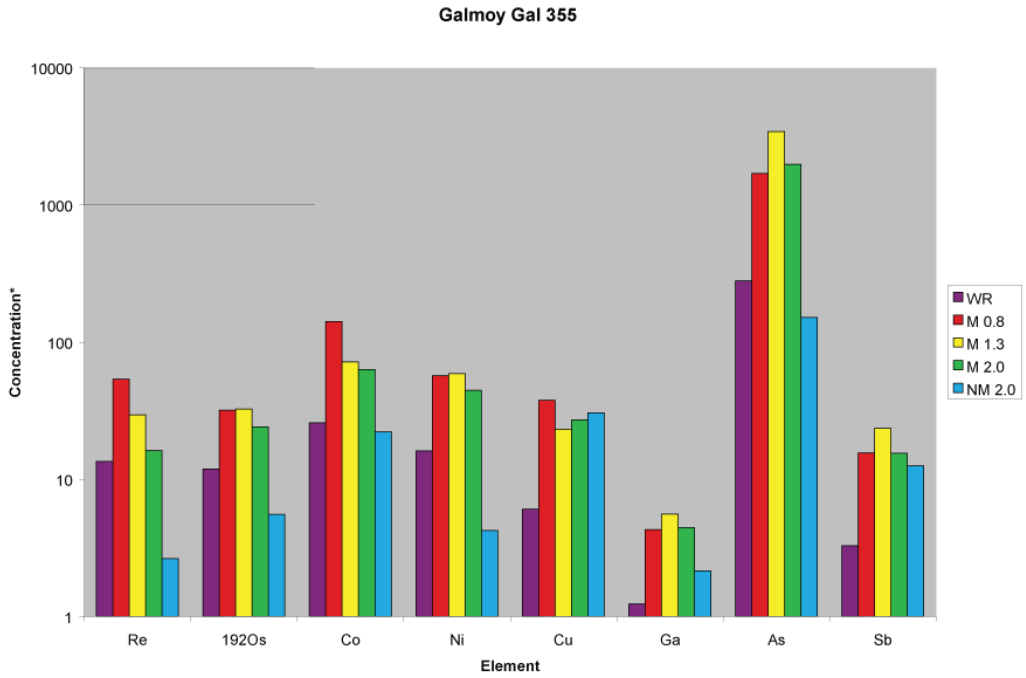

Figure 2.8: Trace element distribution for LK 8S08 and Gal 355.
*Re concentration is in ppb, Os concentration is in ppt, and Ni, Co, Cu, Ga, As, and Sb are in ppm.
** These bulk analyses do not independently indentify which minerals show trace element variations.

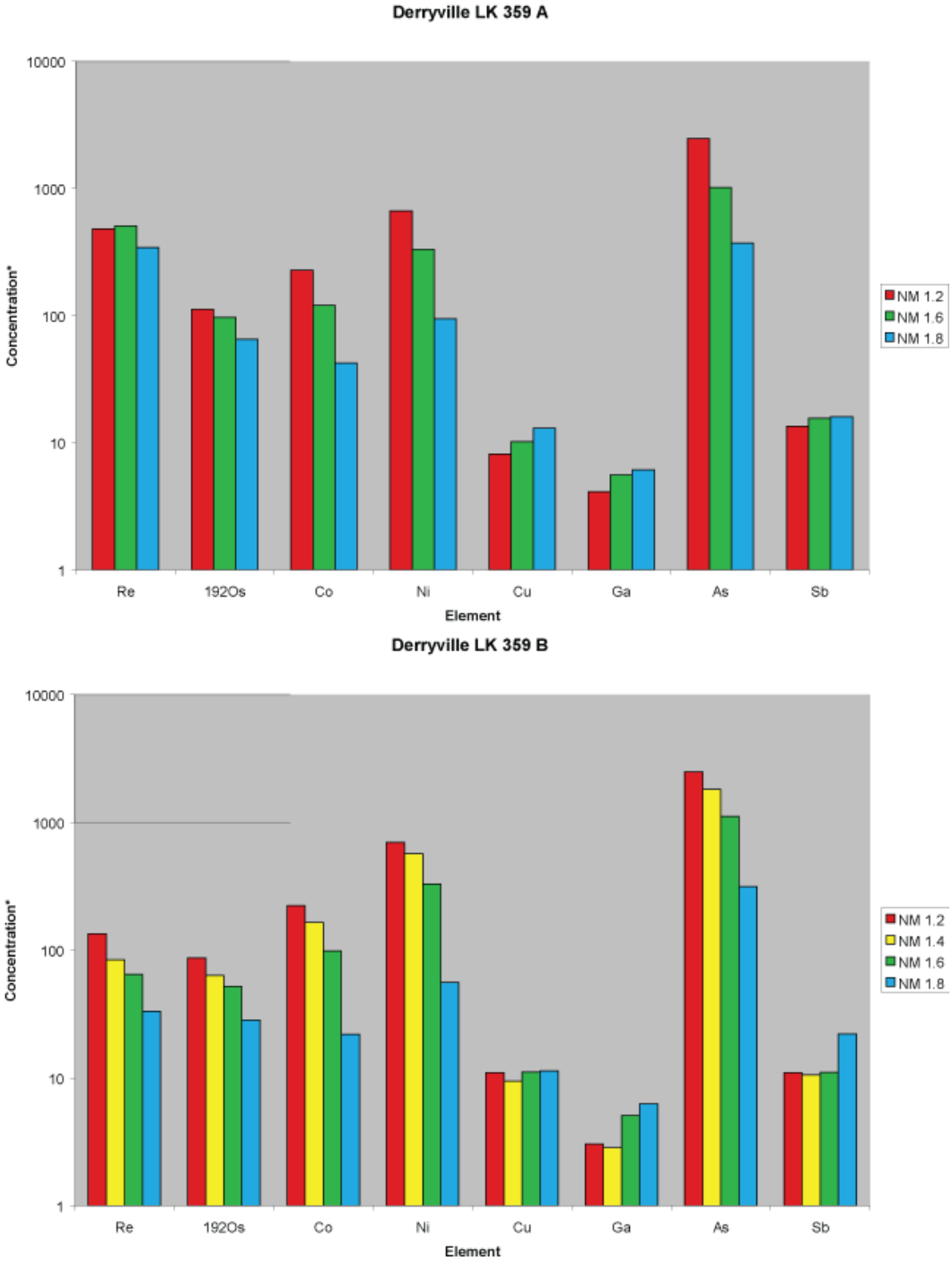

Figure 2.9: Trace element distributions for LK 359.
*Re Concentration is in ppb, Os concentration is in ppt, and Ni, Co, Cu, Ga, As, and Sb are in ppm.
** These bulk analyses do not independently indentify which minerals show trace element variations.

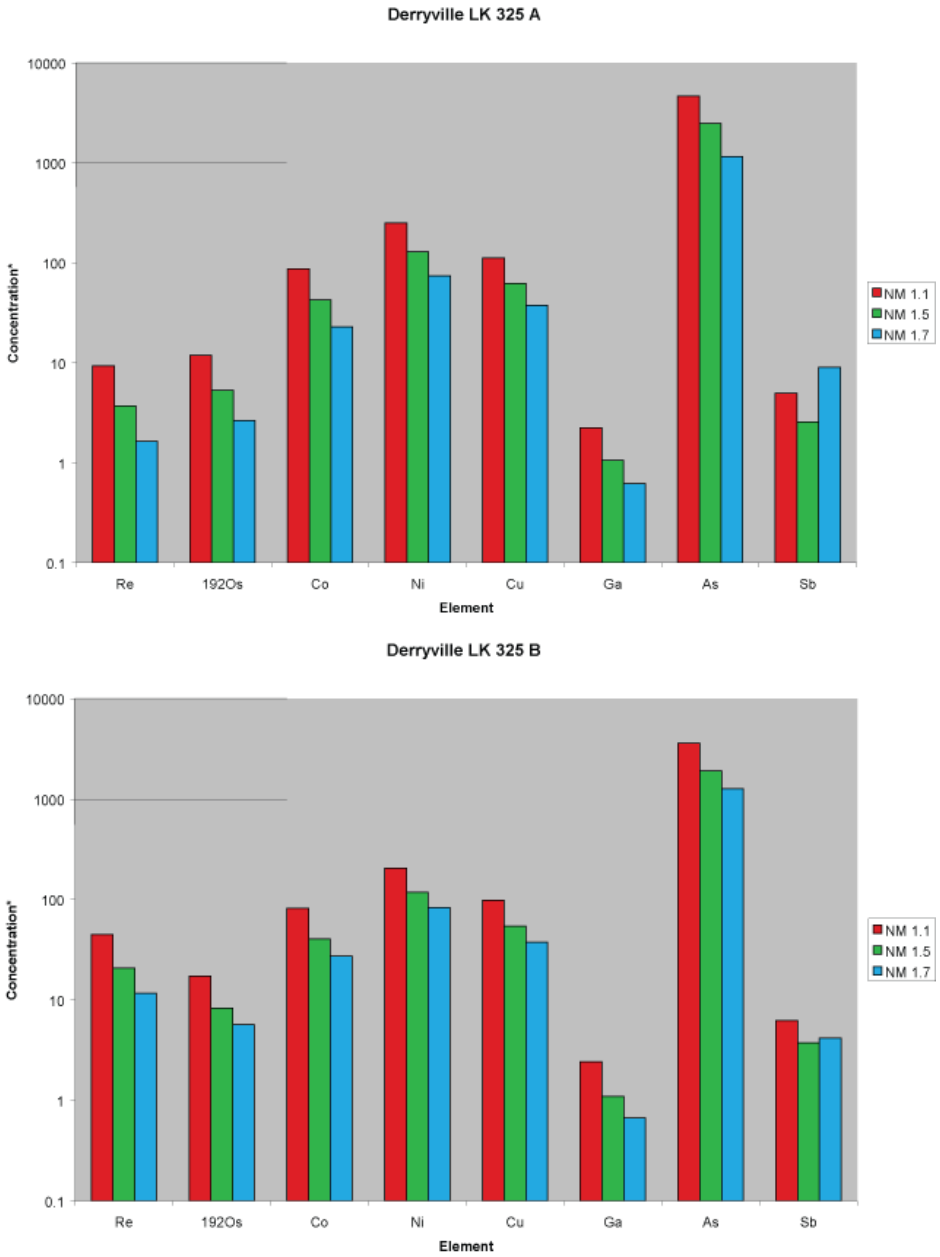

Figure 2.10: Trace Element Distributions for LK 325.
*Re Concentration is in ppb, Os concentration in ppt, and Ni, Co, Cu, Ga, As, and Sb in ppm.
** These bulk analyses do not independently indentify which minerals show trace element variations.

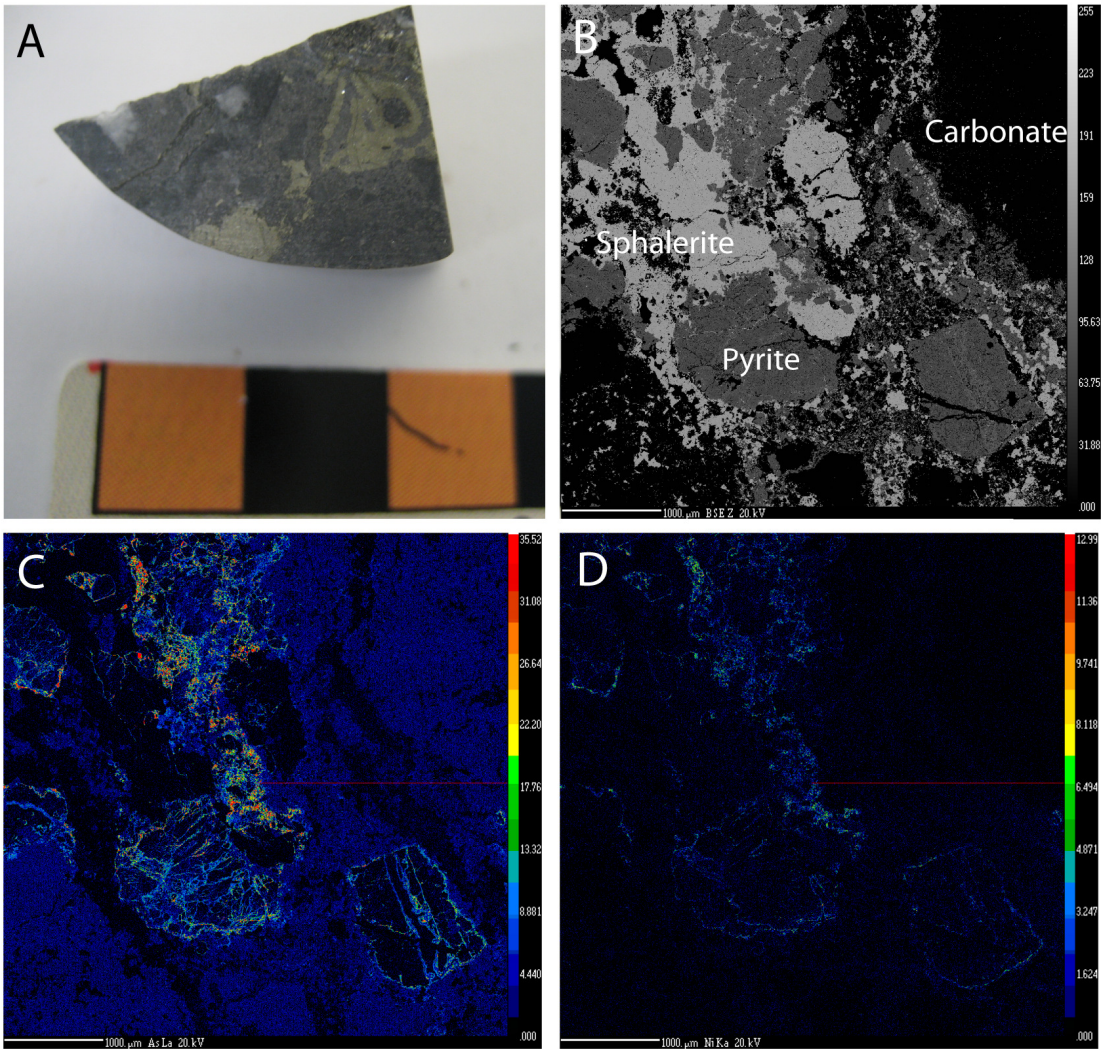

Figure 2.11: Sample LK 121 (A) Original specimen (B) Back Scattered Electron Image (C) Arsenic map showing complex alteration of the pyrite grains (D) Nickel maps that show the correlation between Ni and As.

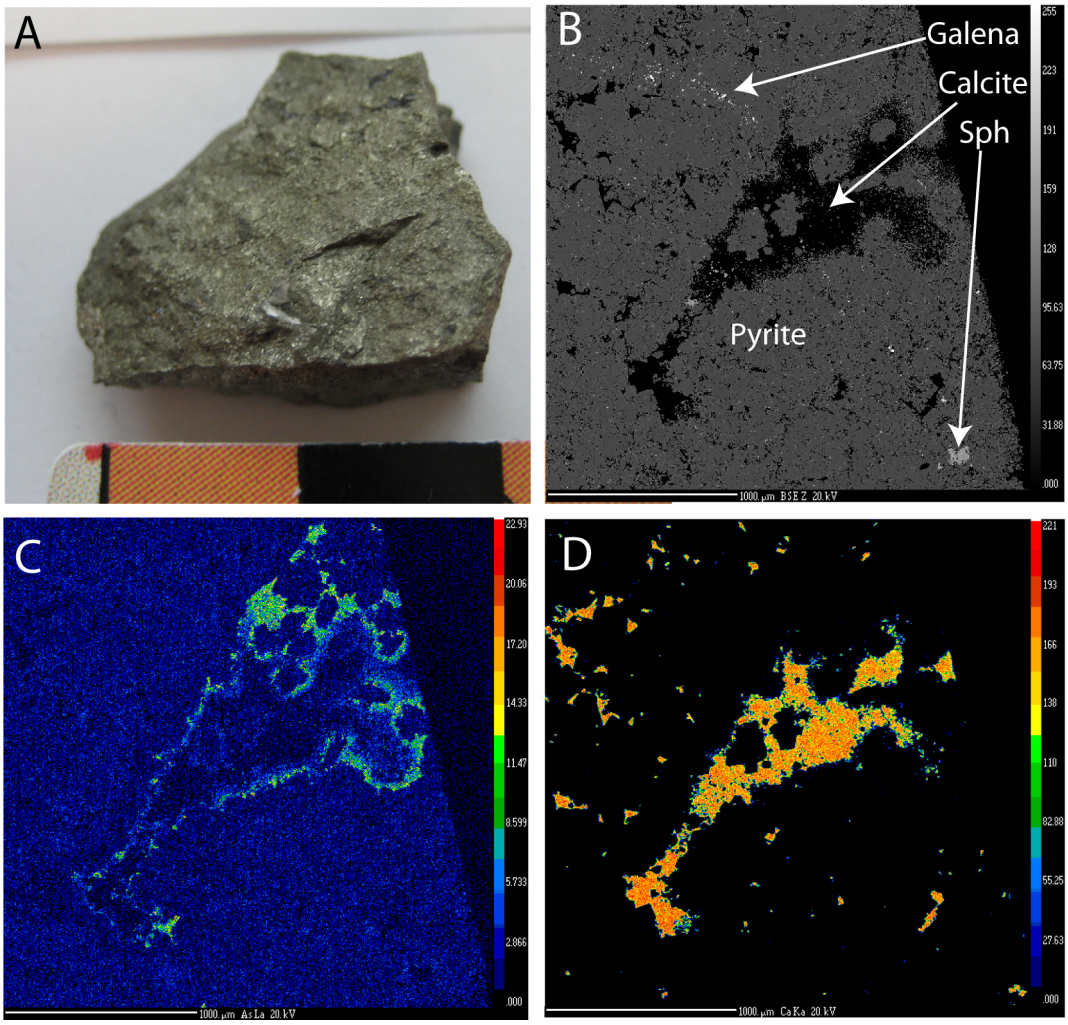

Figure 2.12: Sample LK 8S08 (A) Original specimen (B) Back Scattered Electron Image (C) Arsenic map showing enrichment in areas adjacent to calcite (D) Calcium map showing the calcite veins that crosscut the sample.

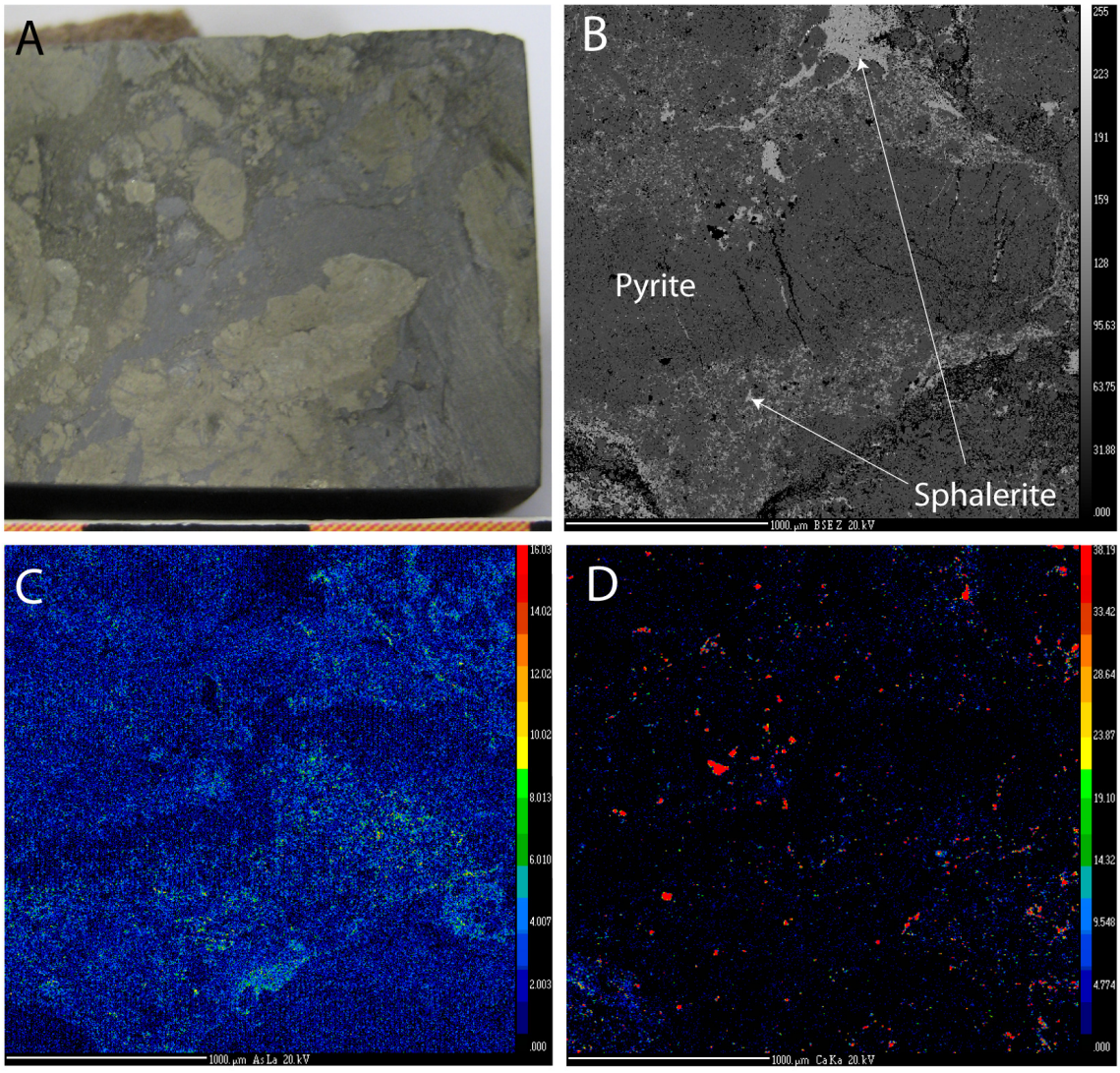

Figure 2.13: Sample LK 359 (A) Original specimen (B) Back Scattered Electron Image (C) Arsenic Map showing a trace element depleted pyrite core surrounded by a rim with a complex As distribution (D) Calcium map.

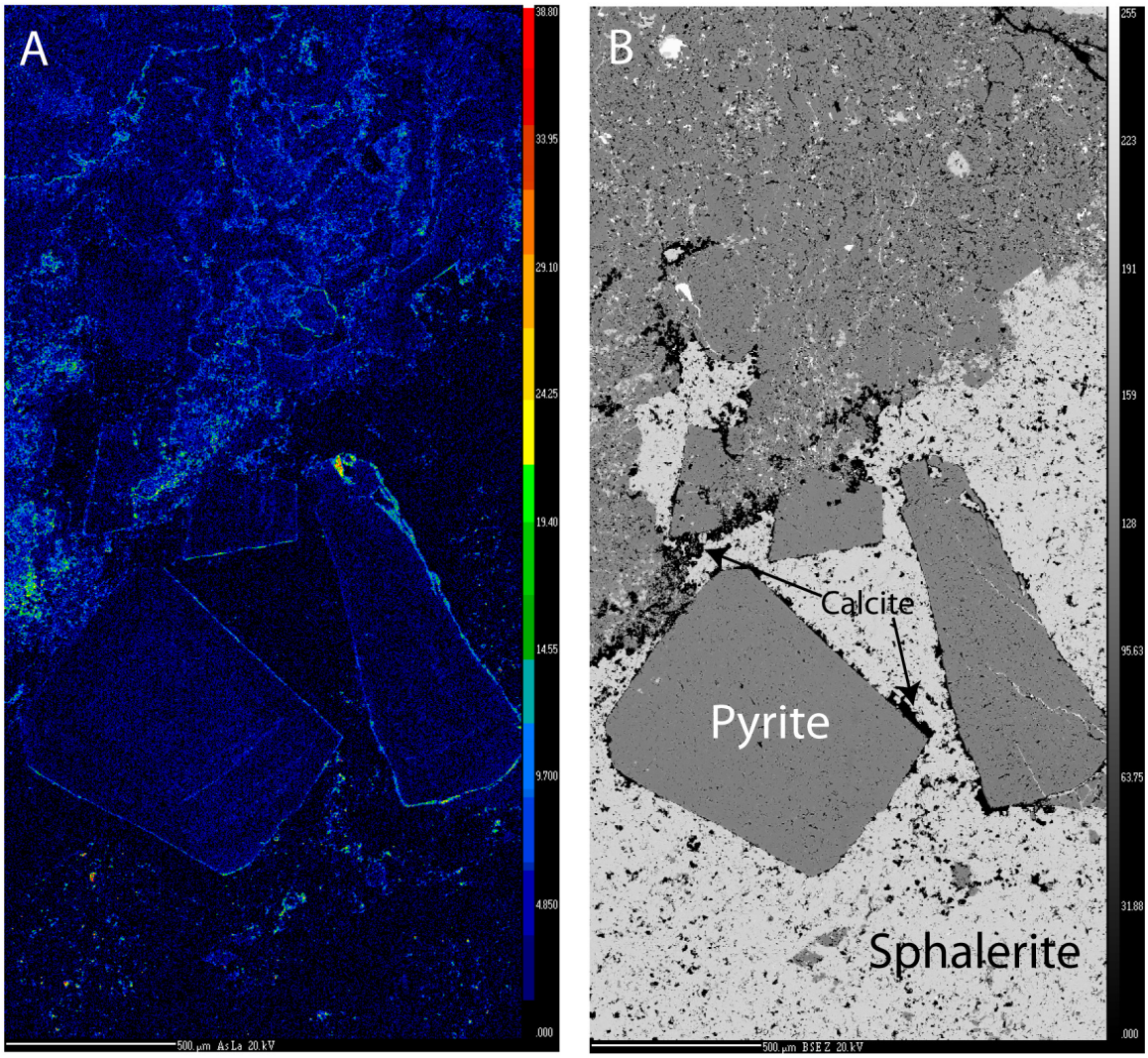

Figure 2.14: Sample LK 325 (A) Arsenic map showing banded zoning in euhedral pyrite crystals and complex zoning and alteration in massive pyrite (B) Back Scattered Electron Image.

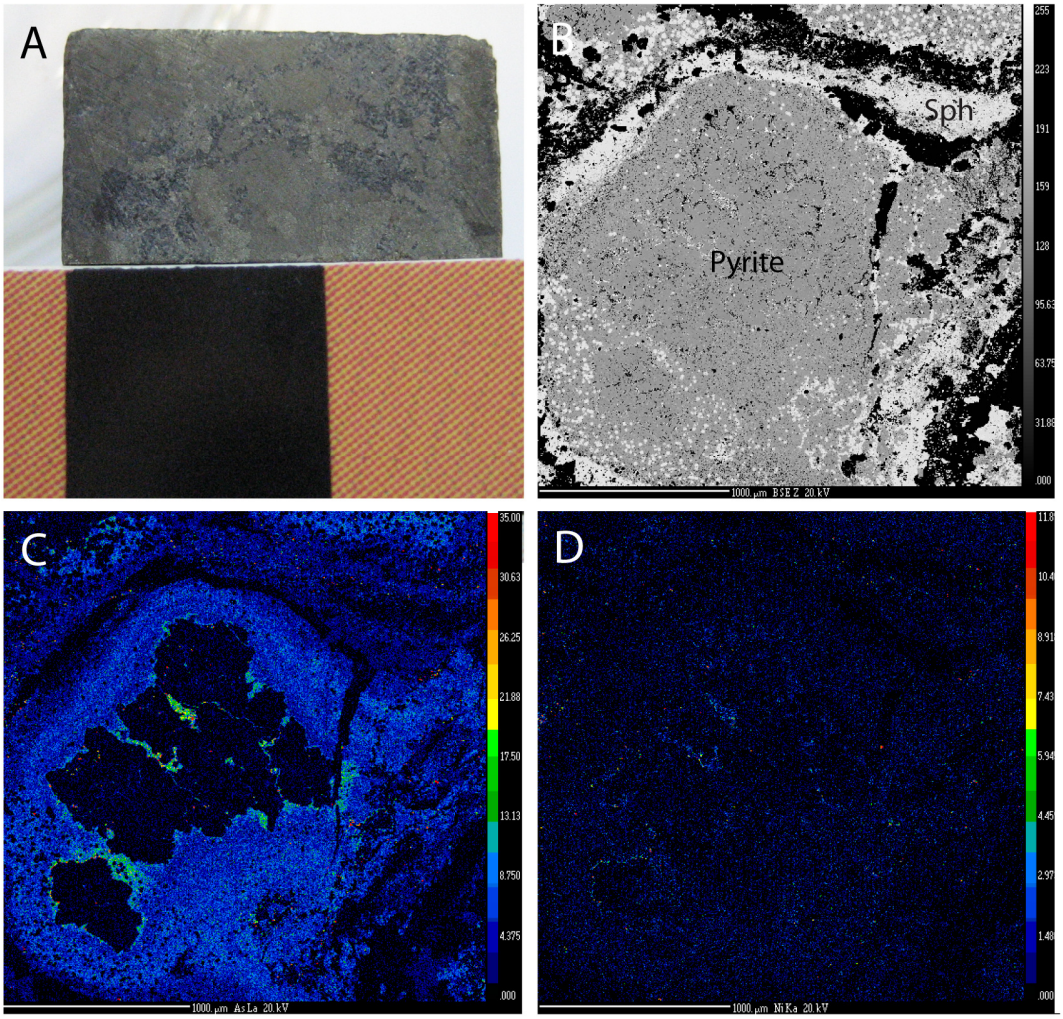

Figure 2.15: Sample LK 451 (A) Original specimen (B) Back Scattered Electron Image (C) Arsenic map showing a trace element depleted pyrite core surrounded by a As rich rim (D) Nickel map showing the correlation between As and Ni contents.

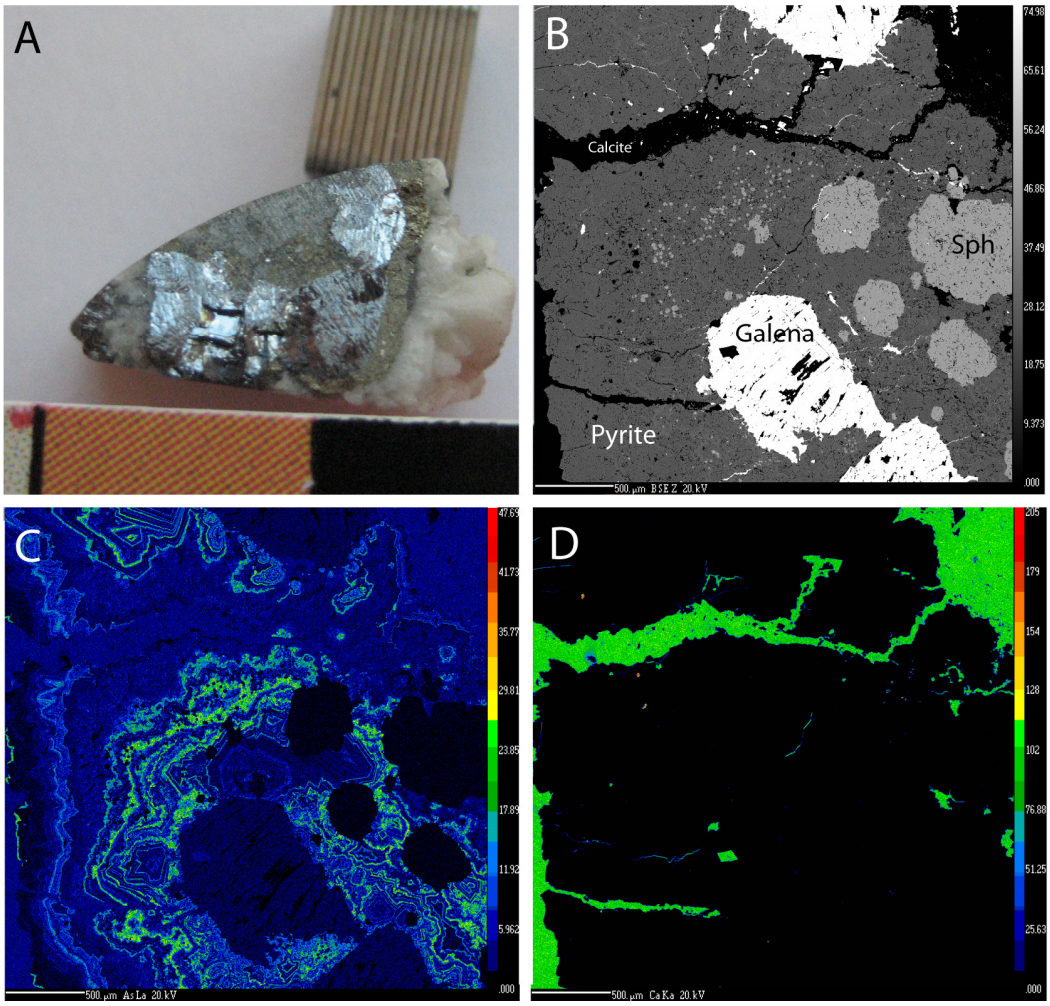

Figure 2.16: Sample Gal 355 (A) Original specimen (B) Back Scattered Electron Image (C) Arsenic map showing zoned pyrite (D) Calcite map of crosscutting calcite veins.

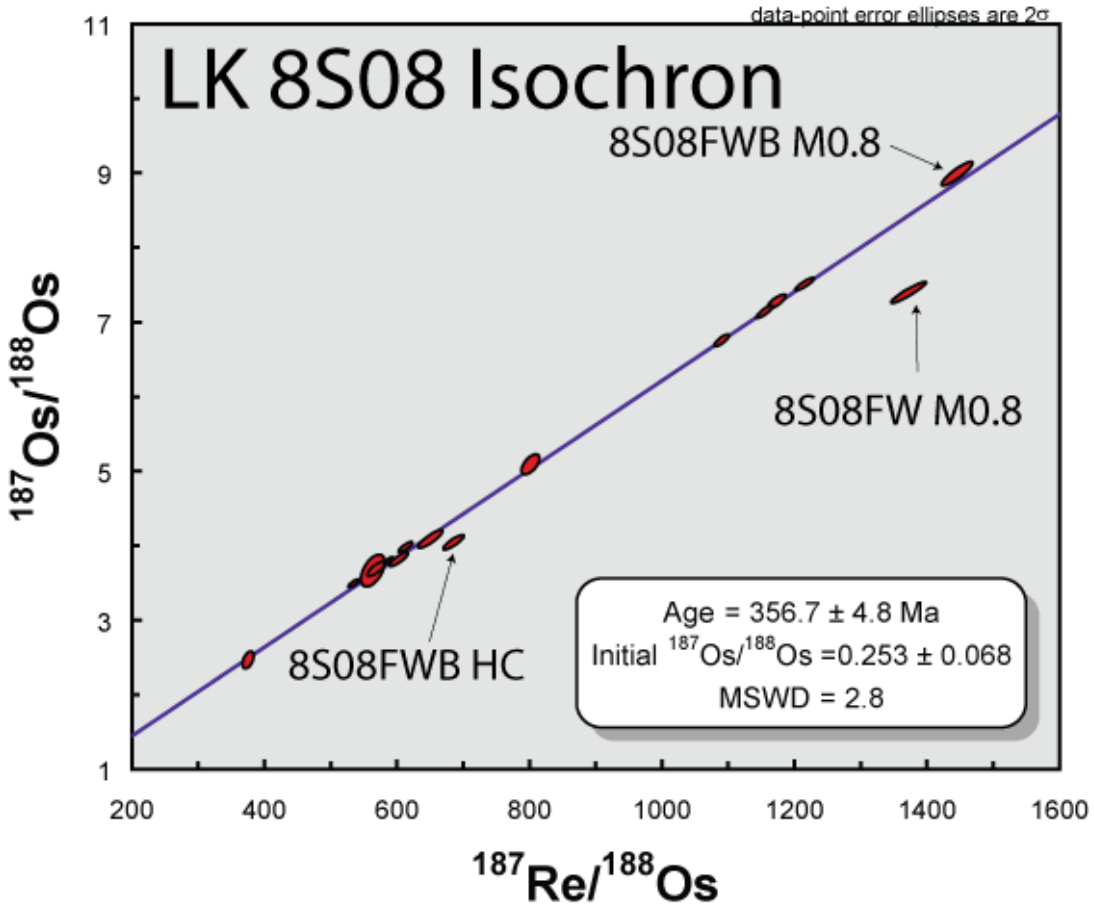

Figure 2.17: Isochron diagram for LK 8S08.

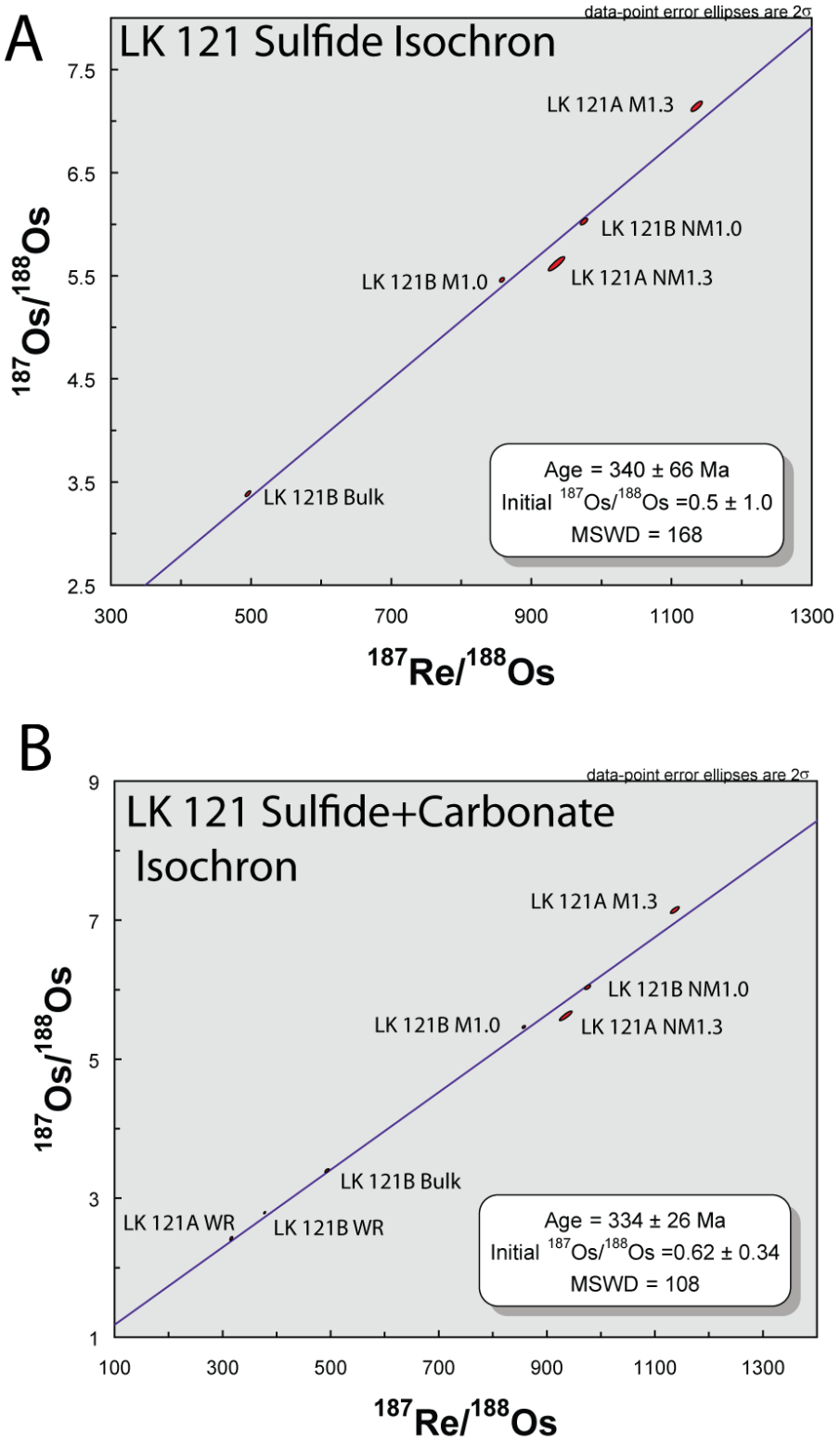

Figure 2.18: Isochron diagram for LK 121 (A) Sulfide samples are only considered (B) Carbonate samples added to isochron diagram.

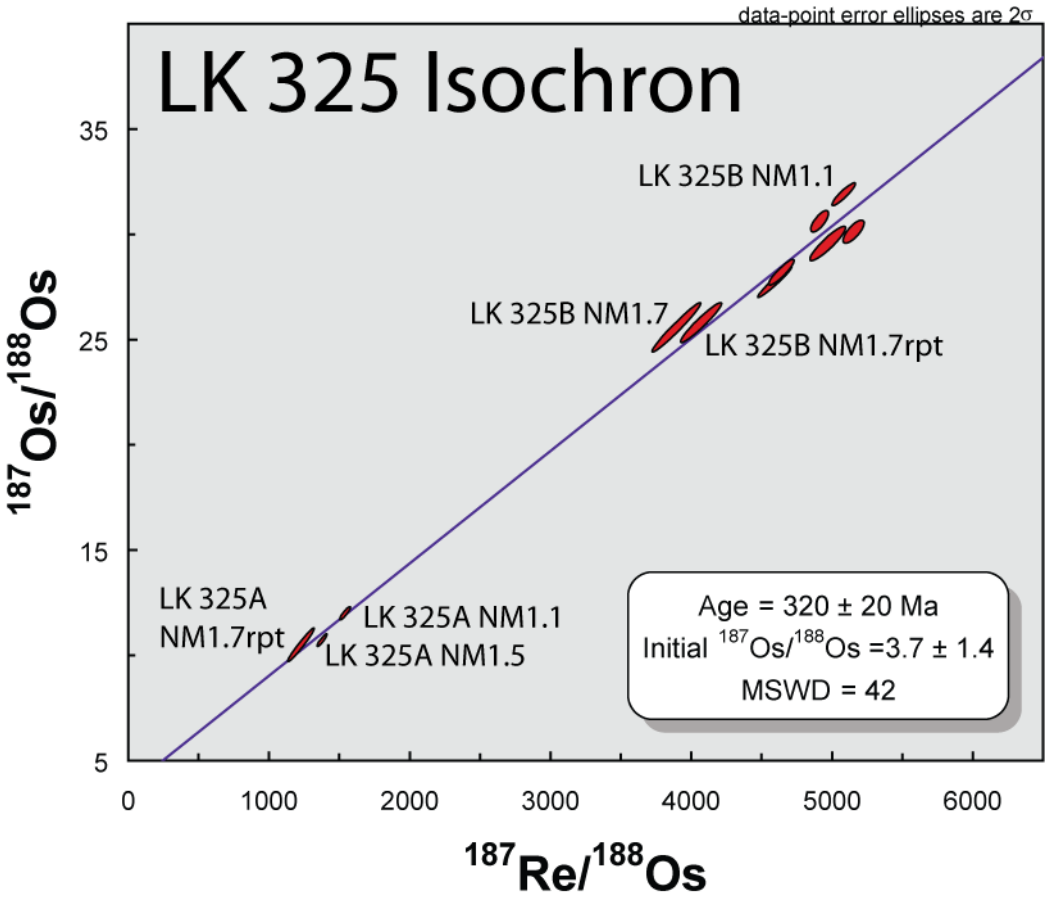

Figure 2.19: Isochron diagram for LK 325. Some data points are labelled for clarity.

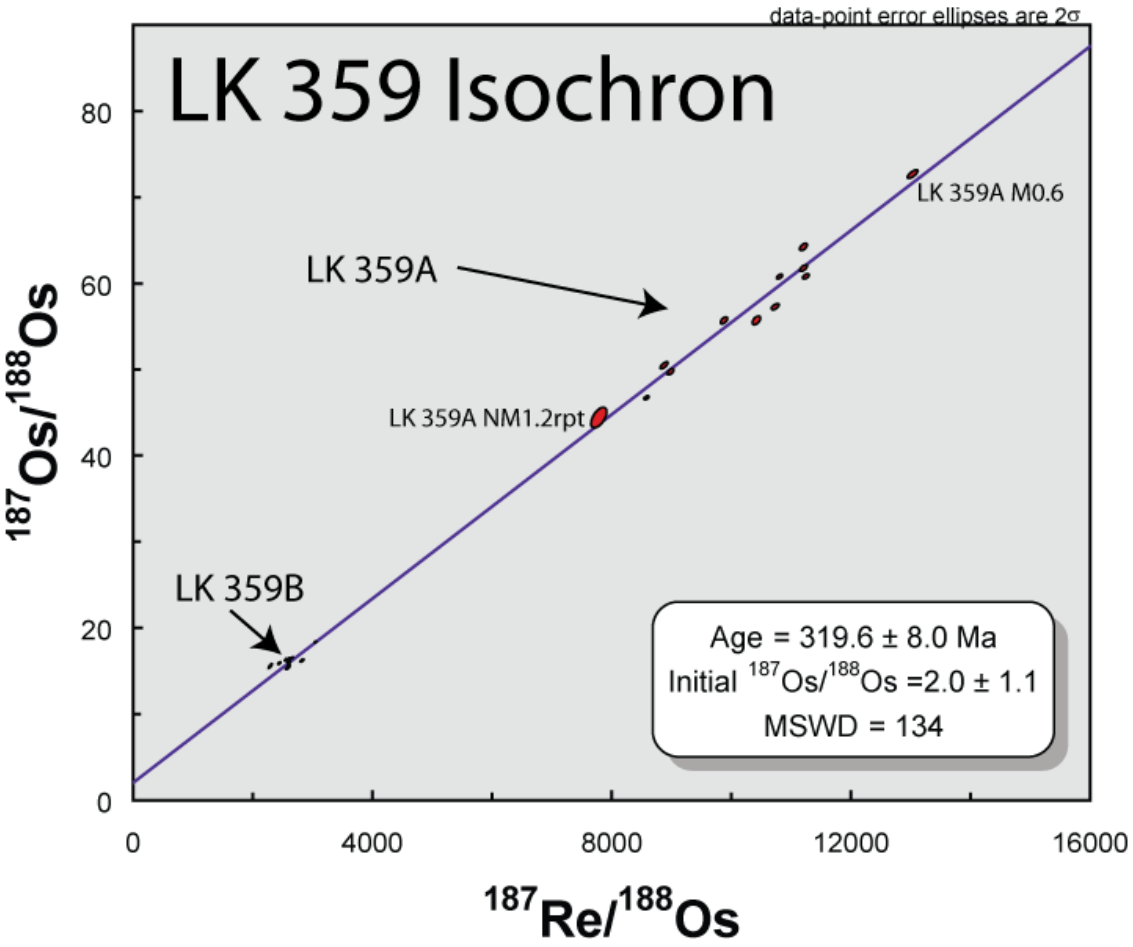

Figure 2.20: Isochron diagram for LK 359. Some data points are labelled for clarity.

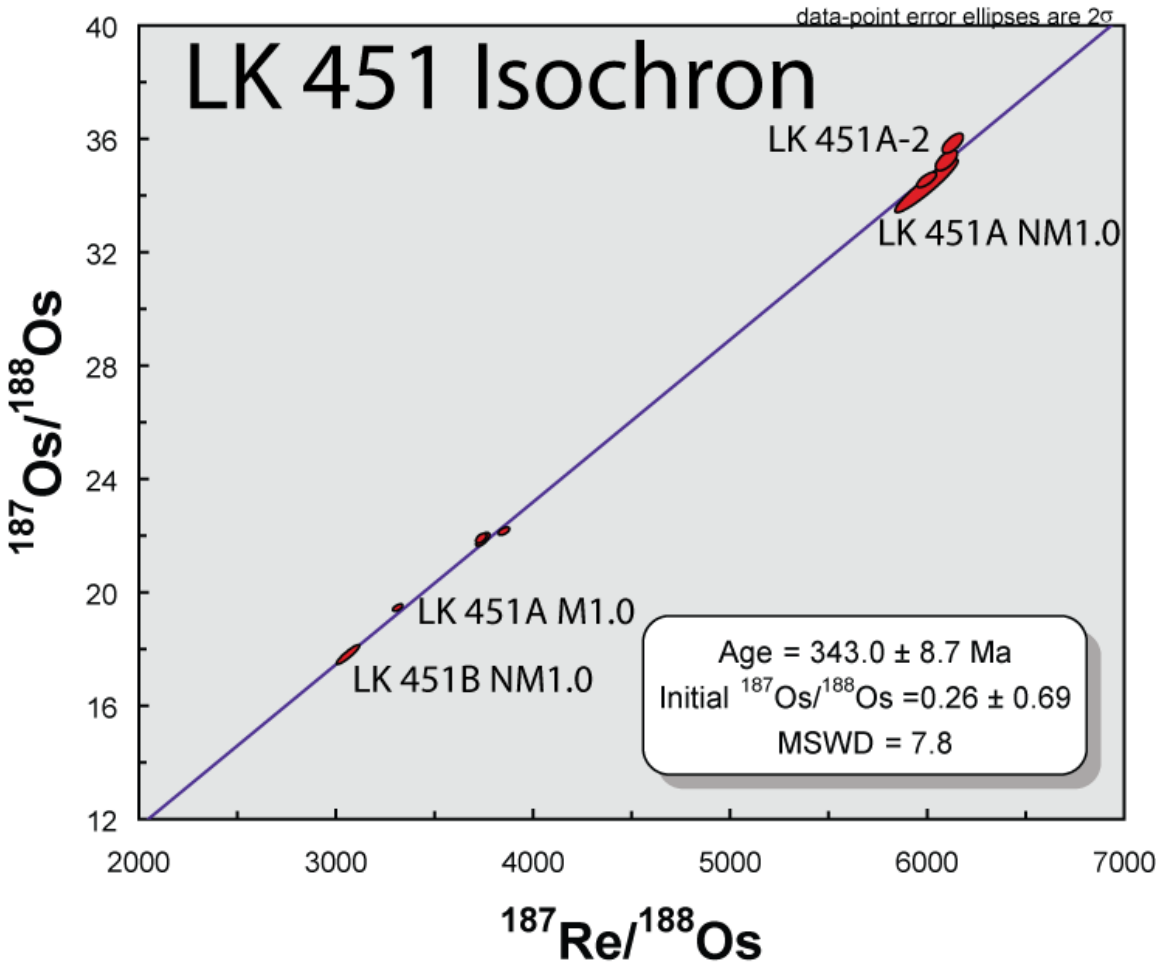

Figure 2.21: Isochron diagram for LK 451. Some data points labelled for clarity.

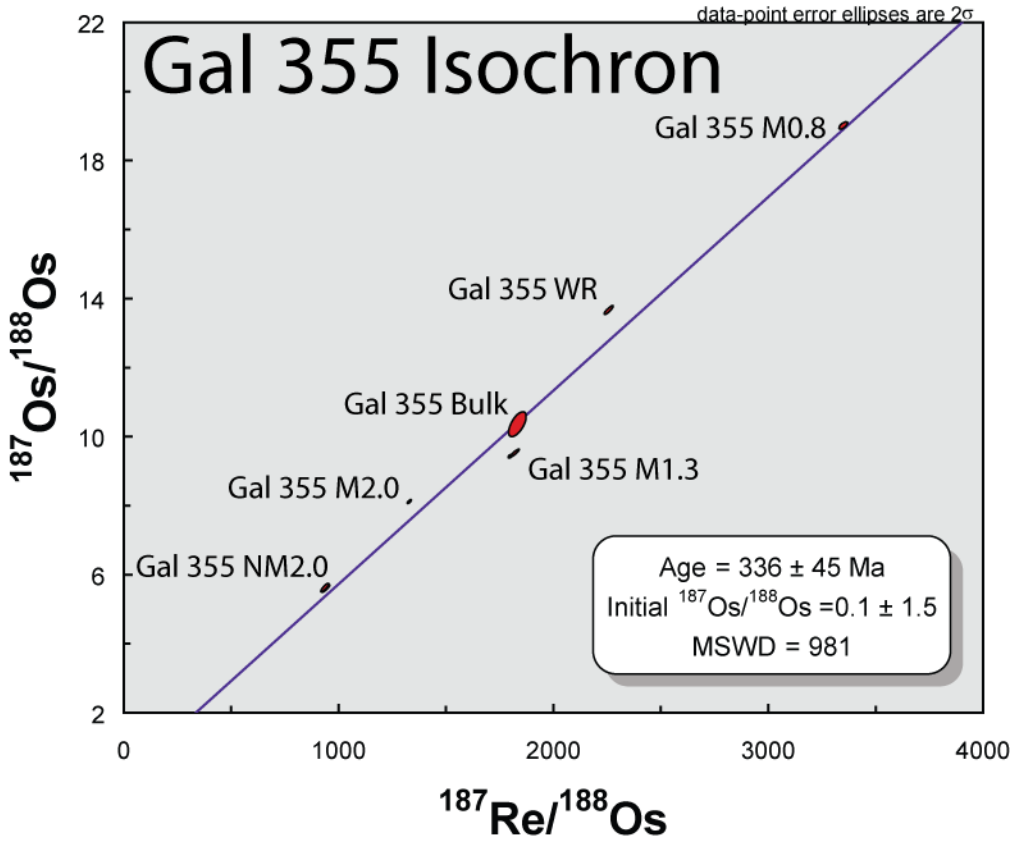

Figure 2.22: Isochron diagram for Gal 355.

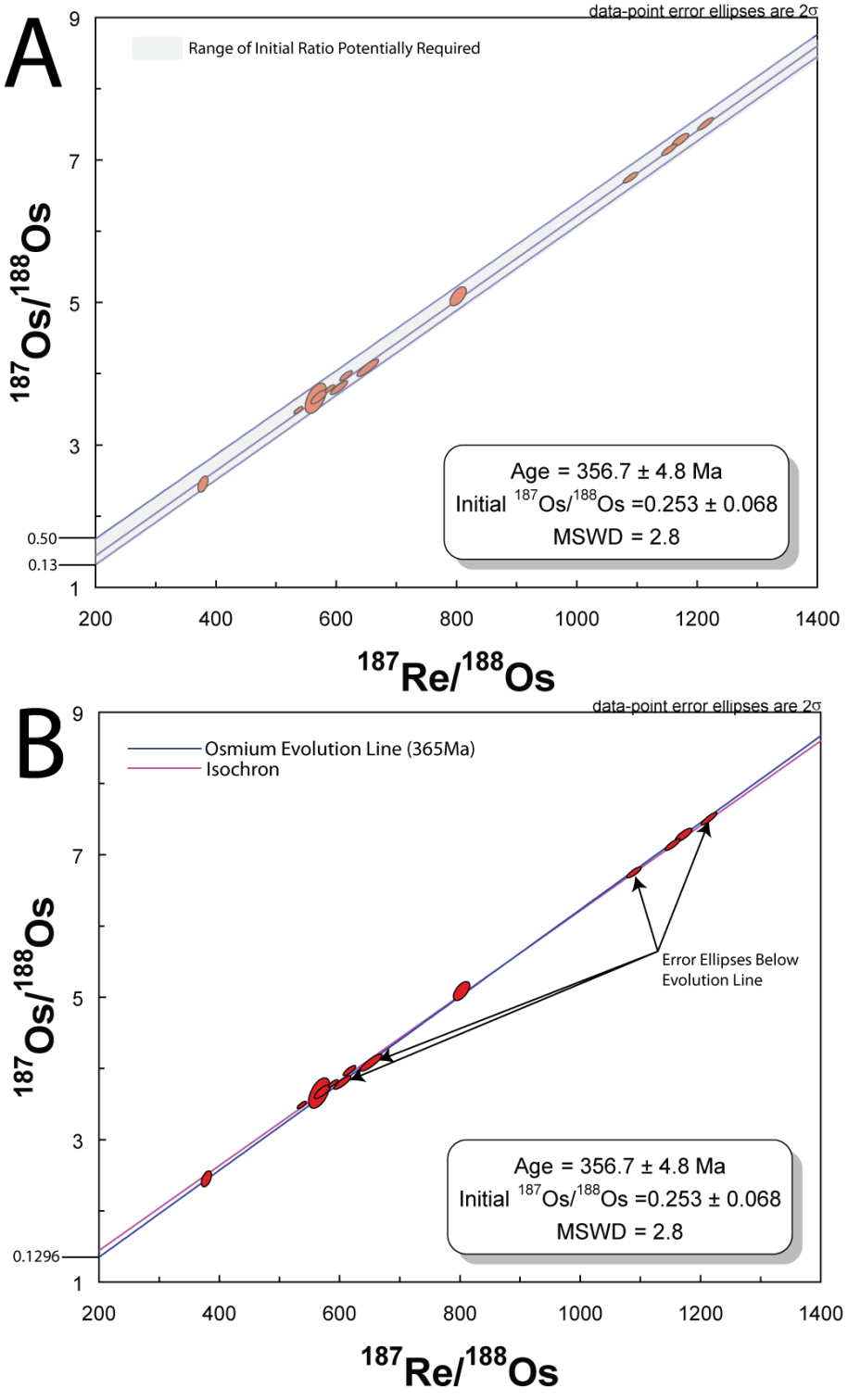

Figure 2.23: Calculating the initial ratio requirements to explain data scatter in LK 8S08. Results for other samples presented in Table 2.8.

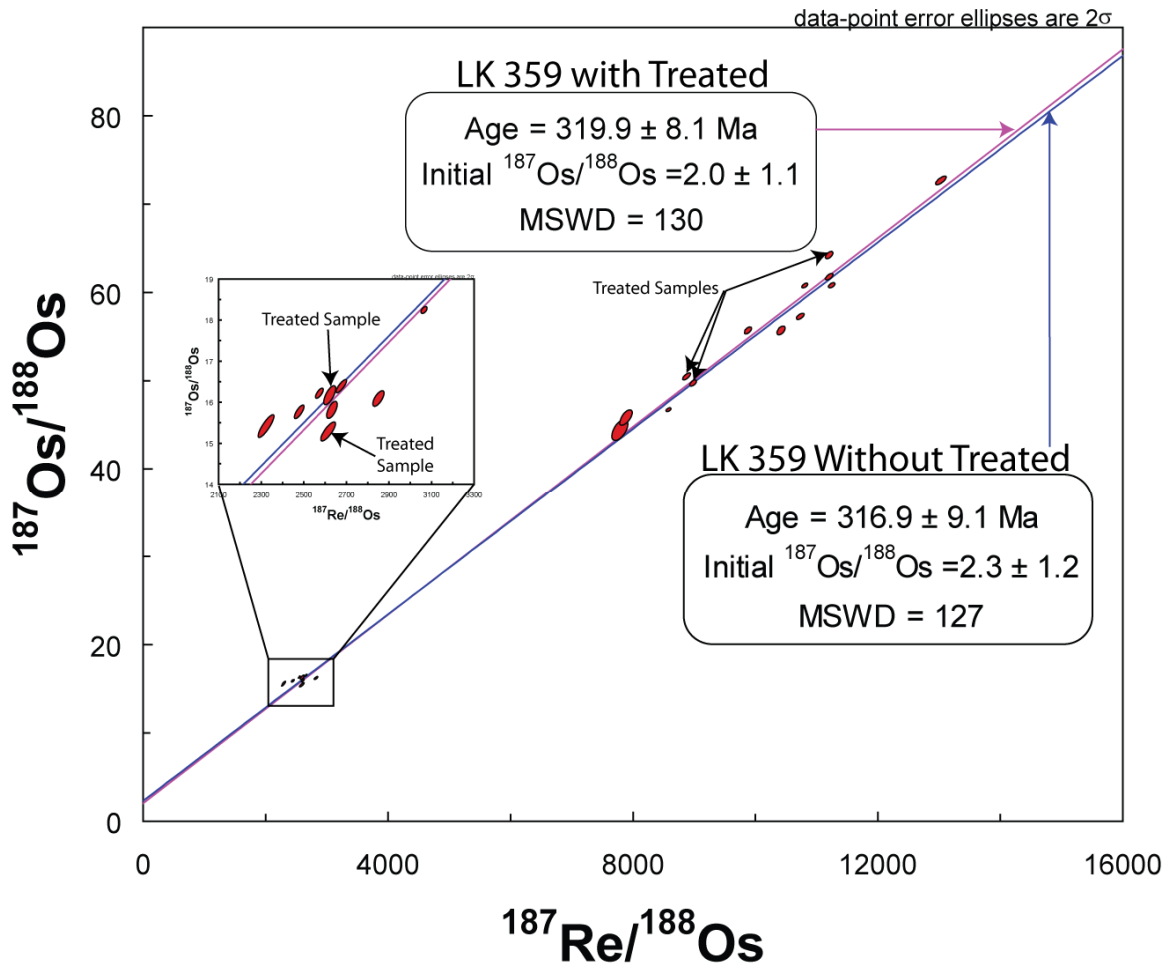

Figure 2.24: Comparison between an isochron that contains acid treated samples and that of non treated samples. The scatter shown by the treated samples is of the same order as the samples that were not treated with acid.

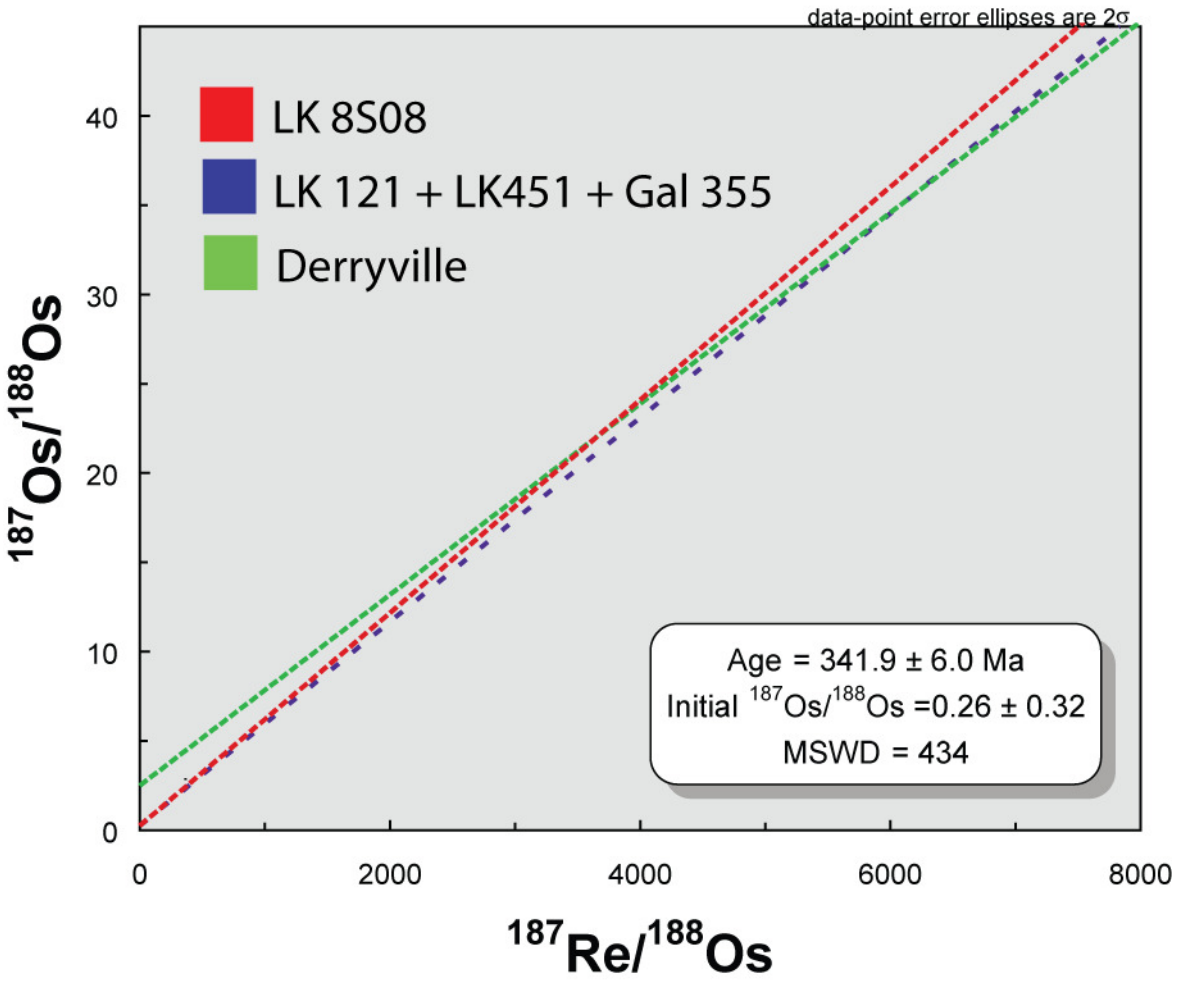

Figure 2.25: Comparison of isochron diagrams showing that the Derryville isochron is rotated with respect to the other samples.

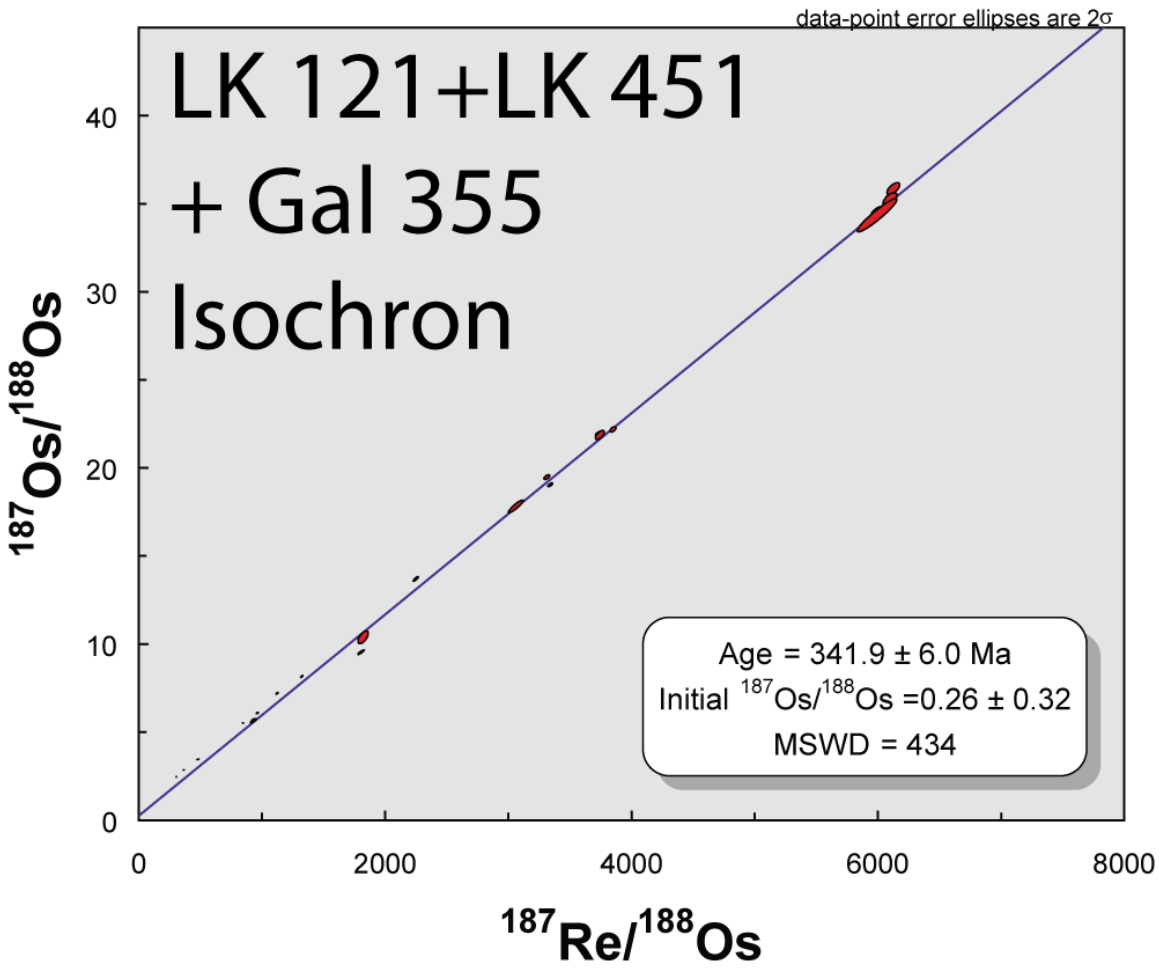

Figure 2.26: Isochron diagram for LK 121 + LK 451 + Gal 355.

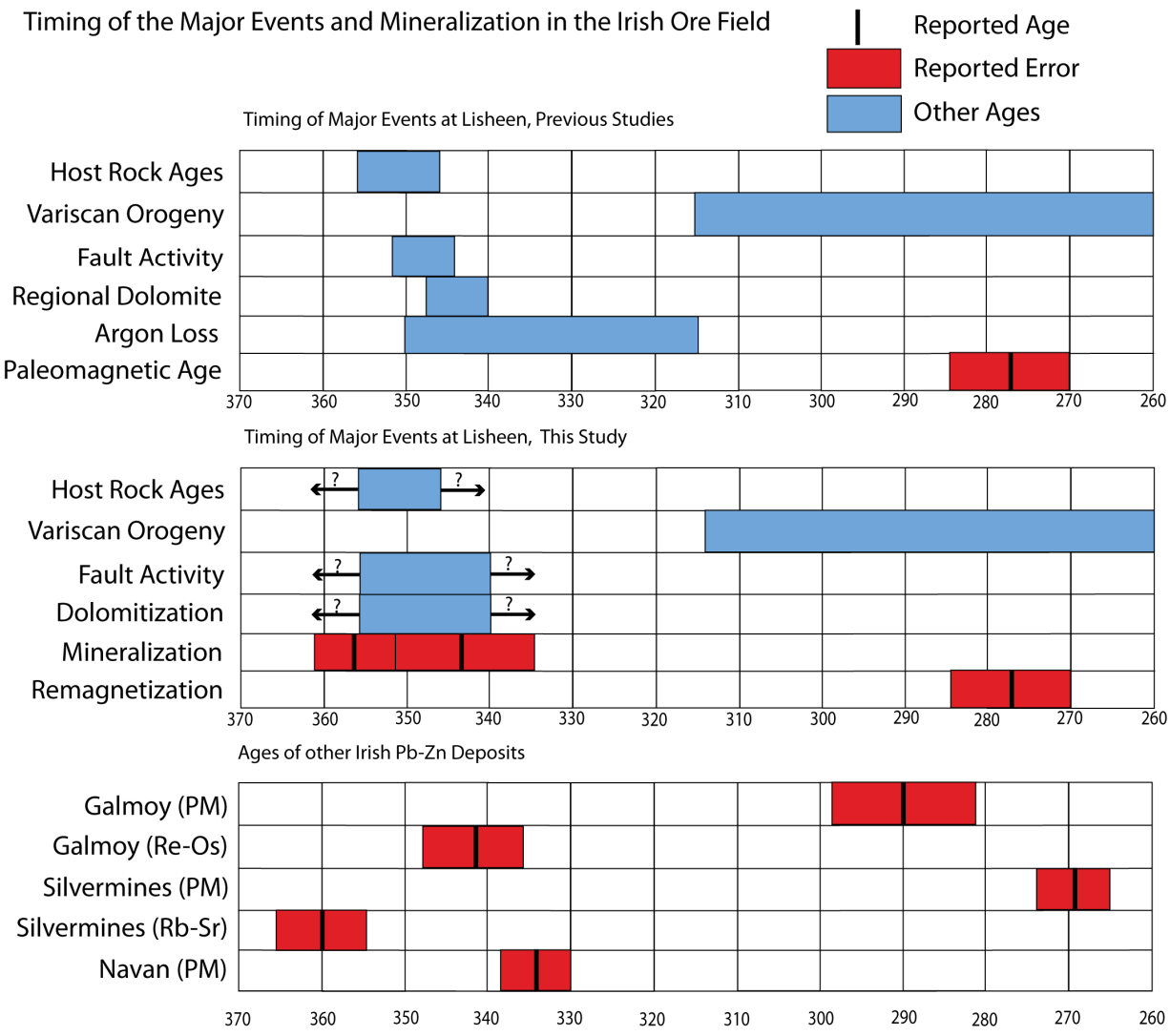

Figure 2.27 A summary of the reported ages for the major events and mineralization in the Irish Ore Field. The host rocks ages represent both the Waulsortian Limestone and the Lisduff Oolite Member.
- Re-Os are dates based on Re-Os geochronology
- Rb-Sr are dates based on Rb-Sr geochronology
- PM are dates based on paleomagnetism.

3.0 - Case Study 2: Re-Os Constraints for the ages of Nanisivik and the Hawker Creek Pb-Zn ore deposits of Nunavut

3.1 Introduction

The Mesoproterozoic Borden basin of northern Baffin Island, Nunavut, is the host to a number of Pb-Zn mineralization showings and deposits, including the once-operating Nanisivik mine. The Nansivik mine began operation in 1976 with reserves of 19Mt at ~10% Pb+Zn and 35g/t Ag, but was closed down in 2002. Since the closing of Nanisivik, there has been continued interest in the Borden basin with regard to economic Pb-Zn mineralization (Figure 3.1). The majority of mineralization, including Nanisivik itself, is found within the newly defined Nanisivik formation (Turner, 2009; Turner, 2011). Although Nanisivik and prospective areas such as Hawker Creek have been explored, there is a lack of knowledge concerning the timing of fluid flow and mineralization within the basin. There are more than a half dozen significant sulphide showings in the Borden basin, however, it is unknown if they temporally related to each other. Answering this question has significant implications for further exploration within the basin by potentially restricting the ages of possible host rocks that can contain economic mineralization.

Proterozoic deposits provide less than 10 percent of all ore mined from Mississippi Valley-type (MVT) ore deposits. This is due to the rarity of MVT deposits being formed in the Proterozoic or hosted in Proterozoic basins (Leach et al., 2010). Previous studies on other deposits such as Bushy Park in South Africa (ca. 2.05Ga) have shown that MVT deposits can form in the Proterozoic (Gleason et al., 2011). The age of Nanisivik is still debated as earlier work in the area has proposed two different ages for the mineralization. One proposal, supported by the work of Sherlock et al. (2004), has mineralization occurring at 461 Ma, on the basis of Ar-Ar dating of adularia. However, ages from Christensen et al. (1993) and Symons et al. (2000) have proposed a much older age of approximately 1100 Ma. Determining which of these ages represents the true age of mineralization of Nanisivik has strong implications for understanding the formation mechanisms and preservation potential of MVT style ore deposits. To help clarify this issue, Re-Os geochronology on main stage ore pyrite from Nanisivik is attempted.

Additionally, the temporal relationship between Nanisivik and smaller prospective areas, such as Hawker Creek, were evaluated using Re-Os geochronology. If the Hawker Creek prospect is the age as that as Nanisivik then further exploration in the basin may need to be restricted to Proterozoic carbonates of greater that 1000Ma in age.

3.2 Geologic Context

A brief overview of the stratigraphy, mineralization, and overall geology will be presented, however, a more in-depth discussion is presented in publications such as Turner (2009) and Turner (2011).

The Borden basin of Baffin Island (Figure 3.1) is part of a group of Mesoproterozoic basins known as the Bylot basins (Fahrig et al., 1981; Jackson and Iannelli, 1981). These basins formed in response to crustal extension due to the very large Mackenzie igneous event at ca. 1270 Ma (LeCheminant and Heaman 1989). Basin deposition initially occurred as a response to rift related grabens (Jackson and Iannelli, 1981), later evolving into a more typical foreland basin (Sherman et al., 2002).

The Proterozoic stratigraphy in the Borden basin dips to the west by 10^{o}-20^{o} and is marked by numerous northwest trending normal faults (Jackson and Iannelli, 1981; Scott and deKemp, 1998). These faults are thought to have been formed during the initial rifting and could have been sporadically active well into the Phanerozoic (Jackson and Iannelli, 1981). Throughout the Canadian arctic, the Franklin age dikes are also a major structural feature (ca. 720 Ma, Heaman et al., 1992), and at Nanisivik the ore has been crosscut by one of these dikes, known locally as the mine dike.

3.3 Stratigraphy

The Borden basin is the largest of the Bylot basins and is composed of a succession known as the Bylot Supergroup. The Bylot Supergroup is composed of volcanic and siliclastic rocks from the Eqalulik Group, which is overlain by the shale and carbonates of the Uluksan Group, and the upper siliclastic material of the Nunatsiaq Group (Figure 3.2). Later stage diabase dikes are known to cut through the Bylot

Supergroup, the majority of which likely are related to the 720 Ma Franklin dikes (Heaman et al., 1992; Pehrsson and Buchan 1999; Denyszyn et al., 2009; Turner, 2011).

Pb-Zn mineralization within the Borden basin is related to a group of unmetamorphosed sedimentary successions within Bylot Supergroup. The lowermost of these units is the shale-dominated Arctic Bay Formation, which conformably transitions into the Nanisivik Formation and locally into the crystalline dolostones of the Ikpiarjuk Formation. The Nanisivik Formation is composed of laminated brown dolostone that conformably lies overtop either the Arctic Bay Formation or the Ikpiarjuk Formation. The Nanisivik Formation is overlain disconformably by the shales, limestone's, and dolomitic mudstones of the Victor Bay Formation. The contact between the Nanisivik Formation and Victor Bay Formation in the vicinity of the Nanisivik mine is extremely variable and complex topographically (See Figure 10 in Turner, 2011). Turner (2011) proposed that this was due to normal faults causing the Nanisivik Formation to split into several horst and graben structures prior to the deposition of the Victor Bay Formation. The majority of mineralization at Nanisivik is related to one of these horst structures (Figure 3.3).

3.4 Mineralization

The mineralization at Nanisivik, and the other prospective areas, is thought to be related to MVT style processes, meaning that the major ore minerals of pyrite, marcasite, galena, and sphalerite are known to replace host carbonate sedimentary rocks, at relatively low temperatures (McNaughton, 1983). The main mineralization at Nanisivik is spatially related to a major horst structure and the Keystone fault (Figure 3.3). The metalliferous fluids that gave rise to mineralization are thought to have moved up through permeable fractures associated with the Keystone fault. Mineralization itself is thought to have been initiated when the metal rich brine interacted with hydrocarbon gas believed to have been trapped underneath the paleotopographic highs of the Victor Bay Formation (Arne et al., 1991; Sutherland and Dumka, 1995; Sherlock et al., 2004; Turner, 2011). This produced a sinuous 3000m long, 200m wide, 10m thick ore body that varies less than 3m topographically. Mineralization styles are typically comprised of massive sulphides, which often contain complex replacement and banded textures, which are

thought to have come from a series of dissolution and replacement events, likely associated with gas-fluid interactions (Arne and Kissin, 1989; Arne et al., 1991; Turner, 2011).

Hawker Creek mineralization is compositionally and texturally very similar to Nanisivik and is exposed at a variety of surface outcrops that have vein filling sulfides and banded massive sulphides. These similarities in textures to Nanisivik led Turner (2011) to suggest that the formation of Hawker Creek may have been associated with gas being accumulated in the paleotopographic highs produced by erosion. Unfortunately, at Hawker Creek much of the overlying Victor Bay Formation has since been eroded leaving some uncertainly to the exact origin of mineralization at Hawker Creek.

3.5 Hydrothermal Activity

Aside from the major hydrothermal activity associated with the precipitation of sulphides, there is a second fluid event associated with a prominent alteration assemblage at Nanisivik. Known as “white rock” adularia alteration, it has extensively altered some areas of the Nanisivik ore zone (Sutherland and Dumka, 1995; Sherlock et al., 2004). Adularia is particularly pervasive throughout the mine itself and is likely a direct product of dike alteration (Sherlock et al., 2004). Alteration is not restricted to the mine dike, as other areas also have adularia alteration, albeit with differing morphologies. These tend to occur as bed-parallel features and as small irregularly shaped features associated with coarse grain sphalerite, and are likely due to alteration of remnant siliclastic material (Sherlock et al., 2004). Textural and crosscutting relationships within the white rock assemblage suggest that sulphide mineralization has taken place during, and after, the formation of the white rock material (Sherlock et al., 2004). While the alteration assemblage is known to significantly affect many areas of Nansivik, its relationship to primary mineralization is unknown. In particular, the magnitude of sulphide mineralization associated with the white rock assemblage is unknown. Complicating the matter is that the actual origin and extent of the associated K-rich fluids, which are atypical of MVT-style mineralization, is currently unknown.

3.6 Existing Age Constraints

The timing of mineralization at Nanisivik, and the other prospects in the Borden basin is very contentious, with age dates from the Mesoproterozoic to Ordovician being proposed. The age of the host rock gives the maximum upper limit of mineralization at Nansivik. Bylot Supergroup deposition likely started close to ~1270 Ma based on correlations of paleomagnetic poles to those of the Mackenzie dike swarms which were dated to ~1270 Ma (Fahrig et al., 1981; LeCheminant and Heaman 1991). Additionally, it was reported in Symons et al., (2000) that Pb-Pb work on the Lower Uluksan Group by L.C Kah and F.Marcantonio suggests a deposition age of 1204 ± 22 Ma. Symons et al. (2000) used updated information to modify that age such that the deposition of the Bylot Supergroup occurred between 1225-1270 Ma, whilst Nanisivik's host rocks likely were deposited at ~1250 Ma.

Remagnetization of the host dolostones directly above the mineralization has been dated to 1095 ± 10 Ma using paleomagnetic methods (Symons et al., 2000). However, because this age is not derived from the ore, it is unclear whether or not remagnetization is directly related to ore forming event at Nanisivik. Direct dating of the ore was attempted by Christensen et al. (1993) using Rb-Sr measurements of sphalerite, which produced an age of mineralization of 1100 Ma, correlating well with the Symons el al. (2000) dates. Pb-Pb analyses have also previously been attempted at both Nanisivik and Hawker Creek, which gave a possible range of 600-800 Ma for mineralization (Olsen, 1984). As it is stated in Olsen (1984) these ages are not particularly robust since it is unclear which Pb-isotope crustal evolution model is required to properly model the Pb-Pb ages in the Borden basin. The most likely minimum age of the deposit corresponds to the age of the mine dike that crosscuts the deposit. Although this dike is undated, it is assumed to be related to the Franklin igneous event, and if so it provides a minimum age of deposit of ~720 Ma (Heaman et al., 1992; Pehrsson and Buchan, 1999). In contrast to these Proterozoic age constraints, Sherlock et al. (2004) determined Ar-Ar dates of 461 ± 3 Ma for the adularia alteration seen at Nanisivik. It was argued by Sherlock et al. (2004) that this date represents the true age of mineralization, with the assumption that formation of the ore body is directly related to adularia alteration. However, if this is the true age of

the deposit it would be hard to reconcile with the apparent minimum age given by the mine dike. It has been suggested by Turner (2011) that the alteration assemblage is disconnected from the main ore forming event, even though the origin of these secondary fluids is currently unidentified.

3.7 Methodology

Sulphide minerals from Nanisivik and Hawker Creek were selected, prepared, and analyzed at the University of Alberta, using samples provided by Dr. E. Turner, Laurentian University Canada.

3.71 Sample Preparation

Below is a brief description of the sample preparation for Re-Os analysis, for a full description of these processes and other supplemental techniques please refer to Appendix I-IV. For Re-Os analysis, samples were processed through a very specific procedure in order to obtain purified sulphide concentrates.

Initial preparation starts with crushing the starting material to approximately 100µm. A hammer is used as to prepare a sample for a shatter box. To keep contamination to a minimum the hammer is wrapped in plastic. The shatter box is then used to crush the sample to the desired size. To separate the unwanted quartz and carbonates from the crushed sample a heavy liquid separation procedure is used to separate these lighter minerals from the sample. The dense material contains pyrite ± sphalerite ± galena, which are subsequently divided up into a number of divisions based on their magnetic susceptibilities using a Frantz isodynamic separator. Galena and sphalerite were dissolved out in some divisions using concentrated hydrochloric acid, leaving behind a pyrite rich division.

3.72 Rhenium-Osmium Analytical Procedure

The Re-Os analyses were carried out by weighing up to 400mg of a sulphide sample and transferring it into a thick-walled Carius tube. The sample is then dissolved in inverse aqua regia (~2mL of 10N HCl and ~6mL 16N HNO_3) with a known amount of

^{185}Re + ^{190}Os spike and is immediately frozen in dry ice/ethanol and sealed with a glassblowing torch using natural gas and oxygen. To equilibrate the sample Re and Os with the spike Re and Os, the sealed Carius tube is heated at 220^{o}C for a minimum of 24 hours. After heating the Carius tube is then frozen in a dry ice-ethanol slurry prior to extraction in order to prevent any loss of Os. Upon opening the Carius tube 10.5mL chloroform is added to the acid solution, in three aliquots of 3.5 mL, which provides a way to separate the Re from the Os. This creates a pair of immiscible liquids where the Os is preferentially partitioned in the chloroform and the Re remains dissolved in the inverse aqua regia.

The chloroform portion containing Os is then transferred into a pre-cleaned 22ml glass scintillation vial containing 3mL of 9N HBr, which is subsequently heated to ~80^{o}C for a minimum of 12 hours. This process transfers the Os from the chloroform into the HBr, via reduction. The HBr solution is then removed from the vial and dried down onto a Teflon cap prior to then next analytical step - micro distillations. To purify the Os, a 7N H_2SO_4 solution containing CrO_3 is added to the dried down HBr and is distilled at ~70^{o}C inside a Teflon conical vial (Savillex) in which the Os rich vapour is transferred to 20ul of clean 9N HBr held in the vial tip via surface tension. The process is repeated one more time; the sample is dried down, and is transferred onto a platinum filament. To ensure a strong signal the sample is activated using $Ba(OH)_2$, dissolved in 0.1N NaOH.

The remaining inverse aqua regia is transferred to a glass vial and dried down. To purify the Re, anion exchange chromatography is used. The dried sample residue is re-dissolved in 0.2N HNO_3 and is transferred into disposable anion column and is washed in the order specified in Figure 2.5. The final solution that contains the dissolved Re is then dried down in a pre-cleaned PMP beaker. The sample is once again dissolved in 0.2N HNO_3. This solution is transferred into a 1mL centrifuge tube where a single ~ 20 mesh anion bead is used to extract the Re over a minimum of 6 hours. The anion bead is then washed and transferred into a clean 1mL centrifuge tube containing 6N HNO_3 in order to back-extract the Re from the bead. The purified Re sample is dried down and placed onto a nickel filament and is activated using $Ba(NO_3)_2$ dissolved in water.

These filaments are run on a thermal ionization mass spectrometer under specific conditions. The Re coated filament is heated to ~650-800^{o}C at a rate of ~200deg/min to

create a stable beam of ReO_4^- for the Faraday cup detectors. Both ^{185}Re and ^{187}Re are analyzed simultaneously 100 times at discrete time intervals to ensure good counting statistics. The Os coated filament is typically heated to between ~650°C - 735°C at a rate of ~30deg/min under a pressure of ~2.00×10^{-7} mbar of O_2 to ensure a stable beam of OsO_3^- is obtained. Due to the low beam intensity associated with Os a secondary electron multiplier is used for analysis. Each isotope is then measured independently 96 times to ensure good counting statistics.

Procedural blanks are also used to define the amount of impurities added through the chemical process. In particular, Os blank values (0.40 ± 0.20 pg) for non radiogenic isotopes of Os can be responsible for up to 25% of ^{188}Os, but values <5% are more typical. Blank values for both Re and Os are used to correct raw data collected from the TIMS instrument. As a sample is run through the TIMS further corrections are made based on the oxygen isotope abundances, since it is the Re and Os oxides that are measured. Finally isotope fractionation corrections and spike unmixing corrections are applied before final analysis.

3.73 Trace Element Analysis

To obtain bulk trace element compositions of the separated mineral fractions a Perkin Elmer Elan 6000 Quadrupole Inductively Coupled Plasma Mass Spectrometer at the University of Alberta was used. For analysis acid digestion is performed on 200mg of sample and was subsequently run on the quadrupole ICP-MS using a DNC-1 standard for the calibration of trace elements. Appropriate dwell times and integration times were selected to optimize counting statistics for each element. For the majority of elements 20ms and 700ms integrations times were used, with the exception being copper where the dwell and integration times were decreased to 10ms and 350ms respectively.

Spot analyses of all phases, back scattered images, and element maps were performed over numerous sessions on a Cameca SX100 electron microprobe. The following standards were used for all analyses, pyrite for S and Fe, nickel metal for Ni, cobalt metal for Co, sphalerite for Zn, arsenopyrite for As, and calcite for Ca. Data was then collected under beam conditions of 20kV and 20nA. Detection limits for trace elements were approximately 300-800ppm, depending on the element analyzed.

3.8 Sample Description

3.81 General Characteristics

Details for the samples chosen for Re-Os and trace element analyses are presented in Table 3.1 and Figure 3.5. The naming convention for the prepared samples is given in Table 3.2. These samples were all divided into various divisions using the procedure explained above and have subsequently been analyzed for bulk trace element composition using a ICP-MS.

The mineralogy for each sample was determined using a combination of optical microscopy, element distributions in the ICP-MS analyses, and electron microprobe analyses. The general trace element distributions for Nansivik and Hawker are determined to be similar (Figure 3.6). It is also observed that higher magnetic susceptibility corresponds to an increase in the concentrations of Re, Os, As, Ni, Co, and other trace elements, as was found previously for Case Study 1 at Lisheen. These analyses suggest that these samples contain chemical/magnetic banding, although in thin section and microprobe examination it was not possible to determine the location, extent, or even the existence of these different zones (Figure 3.7). This was primarily due to the trace element concentrations being below the electron microprobe detection limits.

Table 3.1: Basic description and location of samples used for Re-Os analysis

Sample Name	Deposit/Zone	Ore Minerals	Basic Description
NOV-4	Nanisivik/Main Ore Body	Pyrite, Sphalerite, Galena	Banded Sulfides
04-N-2	Nanisivik/Oceanview Pit	Pyrite, Sphalerite, Galena	Banded Sulfides
01-N-D	Nanisivik/Main Ore Body	Pyrite, Sphalerite, Galena	Banded Sulfides
03-HC-8D	Hawker Creek	Pyrite	Massive Pyrite
03-HC-8F	Hawker Creek	Pyrite, Sphalerite	Massive Pyrite/Sphalerite

Table 3.2: Naming convention for Re-Os analysis

Name	Comment
Sample	Handpicked material
Sample Bulk	Crushed material that has not undergone magnetic separation
Sample NM 2.0	Mineral separate was non-magnetic at a current of 2.0 amps
Sample M 2.0	Mineral separate was magnetic at a current of 2.0 amps
Sample rpt	A sample that has been analyzed more then once.

3.82 Nanisivik

The main sample analyzed for the Nanisivik study was NOV-4 which is composed of banded pyrite, sphalerite, and calcite from the main ore zone at Nanisivik (Figure 3.5D). The pyrite rich bands are ~1cm in thickness and were handpicked to obtain samples for analysis.

Sample 01-N-D is also from the main ore zone and is composed of primarily euhedral pyrite cubes with volumes of ~1cm^3 (Figure 3.5E). A minor component of massive intergrown sphalerite and pyrite is also present in this sample. Pyrite from 01-N-D was split into different magnetic fractions prior to analysis. A relatively narrow range of magnetic susceptibility was measured in this sample compared to that of 04-N-2 and Hawker Creek.

Sample 04-N-2 is from the Oceanview pit just east of the main zone at Nanisivik and is composed of alternating 1cm bands of pyrite, sphalerite, and calcite (Figure 3.5C). This sample was split into three magnetic fractions, two of which contain nearly pure pyrite, whereas the third contains a mix of pyrite and sphalerite.

3.83 Hawker Creek

Sample 03-HC-8D is composed of massive pyrite with minor of sphalerite and calcite (Figure 3.5A). Within this sample there are strong variations in magnetic susceptibility, corresponding to changes in trace element content. From the ICP-MS analyses it is clear that the most magnetic fractions is also associated with the highest trace element content. Although not visible in thin section or backscattered images (Figure 3.7) there may be some form of zoning present based on these chemical observations.

03-HC-8F is a sample of dominated by banded pyrite and orange sphalerite (Figure 3.45).

3.9 Results

For Nansivik, eleven fractions of pyrite were processed and analyzed (Table 3.3). The data obtained from the TIMS measurements were used to construct an isochron

diagram using Isoplot version 3.00 by plotting $\frac{^{187}Os}{^{188}Os}$ vs. $\frac{^{187}\mathrm{Re}}{^{188}Os}$ (Ludwig, 2001). The Hawker Creek analyses (Table 3.3) are not appropriate for an isochron, however, Model Ages were constructed to obtain age information.

Table 3.3: Analytical Results for Nanisivik and Hawker Creek

Sample	Sample Weight (g)	$^{185}Re/^{190}Os$ Spike Weight (g)	Total Re ppb	Total Os ppt	Total ^{192}Os ppt	$^{187}Re/^{188}Os$	$^{187}Os/^{188}Os$
NOV4-A	0.33004	0.00100	6.93 ± 0.03	96.34 ± 1.43	8.83 ± 0.10	1560.83 ± 19.45	26.98 ± 0.40
NOV4-B	0.52406	0.00100	8.55 ± 0.03	121.15 ± 1.40	7.57 ± 0.07	2247.35 ± 21.29	43.12 ± 0.45
NOV4-C	0.41478	0.00100	2.15 ± 0.01	36.08 ± 0.77	4.17 ± 0.08	1023.35 ±19.71	19.83 ± 0.44
NOV4-D	0.42152	0.00100	6.39 ± 0.03	92.24 ± 1.48	9.72 ± 0.11	1307.25 ± 15.58	22.50 ± 0.41
NOV4-E	0.21549	0.00637	4.99 ± 0.02	78.82 ± 1.49	6.06 ± 0.16	1638.31 ± 42.38	33.62 ± 0.88
NOV4-F	0.3911	0.01085	5.41 ± 0.02	86.27 ± 1.24	5.73 ± 0.09	1878.15 ± 28.42	40.09 ± 0.61
NOV4-G	0.26348	0.00710	8.55 ± 0.03	127.63 ± 3.21	10.00 ± 0.18	1700.99 ± 31.55	32.85 ± 0.90
01-N-D M1.75	0.39793	0.00215	0.04 ± 0.01	2.00 ± 0.12	0.52 ± 0.09	153.25 ± 37.55	4.53 ± 0.77
04-N-2 M 1.6	0.40361	0.00536	0.70 ± 0.01	20.36 ± 0.29	4.35 ± 0.09	319.53 ± 7.05	7.27 ± 0.15
04-N-2 M 2.0	0.40188	0.00396	0.53 ± 0.01	16.06 ± 0.26	3.46 ± 0.08	303.46 ± 8.50	7.17 ± 0.18
04-N-2 N M2.0	0.39914	0.00220	0.17 ± 0.01	6.01 ± 0.17	1.35 ± 0.09	251.20 ± 19.08	6.54 ± 0.42
03-HC-8D Bulk	0.39182	0.00545	7.29 ± 0.02	36.02 ± 1.69	0.91 ± 0.09	15980.17 ± 1531.09	118.08 ± 11.82
03-HC-8D M0.8	0.40067	0.00531	19.94 ± 0.06	93.61 ± 2.45	2.08 ± 0.09	19098.64 ± 772.35	135.14 ± 5.61
03-HC-8D M0.8rpt	0.39904	0.02518	12.96 ± 0.04	60.17 ± 10.33	4.07 ± 0.64	6329.54 ± 988.26	39.20 ± 9.70
03-HC-8D M1.25	0.40107	0.00523	3.49 ± 0.01	22.77 ± 1.06	0.65 ± 0.09	10656.63 ± 1363.03	103.09 ± 13.32
03-HC-8D M1.25 rpt	0.39907	0.00486	3.42 ± 0.01	20.82 ± 0.97	0.66 ± 0.09	10359.84 ± 1319.98	92.67 ± 11.94
03-HC-8D M 2.0	0.40347	0.00531	1.07 ± 0.01	8.98 ± 0.56	0.34 ± 0.09	6346.77 ± 1558.68	77.22 ± 19.02
03-HC-8D M 2.0 rpt	0.39879	0.00373	1.51 ± 0.01	12.04 ± 0.74	0.32 ± 0.09	9306.20 ± 2391.50	110.36± 28.37
03-HC-8D NM2.0	0.39970	0.00538	0.29 ± 0.01	3.01 ± 0.40	0.08 ± 0.09	7484.33 ± 8185.25	117.98 ± 129.04
03-HC-8D NM2.0 rpt	0.39449	0.00310	0.36 ± 0.01	3.58 ± 0.35	0.14 ± 0.09	5205.64 ± 3148.41	75.12 ± 45.44
03-HC-8D NM2.0 rpt 3	0.40018	0.00250	0.38 ± 0.01	4.26 ± 0.33	0.22 ± 0.09	3431.21 ± 1280.09	53.07 ± 19.81
03-HC-8D NM2.0 rpt 4	0.40660	0.00263	0.38 ± 0.01	4.57 ± 0.28	0.34 ± 0.09	2260.32 ± 545.61	35.17 ± 8.48
03-HC-8F 2 Bulk	0.39916	0.00534	2.40 ± 0.01	25.30 ± 0.97	0.90 ± 0.09	5312.00 ± 493.64	81.69 ± 7.65
03-HC-8F 3 Bulk	0.27055	0.00539	17.01 ± 0.05	56.08 ± 2.05	1.56 ± 0.13	21761.90 ± 1730.72	106.59 ± 8.61
03-HC-8F A NM 1.2	0.39689	0.00273	1.68 ± 0.01	21.98 ± 0.98	0.75 ± 0.09	4948.29 ± 612.67	91.1 ± 11.32

3.91 Nanisivik Results

The NOV-4 pyrite analyses have a consistent range of Re contents between ~2-10ppb and total Os contents between ~35-130ppt. Samples 01-N-D and 04-N-2 were analytically more challenging to measure due to very low Re contents of less than 1ppb, and therefore have significantly larger uncertainties associated with the isotopic measurements. An 11 point, Model 3 regression from these samples corresponds to an age of 1114 ± 120 Ma (MSWD = 297) with an initial $\frac{^{187}Os}{^{188}Os}$ ratio of 1.1 ± 2.7 (Figure 3.8). However, four analyses appear to be associated with the majority of the scatter present (samples NOV4-A, NOV4-D, NOV4-E, NOV4-F). An alternate 7-point regression yields and age of 1094 ± 26 Ma (MSWD = 7.4) with an initial $\frac{^{187}Os}{^{188}Os}$ ratio of 1.55 ± 0.49. Due to the ages calculated above it is safe to attempt Model Age calculations with a $\frac{^{187}\mathrm{Re}}{^{188}Os}$ ratio approaching 2500. With these high $\frac{^{187}\mathrm{Re}}{^{188}Os}$ ratios the initial $\frac{^{187}Os}{^{188}Os}$ ratio is irrelevant and single-analysis Model Ages can be calculated. For sample NOV4-B, a Model Age of 1100 ± 15 Ma is obtained using an initial $\frac{^{187}Os}{^{188}Os}$ ratio of 1.55 ± 0.49, whereas an age of 1112 ± 70 Ma is obtained if an initial $\frac{^{187}Os}{^{188}Os}$ ratio of 1.1 ± 2.7 is used.

3.92 Hawker Creek Results

The Hawker Creek samples have a range of Re contents between 0.3ppb-20ppb. Both 03-HC-8D and 03-HC-8F contain very high $\frac{^{187}Os}{^{188}Os}$ ratios in conjunction with relatively low total Re contents. As such, there was great difficulty obtaining accurate measurements of ^{188}Os, leading to the extremely large correlated uncertainties in the $\frac{^{187}Os}{^{188}Os}$ and $\frac{^{187}\mathrm{Re}}{^{188}Os}$ ratios, as seen in Table 3.3. Not only do individual sample divisions have large errors, but the sample divisions do not lie on any isochron. However, the high

proportion of radiogenic Os in these samples allows for Model Age calculations to be useful. A clear pattern emerges between Re content, magnetic susceptibility, and Model Ages (Figure 3.10). In particular, the higher Re contents are associated with pyrite of higher magnetic susceptibility and younger Model Ages (Table 3.4). The oldest of these Model Ages is quite similar to that of Nanisivik at ~ 1121 Ma whereas the youngest age is ~ 420 Ma.

Table 3.4: Re-Os Model Ages for Hawker Creek samples

Sample	Re Content (ppb)	Model Age (Ma)
03-HC0-8D Bulk	7.29 ± 0.02	438 ± 16
03-HC-8D NM2.0 rpt4	0.38 ± 0.01	898 ± 73
03-HC-8D M2.0	1.07 ± 0.01	716 ± 29
03-HC-8D M1.25	3.49 ± 0.01	572 ± 18
03-HC-8D M1.25rpt	3.42 ± 0.01	528 ± 18
03-HC-8D M0.8	19.94 ± 0.06	420 ± 9.3
03-HC-8D M0.8rpt	12.96 ± 0.04	360 ± 74
03-HC-8F NM 1.2	1.68 ± 0.01	1121 ± 42
03-HC-8F 2 Bulk	2.40 ± 0.01	904 ± 32
03-HC-8F 3 Bulk	17.01 ± 0.05	290 ± 8.4

* All Model Ages assume an initial ratio of 1.1 ± 2.7 and uncertainties are given as 2σ

3.10 Discussion

3.10.1 Constraints on the age of Nanisivik Mineralization from Re-Os geochronology

The isochron diagram from ore stage pyrite at Nansivik suggests a mineralization age of 1114 ± 120 Ma and correlates well with the Model Age of 1112 ± 70 Ma calculated from the most radiogenic sample division. Excluding four analyses that scatter farthest from the 1114 Ma regression line, enables a more precise isochron age (1094 ± 26 Ma) and Model Age (1100 ± 15 Ma) to be obtained. Although there is significant uncertainty in the age of Nanisivik based on these regressions and Model Ages, it is clear that Nanisivik ore stage pyrite is Proterozoic in age based on Re-Os analysis.

One possible explanation for the significant scatter is that the samples chosen could have come from a variety of different fluids and as such, would likely contain variations in the initial $\frac{^{187}Os}{^{188}Os}$ ratio. This is possible given that the isochron is composed

of pyrite from 3 different areas of the deposit that may or may not be directly related to the same fluid. Furthermore, the NOV-4 sample is a banded ore and as such, represents evidence for changing fluid chemistry throughout Nanisivik's history. However, even if drastic changes in fluid chemistry occurred throughout mineralization, the scatter observed in the isochron cannot be entirely accounted for. In particular if it is assumed that all samples formed at ~1100 Ma it would require that some of the sample divisions formed with an impossible negative initial $\frac{^{187}Os}{^{188}Os}$ ratio.

A second possible explanation is that some of the ore has undergone partial recrystallization or chemical alteration in response to secondary fluids events, possibly by the fluids associated with the younger adularia alteration. Mixtures between these altered/recrystallized pyrites and the primary pyrite may account for the scatter, but textural evidence of such effects is not evident. Further studies are needed to follow up on any hypothesis used to explain the scatter seen in the isochron diagrams.

The Nanisivik Re-Os age determination is supported by the 1100 Ma Rb-Sr sphalerite age reported in Christensen et al. (1993), as well as the paleomagnetic age of 1095 Ma reported by Symons et al. (2000), and is within the minimum age constraint provided by the mine dike. Other published ages are more difficult to reconcile with the 3-fold determinations of Re-Os, Rb-Sr and paleomagnetic dating, which at Nanisivik appear well-correlated with one another.

The Pb-Pb galena ages (600-800 Ma) reported in Olsen (1984) are inconsistent with the Re-Os ages determined here. These ages were calculated based on a particular two stage evolution of Pb in the Borden basin. However, there may be insufficient knowledge of the evolution of Pb in the basin to properly interpret the Pb-Pb data published in Olsen (1984). Complicating the story is that secondary mineralization and/or alteration has taken place at both Nanisivik and Hawker Creek. At Nanisivik there is even some degree of galena mineralization/recrystallization associated with the later stage adularia alteration (Sherlock et al., 2004). Therefore, the complex behaviour of the Pb isotope system appears to give a spurious age for both Nanisivik and Hawker Creek. For other locations within the Borden basin Olsen (1984) reports Pb isotope data that correspond to Model Ages of ~1.0Ga.

The Palaeozoic age of 461 Ma by Sherlock et al. (2004) is likely not related to primary sulphide mineralization. It is likely the adularia was formed from a completely separate fluid event, perhaps even causing the scatter seen in the Nansivik pyrite Re-Os isochron. Although younger fluid flow events are not recorded from the Hawker Creek area, the similarity in age between the 461 Ma adularia alteration at Nanisivik and the youngest ~420 Ma Re-Os pyrite Model Ages calculated for Hawker Creek, suggests a younger Paleozoic event may be more widespread than Nanisivik .

3.10.2 Timing of mineralization elsewhere in the Borden basin

The Hawker Creek data in conjunction with the Nansivik ages currently provides the best opportunity to address the question of whether or not the various sulphide occurrences in the Borden basin are temporally related.

The complex data for Hawker Creek requires special care when interpreting. In particular, the fact that there is strong coupling between the trace element contents and Re-Os Model Ages suggest that multiple events have been recorded in the pyrite at Hawker Creek. For simplicity, it could be proposed that only two separate events have been recorded, although that doesn't preclude the possibility that other fluid events have also been recorded. The two best defined end member ages for Hawker Creek are 1121 ± 42 Ma and 420 ± 9.8 Ma. These ages can be treated as constraints on the presumed two events preserved at Hawker Creek. The younger age is associated with the highest Re and highest magnetic susceptibility pyrite, whereas the older age is correlated with lowest Re contents and lowest magnetic susceptibility in pyrite. Whether the Re associated with this younger age is due to growth of new pyrite, recrystallization, or chemical alteration of primary pyrite remains unclear. What is clear is that no obvious zonation or recrystallization can be seen in optical, backscattered electron, or element map images for Hawker Creek pyrite (Figure 3.7). Based on these observations, the simplest interpretation is that chemical overprinting that took place at ~420 Ma on the ~1120 Ma primary pyrite.

The younger alteration event at Hawker Creek is similar in age to the adularia alteration seen at Nanisivik. Together these ages provide evidence for active fluid flow in the Borden basin during the Palaeozoic. At this point there is no evidence that the

Palaeozoic fluid flow is related to large scale sulphide mineralization within the Borden basin. This is in contrast to Mesoproterozoic fluid flow at ~1100 Ma, which appears responsible for mineralization at Nanisivik, Hawker Creek, and presumably other sulphide prospects in the Borden basin. A summary of these results are presented in Figure 3.11.

Although the age of Hawker Creek mineralization was previously unknown, it is proposed that initial mineralization took place around 1121 Ma based on the Re-Os pyrite data obtained here. This age overlaps with that of mineralization at Nanisivik and suggests these mineralizing events are temporally related to the same general process of basinal fluid flow. This is supported in part by the Pb-Pb data from Olsen (1984), which gave similar age ranges for both Hawker Creek and Nanisivik. In absolute terms, the Olsen (1984) dates do not appear to have been correct, the relative ages may still be valid if it is assumed that Nanisivik and Hawker Creek had their Pb evolve in a similar, albeit unknown fashion.

3.11 Conclusion

Radiometric dating of Nanisivik using Re-Os in pyrite, coupled with previous Rb-Sr studies on sphalerite, and paleomagnetism, place the timing of mineralization squarely in the Proterozoic, likely at ~1100 Ma. Similar ages for both Nanisivik and Hawker Creek bolster the idea that mineralization in the basin may be temporally and perhaps genetically connected with the processes responsible for formation of the Borden basin. All major mineralization so far appears to be linked to fluid flow in the Mesoproterozoic, but overprinting by later Palaeozoic fluids also appears to have occurred. These ages put Nansivik and related Pb-Zn showings into the rare class of Precambrian hosted MVT systems. This knowledge will be invaluable for any future research that deals with the evolution and characterization of MVT deposits through time. It is clear that MVT style mineralization can occur during the Proterozoic while still being preserved to the present day.

3.12 References

Arne, D.C., and Kissin, S.A., 1989, The significance of “diagenetic crystallization rhythmites” at the Nanisivik Pb-Zn-Ag deposit, Baffin Island, Canada: Mineralium Deposita, v. 24, p. 230–232.

Arne, D.C., Curtis, L.W., and Kissin, S.A. 1991, Internal zonation in a carbonate-hosted Zn-Pb-Ag deposit, Nanisivik, Baffin Island, Canada: Economic Geology, v. 86, p. 699–717.

Christensen, J.N., Halliday, A.N., Kesler, S.E., and Sangster, D.F., 1993, Further evaluation of the Rb-Sr dating of sphalerite: the Nanisivik Precambrian MVT deposit, Baffin Island, Canada [abs.]: Geological Society of America Abstracts with Programs v. 25, p.471.

Denyszyn, S.W., Davis, D.W., and Halls, H.C., 2009, Paleomagnetism and UPb geochronology of the Clarence Head dikes, Arctic Canada: Orthogonal emplacement of mafic dikes in a large igneous province: Canadian Journal of Earth Sciences, v. 46, p. 155–167.

Fahrig, W.F., Christie, K.W., and Jones, D.L., 1981, Paleomagnetism of the Bylot basins: evidence for Mackenzie continental tensional tectonics: Geological Survey of Canada Paper 81-10, p. 303–312.

Gleason, J.D., Gutmer, J., Kesler, S.E., Zwingmann, H., 2011, 2.05-Ga Isotopic Ages for Transvaal Mississippi Valley–Type Deposits:Evidence for Large-Scale Hydrothermal Circulation around the Bushveld Igneous Complex, South Africa: The Journal of Geology, 2011, volume 119, p. 69–80.

Heaman, L.M., LeCheminant, A.N., and Rainbird, R.H., 1992, Nature and timing of Franklin igneous events, Canada: Implications for a Late Proterozoic mantle plume and the breakup of Laurentia: Earth and Planetary Science Letters, v. 109, p. 117–131.

Jackson, G.D., and Iannelli, T.R., 1981, Rift-related cyclic sedimentation in the Neohelikian Borden basin, northern Baffin Island: Geological Survey of Canada Paper 81-10, p. 269–302.

Leach, D.L., Taylor, R.D., Fey, D.L., Diehl, S.F., and Saltus, R.W., 2010, A deposit model for Mississippi Valley-Type lead-zinc ores, chap. A *of* Mineral deposit models for resource assessment: U.S. Geological Survey Scientific Investigations Report 2010–5070–A, 52 p.

LeCheminant, A.N., and Heaman, L.M., 1989, Mackenzie igneous events, Canada: Middle Proterozoic hotspot magmatism associated with ocean opening: Earth and Planetary Science Letters, v. 96, p. 38–48.

Ludwig, K.R., 2001, Isoplot 3.0—A geochronological toolkit for Microsoft Excel: Special publication No. 4, Berkeley Geochronology Center, Berkeley, Calif., 71 p.

McNaughton, K. C. (1983) A fluid inclusion study of the Nanisivik lead-zinc deposits, Baffin Island, N.W.T. Unpublished M.A.Sc. Thesis, University of Windsor.

Olson, R.A., 1984, Genesis of paleokarst and strata-bound zinc-lead sulfide deposits in a Proterozoic dolostone, northern Baffin island, Canada: Economic Geology, v. 79, p. 1056–1103.

Pehrsson, S.J., and Buchan, K.L., 1999, Borden dikes of Baffin Island, N.W.T.: A Franklin U-Pb baddeleyite age and a paleomagnetic interpretation: Canadian Journal of Earth Sciences, v. 36, p. 65–73.

Scott, D.J., and deKemp, E.A., 1998, Bedrock geology compilation, northern Baffin Island and northern Melville Peninsula: Geological Survey of Canada Open File 3633.

Sherlock, R.L., Lee, J.K.W. and Cousens, B.L., 2004, Geologic and geochronologic constraints on the timing of mineralization at the Nanisivik zinc-lead Mississippi Valley-type deposit, northern Baffin Island, Nunavut, Canada: Economic Geology, v. 99, p. 279–293

Sherman, A.G., James, N.P., and Narbonne, G.M., 2002, Evidence for reversal of basin polarity during carbonate ramp development in the Mesoproterozoic Borden basin, Baffin Island: Canadian Journal of Earth Sciences, v. 39, p. 519–538.

Sutherland, R.A. and Dumka, D., 1995, Geology of Nanisivik mine: Society of Economic Geologists Guidebook Series 22, p. 4–12.

Symons, D.T.A., Symons, T.B., and Sangster, D.F., 2000, Paleomagnetism of the Society Cliffs dolostone and the age of the Nanisivik zinc deposits, Baffin Island, Canada: Mineralium Deposita, v. 35, p. 672–682.

Turner, E.C., 2009, Mesoproterozoic carbonate systems in the Borden basin, Nunavut: Canadian Journal of Earth Sciences, v. 46, p. 915–938.

Turner, E.C., 2011, Structural and Stratigraphic Controls on Carbonate-Hosted Base Metal Mineralization in the Mesoproterozoic Borden basin (Nanisivik District), Nunavut Economic Geology, v. 106, p. 1197–1223.

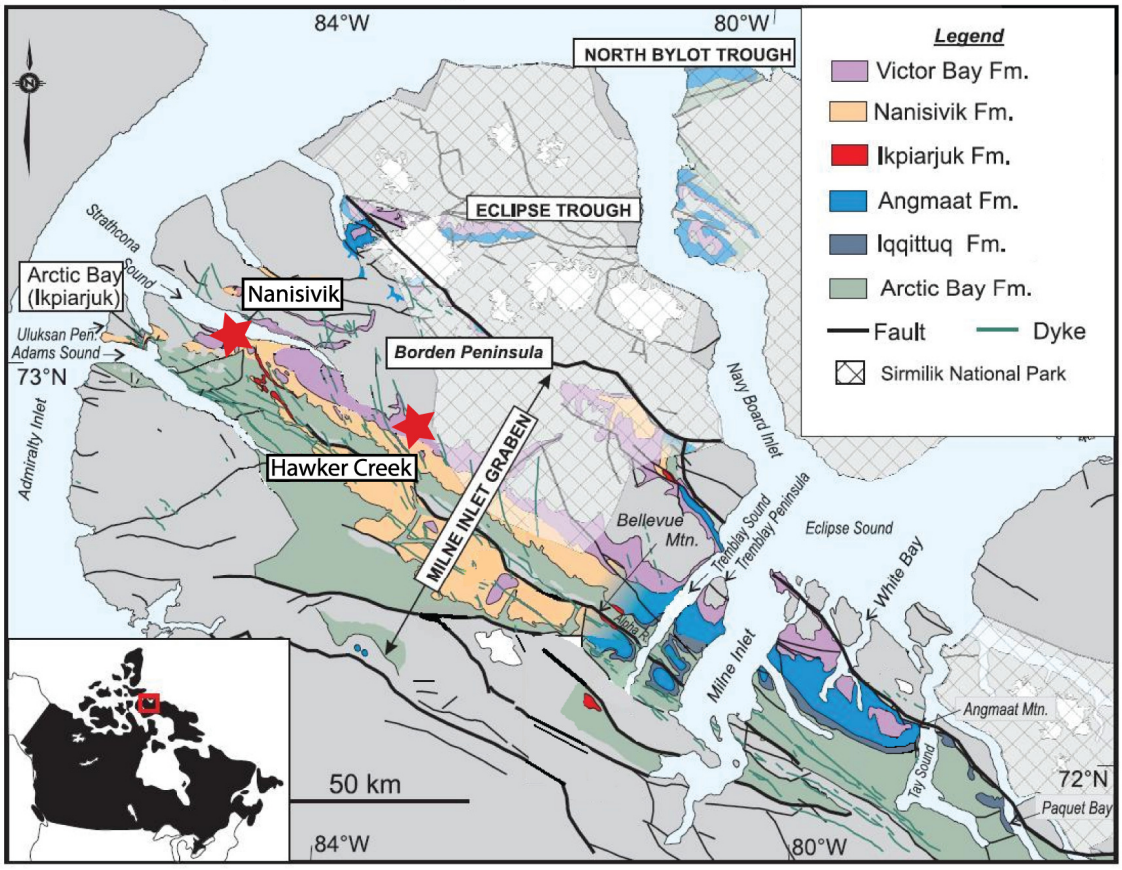

Figure 3.1: Borden basin of Baffin Island (modified from Turner, 2009).

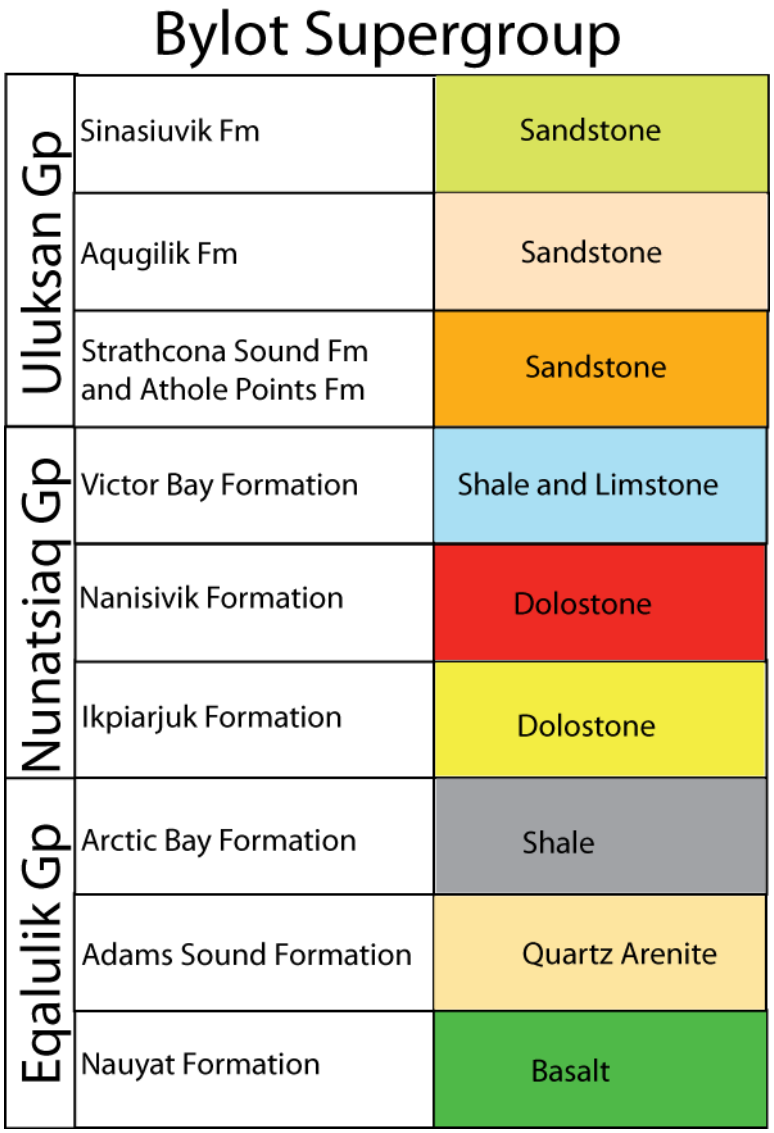

Figure 3.2: Basic stratigraphy of Bylot Supergroup.

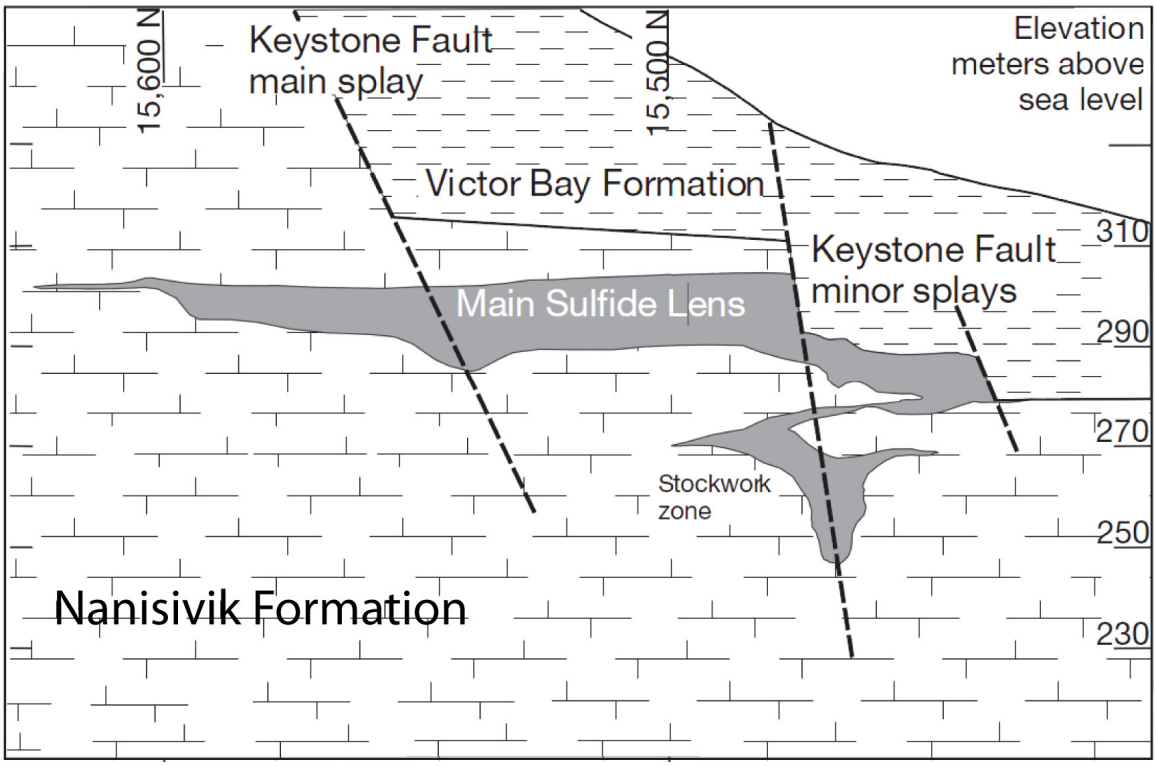

Figure 3.3: Nanisivik Mineralization (modified from Sherlock et al., 2004).

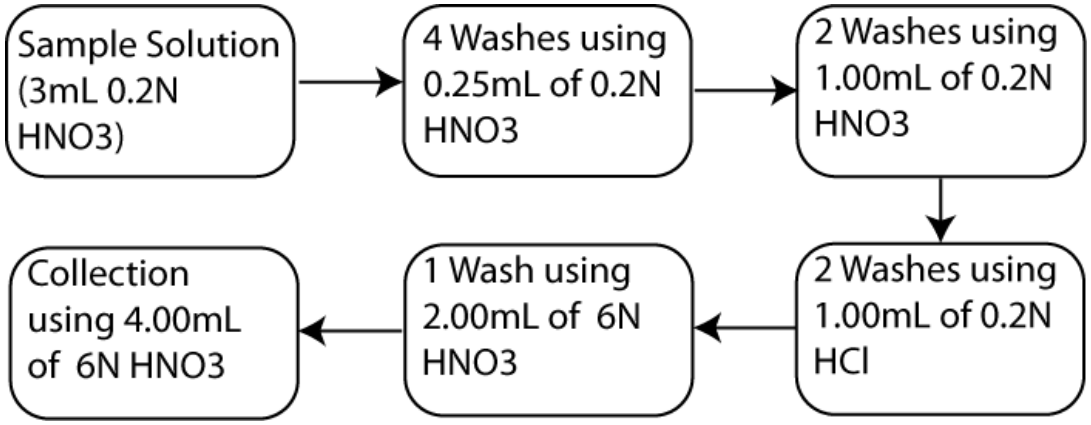

Figure 3.4: Rhenium column chromatography procedure.

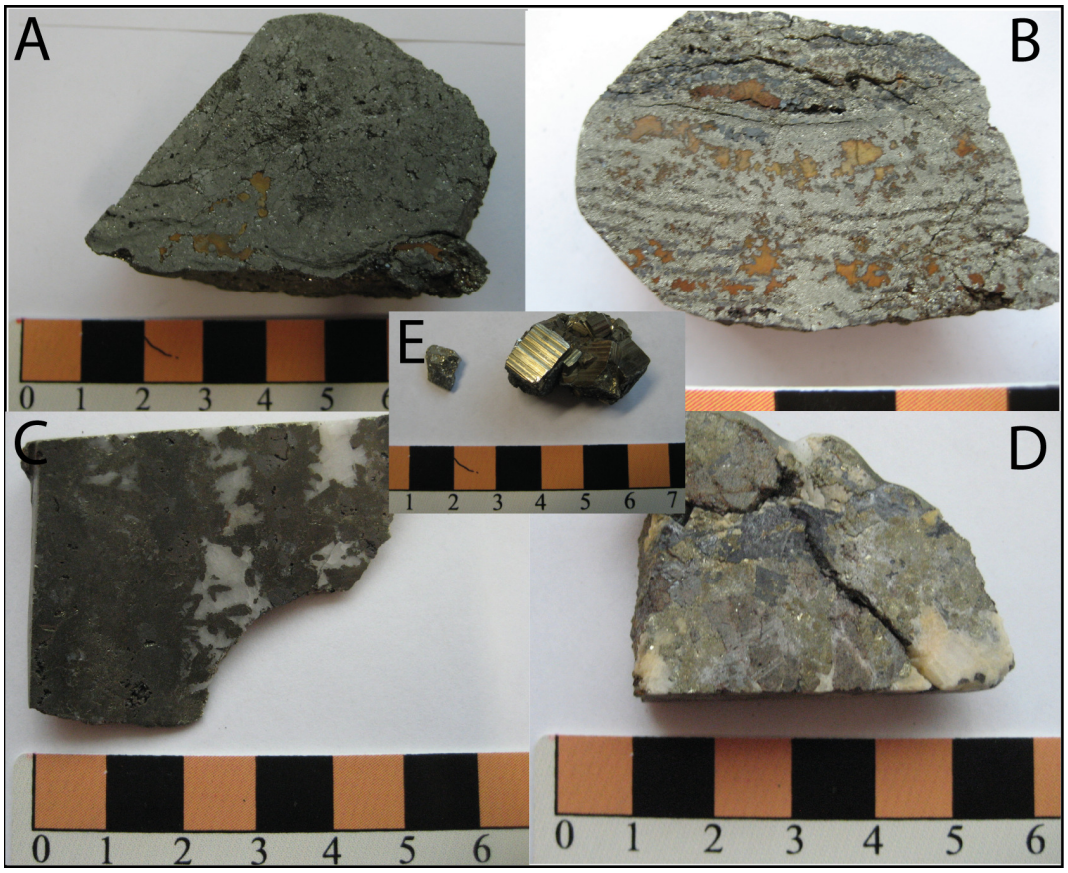

Figure 3.5: Samples selected for Re-Os analysis. A) 03-HC-8D, B) 03-HC-8F, C) 04-N-2, D) NOV4, E) 01-N-D.

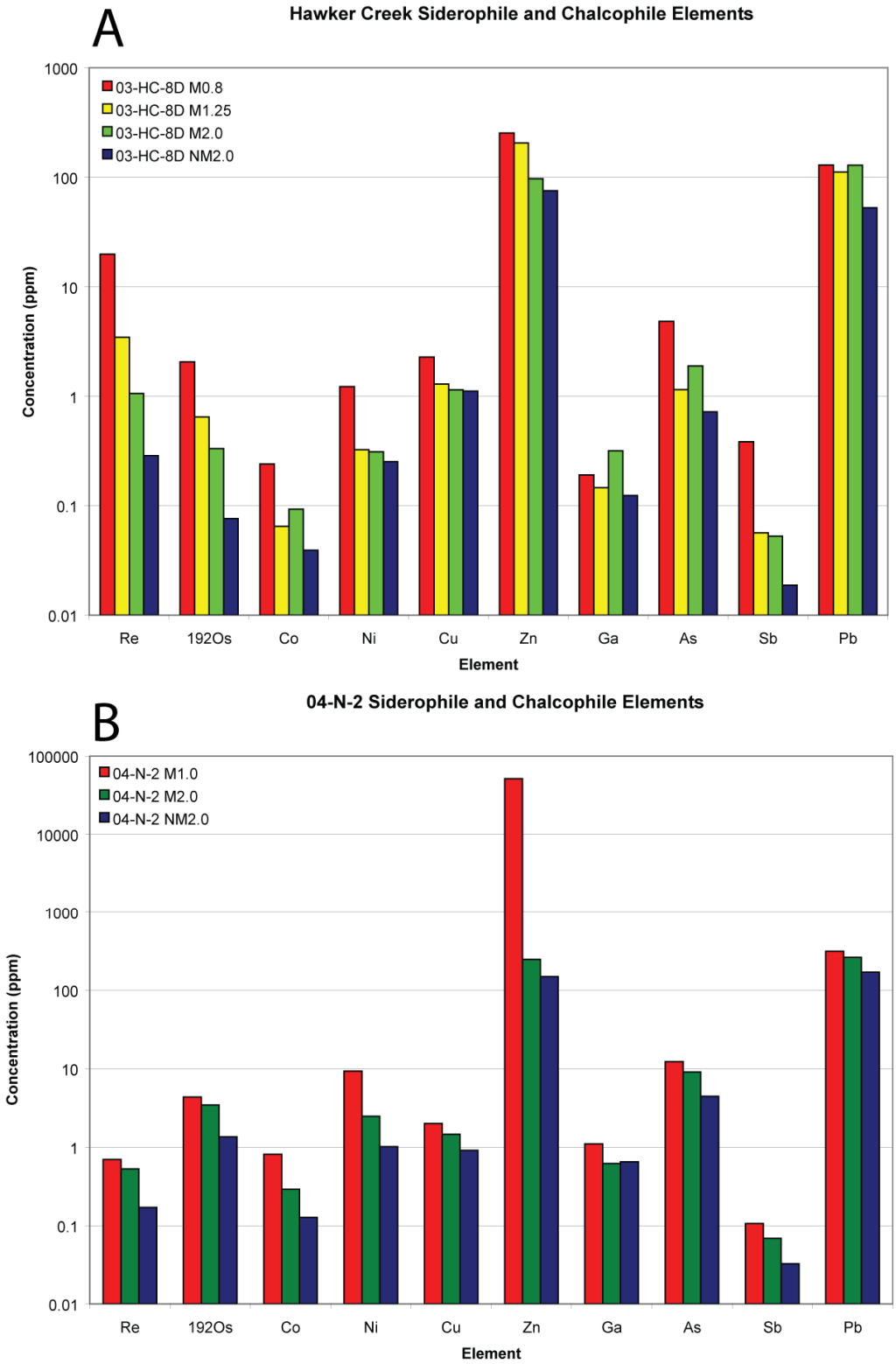

Figure 3.6: Trace element analyses for Hawker Creek (A) and Nanisivik (B). Concentrations for Re are given in ppb, and concentrations of Os are given in ppt.

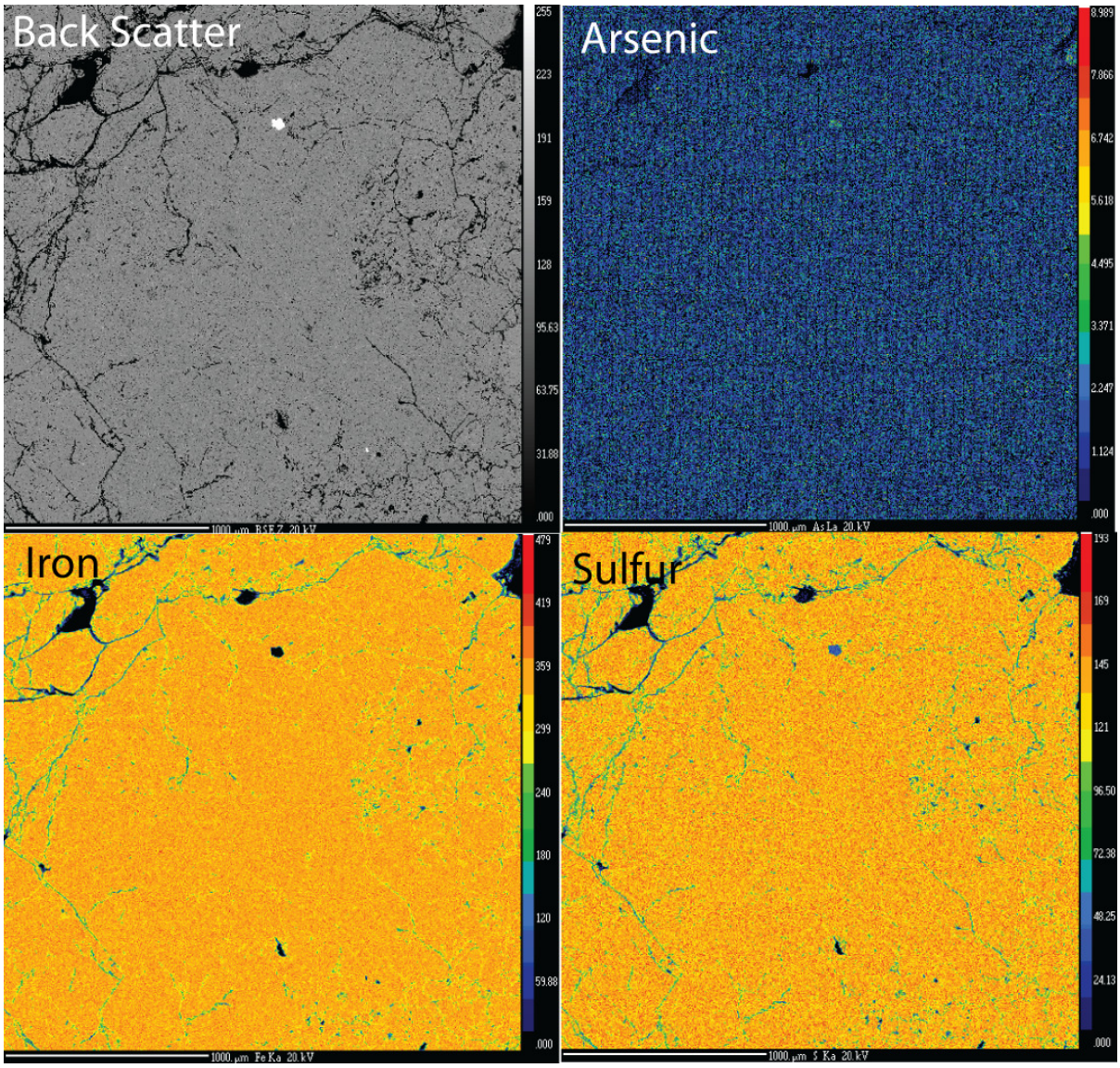

Figure 3.7: Sample 03-HC-8D images showing no discernable zonation in backscattered images or elemental maps.

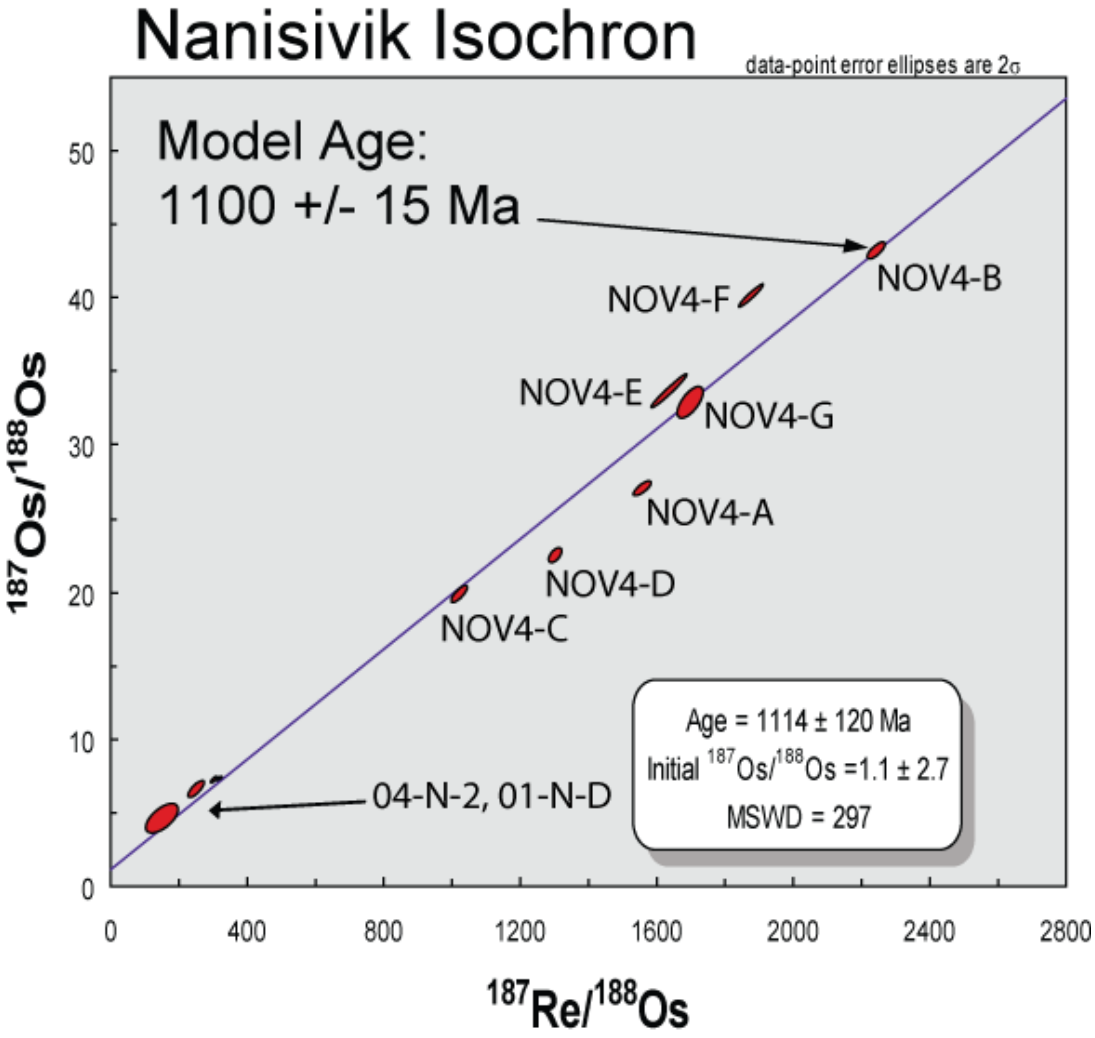

Figure 3.8: Isochron diagram and associated Model Age for Nanisivik. Some data points labelled for clarity.

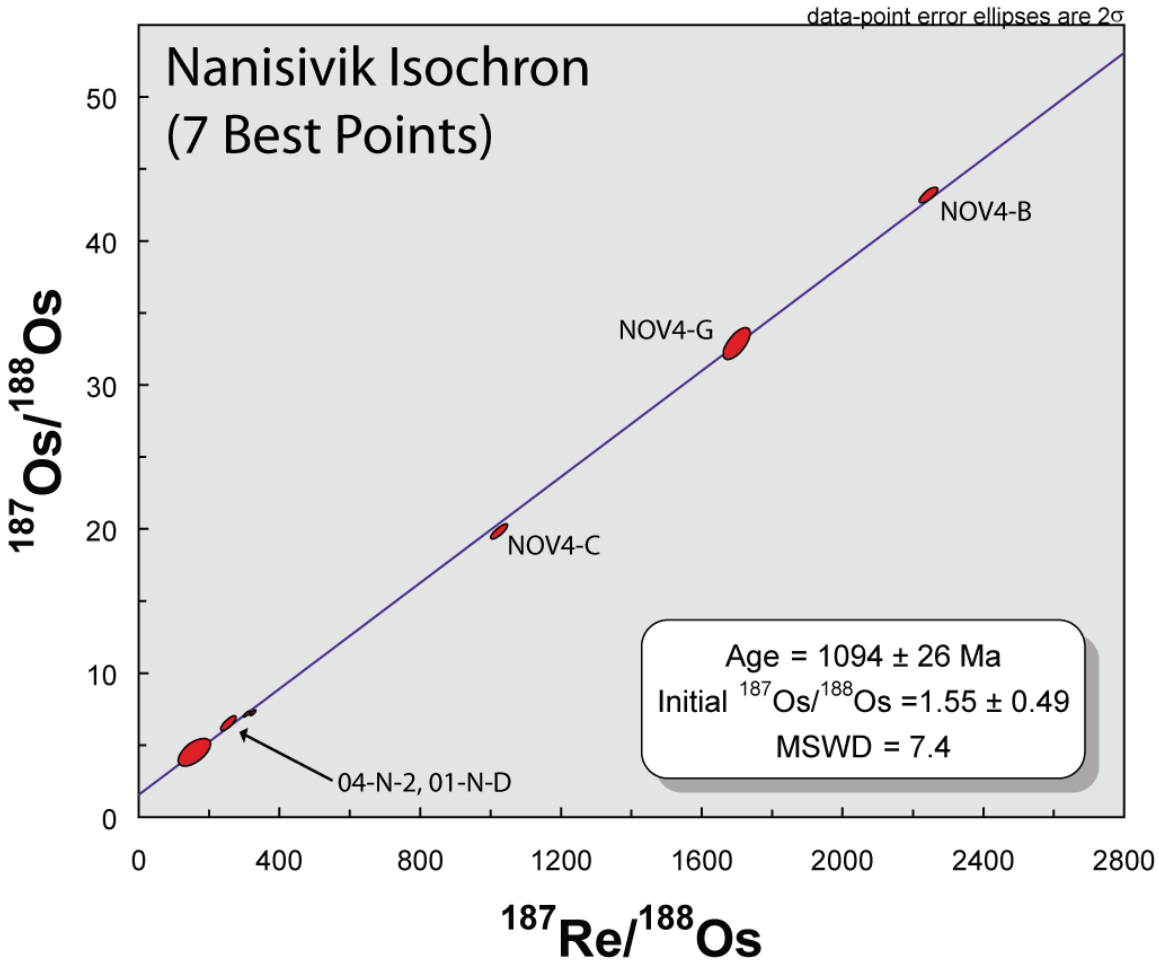

Figure 3.9: Isochron diagram using best 7 data points for Nanisivik. Some data points labelled for clarity.

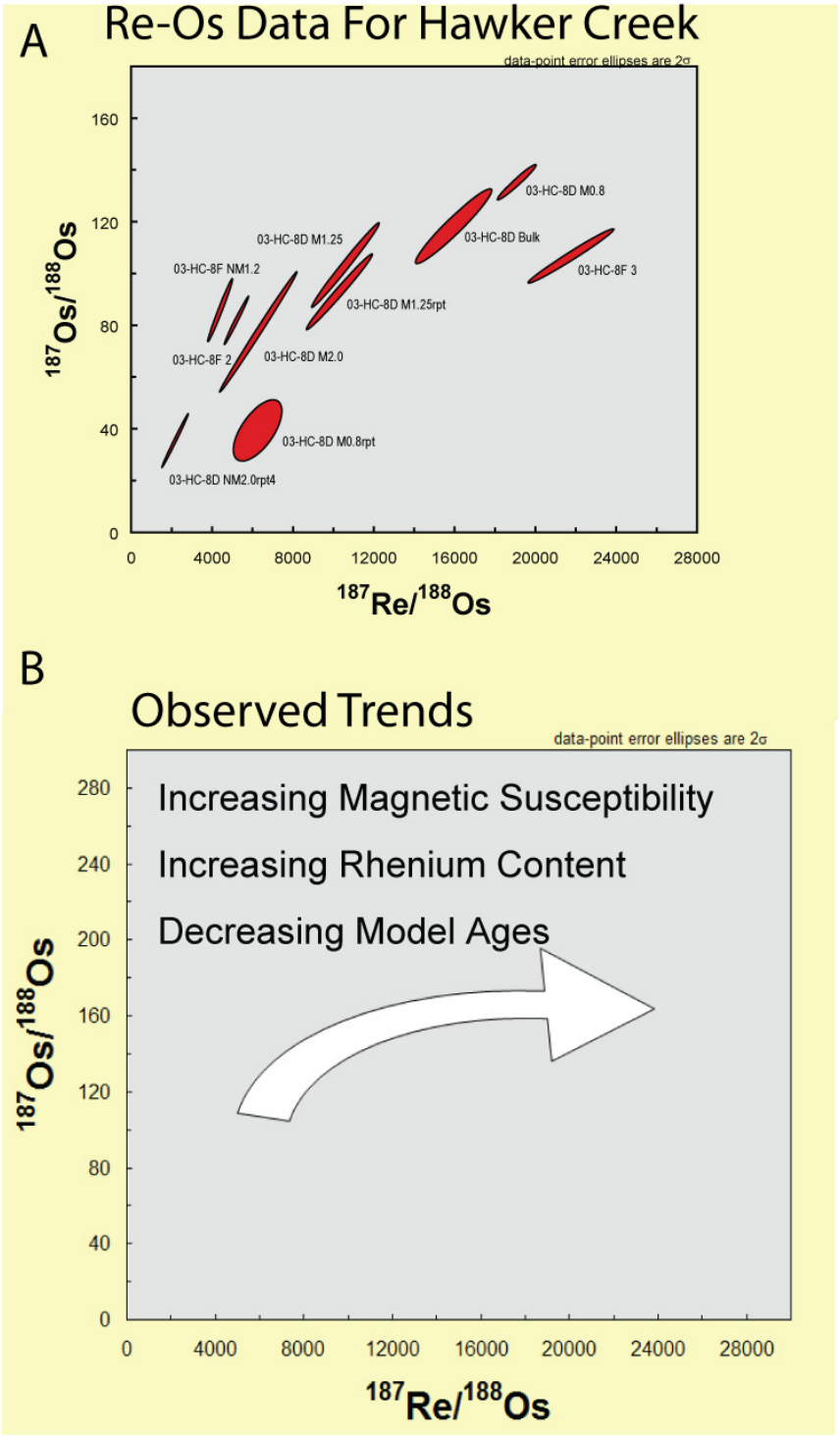

Figure 3.10: Re-Os data for Hawker Creek. A) Sample $\frac{^{187}Os}{^{188}Os}$ and $\frac{^{187}\mathrm{Re}}{^{188}Os}$ data points B) Observed trends for the Re-Os data.

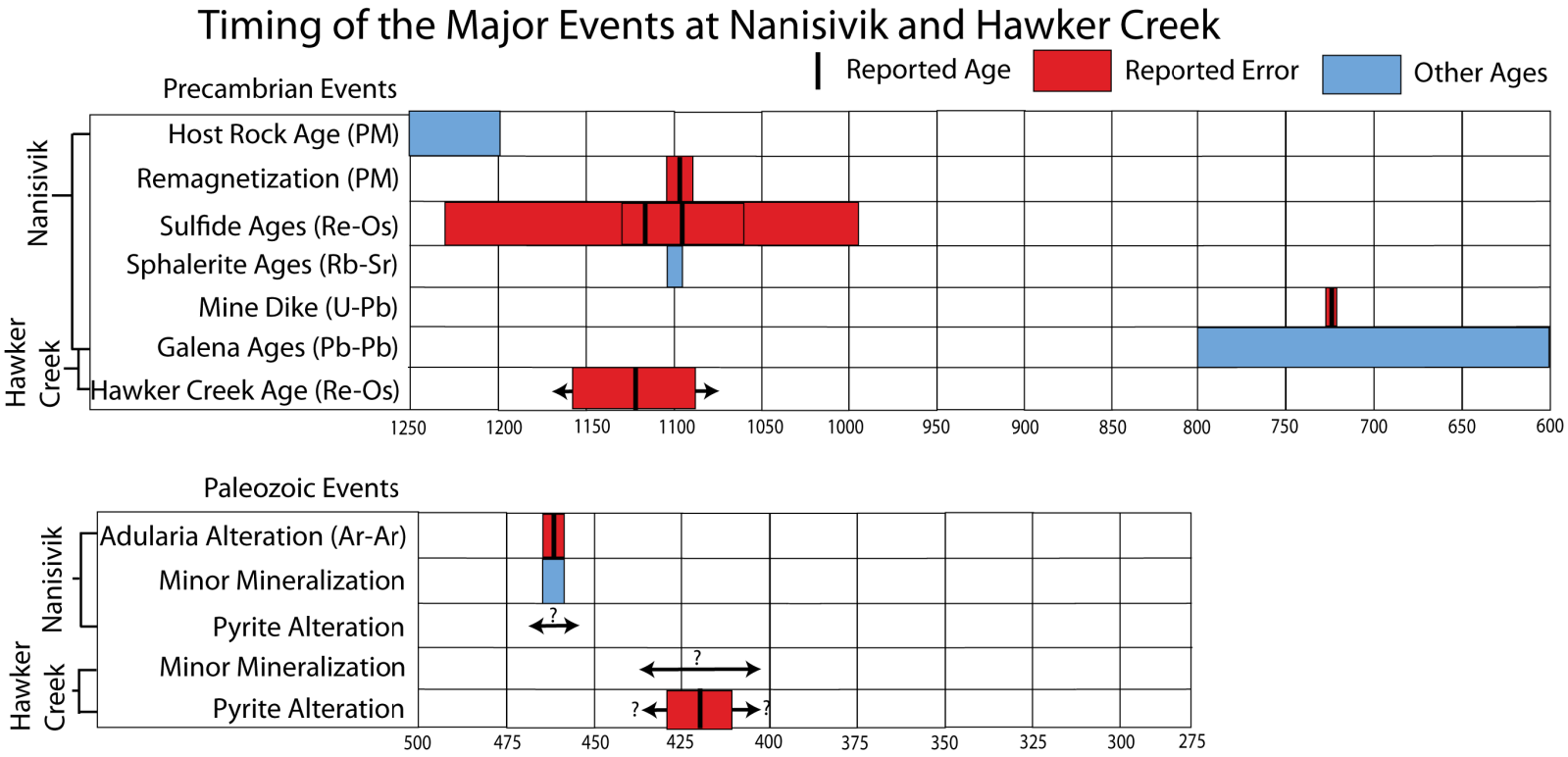

Figure 3.11: Timing of major events at Nanisivik and Hawker Creek

4.0 Supplementary Findings and Conclusions

4.1 Magnetic Properties of Minerals

4.11 Introduction

The magnetic behaviour of minerals can be used for both mineral separation (See Appendix I for details) and to track variations within crystals. The most common types of magnetization associated with minerals are diamagnetic, paramagnetic, ferromagnetic, and antiferromagnetic. Purely diamagnetic materials are slightly repelled by external magnetic fields; examples of these include quartz, calcite, and pyrite. Paramagnetic materials, like many iron bearing minerals, are attracted by magnetic fields. Ferrimagnetic and antiferromagnetic materials contain localized zones known as domains that have a specific magnetization. In ferrimagnetic materials the domains line up such that there is a net magnetic moment, examples of such minerals are pyrrhotite and magnetite. Ideal ntiferromagetic materials carry no net magnetic moment, but in practice minerals typically have structural defects that will give these materials a variable magnetic moment; an example of such a mineral is hematite.

A particularly important parameter that characterizes the strength of magnetization of a mineral in a magnetic field is called magnetic susceptibility. Magnetic susceptibilities can be negative, as in diamagnetic minerals, or positive in the case of paramagnetic and ferromagnetic minerals. Magnetic susceptibility varies from mineral to mineral based on its composition and structure.

In nature, pure minerals and rocks are exceedingly rare and impurities cause a mineral to diverge from its ideal magnetic properties. Within single crystals, minor elements, trace elements, grain size, and crystal structure can cause variations in magnetic susceptibility (Beegart and Seehra, 1977; Dekkers, 1988). Mineral impurities also dictate the measured magnetic susceptibly of a sample. This effect is especially important if grains of magnetite or pyrrhotite are present in the sample. Together, these factors often cause large variations in magnetic susceptibility between different minerals and rocks.

4.12 Measuring Magnetic Behaviour

Relative differences in magnetic susceptibility were measured on a Frantz isodynamic separator. Absolute measurements of magnetic susceptibility were not measured due to lack of calibration for the Frantz isodynamic separator. For magnetic separation, all samples were crushed to a similar in grain size (~100μm) and were run using the same slope settings (see Appendix I). The magnetic field produced by the Frantz isodynamic separator is controlled by the current applied to the electromagnet. The current is set at a point where the force between a mineral grain and the magnet can overcome that of the force of gravity. The current at which a mineral is separated gives an indirect measurement of its magnetic susceptibility. For example, a mineral fraction that is separated out at a high current will have a relatively low magnetic susceptibility, whereas a fraction that is separated out at low current will have a correspondingly high magnetic susceptibility.

4.13 Magnetic Behaviour of Case Study 1 and Case Study 2

Both case studies contained samples of similar mineralogy. In general, samples were composed of pyrite, sphalerite, galena, calcite, and dolomite. It is expected that these minerals should be dominated by diamagnetic behaviour if they are free of impurities. However, this is not observed, as all minerals were measured to have positive magnetic susceptibility. The range of current required to magnetically separate a mineral varies depending on the sample (Table 2.3). Both pyrite and sphalerite typically have a large range in magnetic susceptibility, whereas galena typically has a much lower magnetic susceptibility and it is typically found in the non-magnetic division of a sample.

4.14 Relationship to Trace Element Content

A direct correlation between magnetic susceptibility and trace element contents is observed in the Nansivik and Lisheen data (Chapters 2 and 3). In particular, the ICP-MS and TIMS measurements of Ni, Co, Cu, As, Re, and Os contents are generally enriched in divisions with higher magnetic susceptibility. These trace element trends can be linked to changes in pyrite, since pyrite contains the highest concentration of these trace elements.

The relationship between the different elements and magnetic susceptibility allows elements with of high concentrations (e.g. As) to as act as a proxy for those at lower concentrations (e.g. Re). This was used in Case Study 1 to investigate possible locations of Re enrichment in microprobe images.

4.14 Rhenium Enrichment

The link between magnetic susceptibility and Re concentration is particularly interesting for Re-Os geochronology. There is a clear correlation between high Re contents and high magnetic susceptibility seen in all samples studied (Figure 4.1, 4.2, 4.3). A common observation is that the Re content within a single sample can vary by up to an order of magnitude. Looking at a deposit as a whole, such as Lisheen, it is possible to find pyrite that differs in Re contents by a factor of 5000 as seen with samples LK 8S08 NM1.5 and LK 359 M0.6.

The observed behaviour of Re and other trace elements with respect to magnetic susceptibility strongly suggests that they are all spatially related within the crystal structure. Magnetic separation therefore allows Re-Os geochronology to probe smaller scale features than would typically be accessible for a bulk analysis technique. Additionally, magnetic separation also allows the extraction of Re bearing material from relatively barren material (e.g. 01-N-D).

4.15 Origin of Magnetic Susceptibility

It is clear from all measurements that minerals have deviated from their ideal magnetic character. Both mineralogical and chemical impurities may be the cause of these deviations. The fact that higher trace element concentrations are associated with higher magnetic susceptibility suggests that trace element concentrations may be partly responsible for the measurements. However, there is no quantitative link between the two. The most extreme examples of this are seen when comparing Hawker Creek to Lisheen. Between these two deposits the sulphides have overlapping ranges in magnetic susceptibility, however, their bulk trace element contents are in some cases several orders

of magnitude different. This suggests that bulk trace element content is not the main control on magnetic susceptibility.

Mineral impurities such as pyrrhotite and magnetite are not known to exist in any of the samples studied based on thin section and microprobe examination. However, based on the measurements of Pannalal (2008) single domain magnetite grains are found in samples throughout Lisheen. Unfortunately, these grains are likely too small to be measured or mapped out, therefore any link between these magnetite grains and areas of trace element enrichment cannot be explored. Furthermore, it is unknown if the concentration of these single domain magnetite crystals is sufficient to even explain the magnetic behaviour seen.

The root causes of both magnetic susceptibility and its relationship to trace elements such as Re remains enigmatic.

4.2 Carbonate Rhenium Contents

Carbonate minerals would not typically be expected to contain large amounts of chalcophile elements such as Re or Os due to carbonates being lithophile in nature. However, analysis of carbonates from Lisheen and Galmoy show that Re and Os are present in significant quantities. In fact, when comparing the Re contents in the carbonate to that of the related sulphides it appears that a substantial fraction of the Re contained within the rock can be found within the carbonates (Figure 4.4). This is quite surprising as it would be expected that chalcophile elements would preferentially substitute inside sulphide minerals.

It is unclear where the Re would be located inside these carbonates. One possibility is within fluid inclusions, however, this would require either carbonates to contain a large proportion of fluid and/or that the fluids themselves would have very high Re contents. Another possibility is that sulfide inclusions provide the rhenium, however to explain to observed concentration, these sulfides would require much higher Re content than would be expected for a given sample. These possibilities are probably unrealistic, and therefore Re may be present within the carbonate structure itself. Rhenium would likely be restricted to substituting in the Fe or Mg layers present within a carbonate structure, due to these elements having a similar ionic radius. However, due to

lack of proper constraint on rhenium's ionic radii(s) at appropriate oxidation states, coordination number, and atomic environment, this substitution into the carbonate structure is purely speculative. Although much more study is required, carbonates are a candidate for further Re-Os geochronology research, as there is enough Re in at least these particular samples to theoretically produce an isochron. Questions, such as how robust such an isochron would be, and whether these high Re contents are seen in other samples beyond the hydrothermal carbonates of Lisheen and Galmoy, will need to be answered in the future.

At the very least these observation emphasize the need for purified samples when undertaking Re-Os geochronology, because any impurities may, and often do, contain sufficient Re contents to skew any results.

4.3 Applicability of Re-Os Geochronology to Carbonate-Hosted (MVT) Pb-Zn Ore Deposits

Rhenium contents within the pyrite associated with the MVT deposits studied are highly variable, ranging from below detection limits in a few of the Nanisivik sulphide divisions (< 0.2ppb) to greater than 1ppm in some samples from Lisheen. However, in the two cases studied here, it has been established that pyrite can contain sufficient Re contents to potentially produce an isochron or Model Age, enabling valuable age constraints to be placed on a class of ore deposits hitherto difficult to date.

The major complexity seen in the Re-Os data for these deposits, is that there are often multiple fluid events responsible for ore formation and subsequent alteration. This causes variability in the trace elements contents, textures, and magnetic susceptibilities in samples. Variability often occurs on sub-millimetre scales, which makes it next to impossible to extract single generation mineral separates from a sample for Re-Os analysis. This can potentially lead to significant scatter if the different generations of fluids contain different Os isotope ratios, or had occurred at vastly different times.

Due to these complexities it is extremely important to carefully select any samples that are to be analyzed for Re-Os geochronology. For the best results, single generation pyrite should be analyzed. In some cases, this will be impossible due to the complex intergrowth and alteration, as was seen in the majority of the samples studied. The

samples that are likely to have the most success will be massive sulphides that have only minor variations in trace element contents (e.g. LK 8S08). However, there were notable examples in Case Study 2 where even massive sulphides have isotopic complexities that are not evident by regular imaging methods (i.e. 03-HC-8D).

To best deal with these complications it may be best to prepare a sample by magnetic separation as opposed to hand picking separates. This gives the best chance to separate the different growth zones within the sulphides as different magnetic susceptibility appears to be associated with areas containing different trace element contents. Additionally, this can provide age information that would otherwise be overlooked, as was seen with the Hawker Creek samples.

4.4 Implications for Mineral Prospectivity

Knowing the age of mineralization for any ore deposit, and especially for deposits formed in sedimentary basins like carbonate-hosted Pb-Zn ore deposits, has specific applications for future exploration. Since these ore deposits are formed by fluid flow in a basin, knowing the age of fluid flow as well as constraining fluid origin(s) can help focus any future exploration. Dating ore deposits and obtaining an accurate time for their mineralization is equivalent to obtaining information the age of these important fluid events that initiated mineralization at a specific deposit. If it is assumed or known that these fluids existed in a larger scale region outside the immediate vicinity of the known ore deposit, then these mineralization ages can help put age constraints on the possible age of host rocks for undiscovered ore deposits. Additionally, dating several deposits or prospects can strengthen this argument if they are found to have formed at the same time. Knowing the age of the deposit also helps pin down its associated formation mechanism. Knowing how a deposit forms constrains the types of structures, fluids, and rocks that are required to initiate mineralization, an invaluable tool for future exploration.

The dating of the Lisheen deposit has significant implications for future exploration of Irish-type deposits throughout Ireland. From this research both Lisheen and Galmoy appear to be of Early Carboniferous origin, and therefore future prospecting in the Rathdowney trend should focus on the Waulsortian limestone as the potential hosts of economic mineralization. Now that the paleomagnetic ages of other ores in the Irish

ore field have been put in question a Early Carboniferous age is now more likely to be ubiquitous throughout the region. Irish-type ores in Ireland are likely to be restricted to the lowest clean carbonates from a particular district, as has been described in Wilkinson et al. (2005), but now with an additional requirement that the these carbonates must be from the Early Carboniferous.

Turner (2011) provides relevant descriptions of the mineralization styles in the Borden basin, as well as a discussion of metal prospectively within this basin. The geochronology of Nansivik and of Hawker Creek updates Turner (2011) by restricting economic mineralization in the Borden basin to the Proterozoic. Therefore carbonates with ages of ~1100Ma or older would be a requirement for carbonates to host economic Pb-Zn mineralization within the Borden basin. Younger fluids events associated with the younger Hawker Creek Model Ages and the adularia from Nanisivik (Sherlock et al. 2004) are not known at this time to be associated with primary mineralization. However, until these fluid are better understood, mineralization associated with these fluids cannot be entirely ruled out.

4.5 References

Burgardt, P. and Seehra, M.S., 1977, Magnetic Susceptibility of Iron Pyrite (FeS_2) Between 4.2 and 620K: Solid State Communications, Vol.22, pp. 153-156

Dekkers, M. J., Magnetic properties of natural pyrrhotite Part I: Behaviour of initial susceptibility and saturation-magnetization-related rock-magnetic parameters in a grain-size dependent framework, Physics of the Earth and Planetary Interiors, Volume 52, Issue 3-4, p. 376-393.

Pannalal, S.J., Symons, D.T.A., Sangster, D.F., 2008, Paleomagnetic Evidence for an Early Permian Age of the Lisheen Zn-Pb Deposit, Ireland: Economic Geology, v.103, p.1641-1655.

Sherlock, R.L., Lee, J.K.W. and Cousens, B.L., 2004, Geologic and geochronologic constraints on the timing of mineralization at the Nanisivik zinc-lead Mississippi Valley-type deposit, northern Baffin Island, Nunavut, Canada: Economic Geology, v. 99, p. 279–293.

Turner, E.C., 2011, Structural and Stratigraphic Controls on Carbonate-Hosted Base Metal Mineralization in the Mesoproterozoic Borden basin (Nanisivik District), Nunavut Economic Geology, v. 106, p. 1197–1223.

Wilkinson, J.J., Eyre, S.L., and Boyce, A.J., 2005, Ore-forming processes in Irish-type carbonate-hosted Zn-Pb deposits: Evidence from mineralogy, chemistry, and isotopic composition of sulfides at the Lisheen mine: Economic Geology , v. 100, p. 63–86.

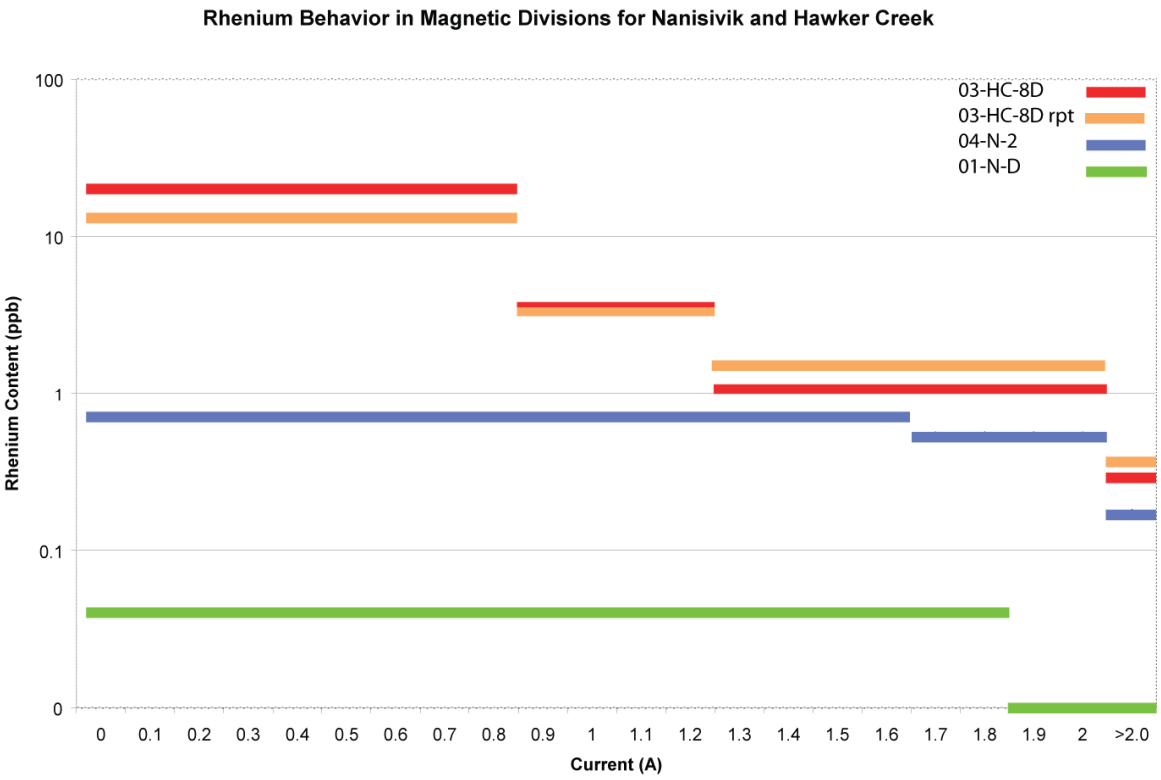

Figure 4.1: The behaviour of rhenium in a variety of magnetic divisions for Nanisivik and Hawker Creek. The general trend seen is as currents increased there is a corresponding decrease in rhenium content.
* Horizontal lines represent a magnetic division that contains minerals that become "strongly magnetic" somewhere within the stated range of currents.

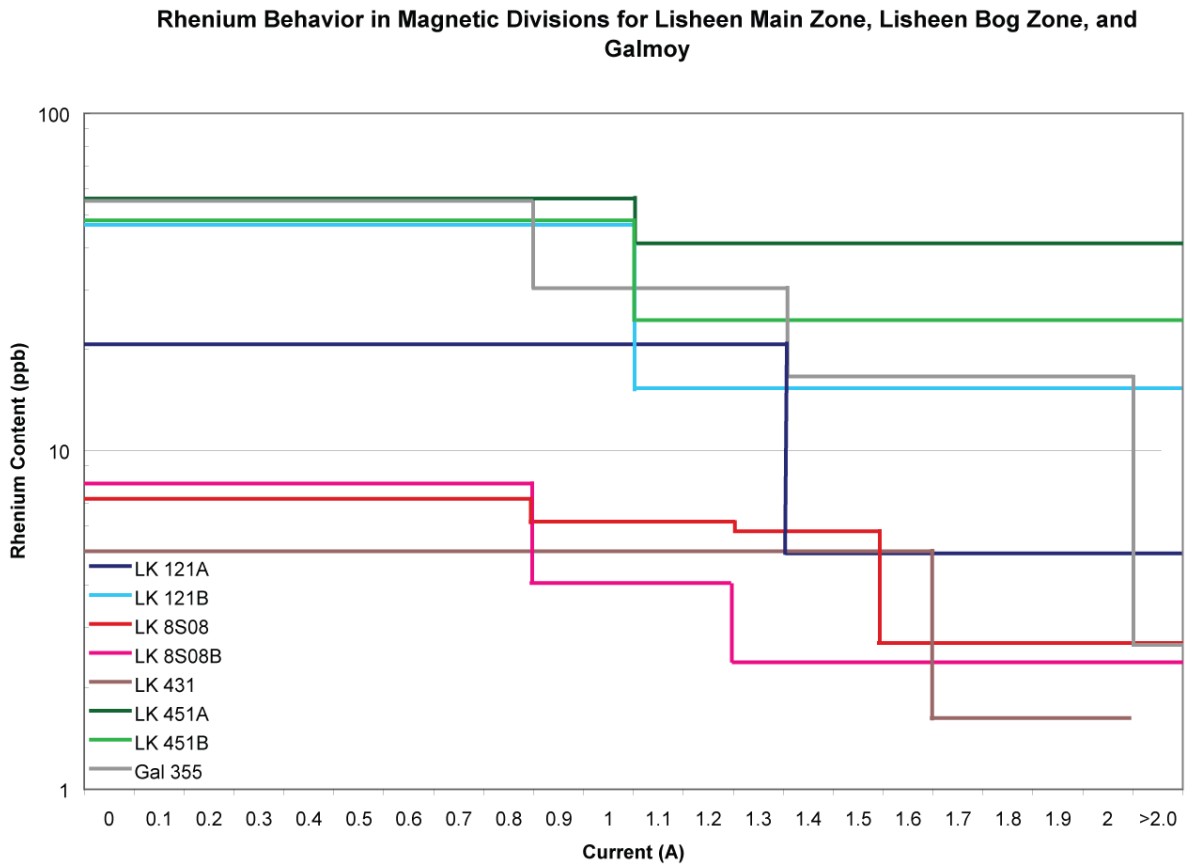

Figure 4.2: The behaviour of rhenium in a variety of magnetic divisions for Lisheen Main zone, Lisheen Bog zone, and Galmoy. As the current is increased there is a corresponding decrease in rhenium content.
* Horizontal lines represent a magnetic division that contains minerals that become "strongly magnetic" somewhere within the stated range of currents.

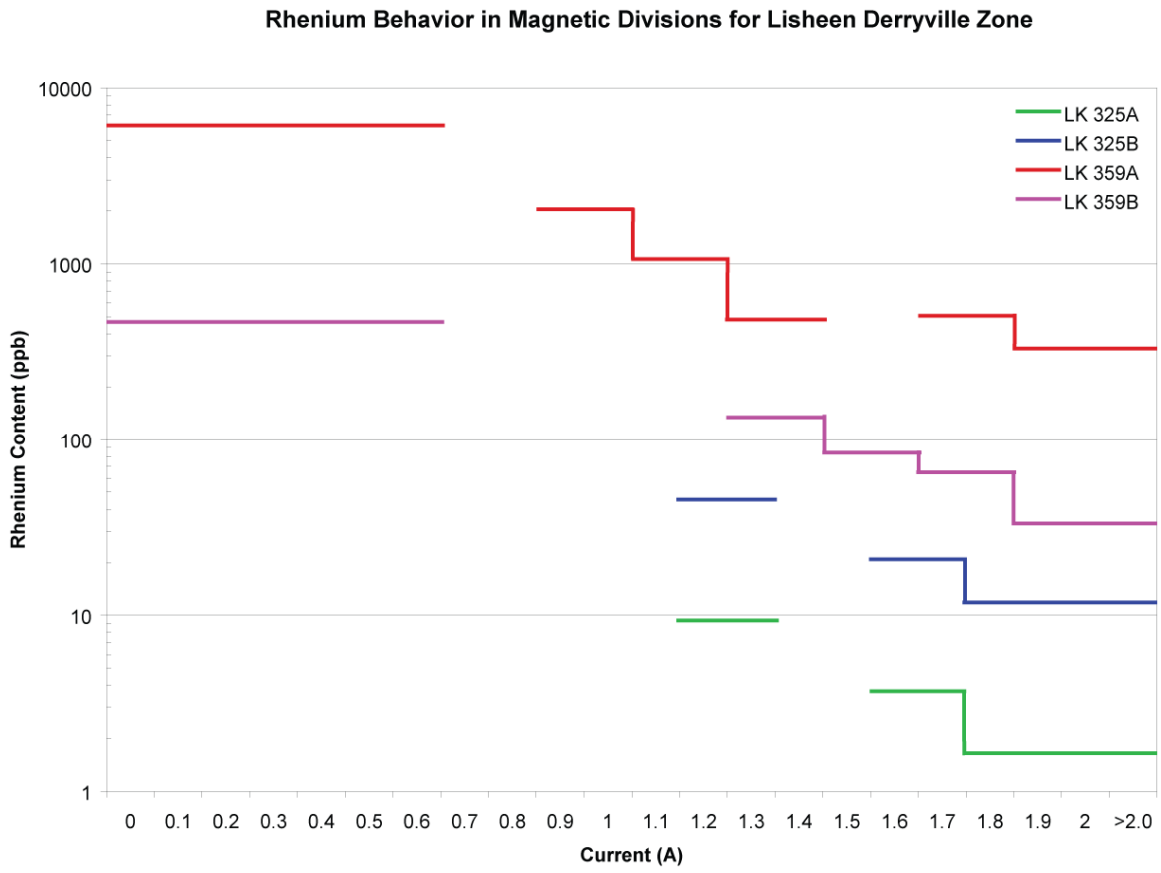

Figure 4.3: The behaviour of rhenium in a variety of magnetic divisions for Lisheen Derryville zone. As the current is increased there is a corresponding decrease in rhenium content.
* Horizontal lines represent a magnetic division that contains minerals that become "strongly magnetic" somewhere within the stated range of currents.

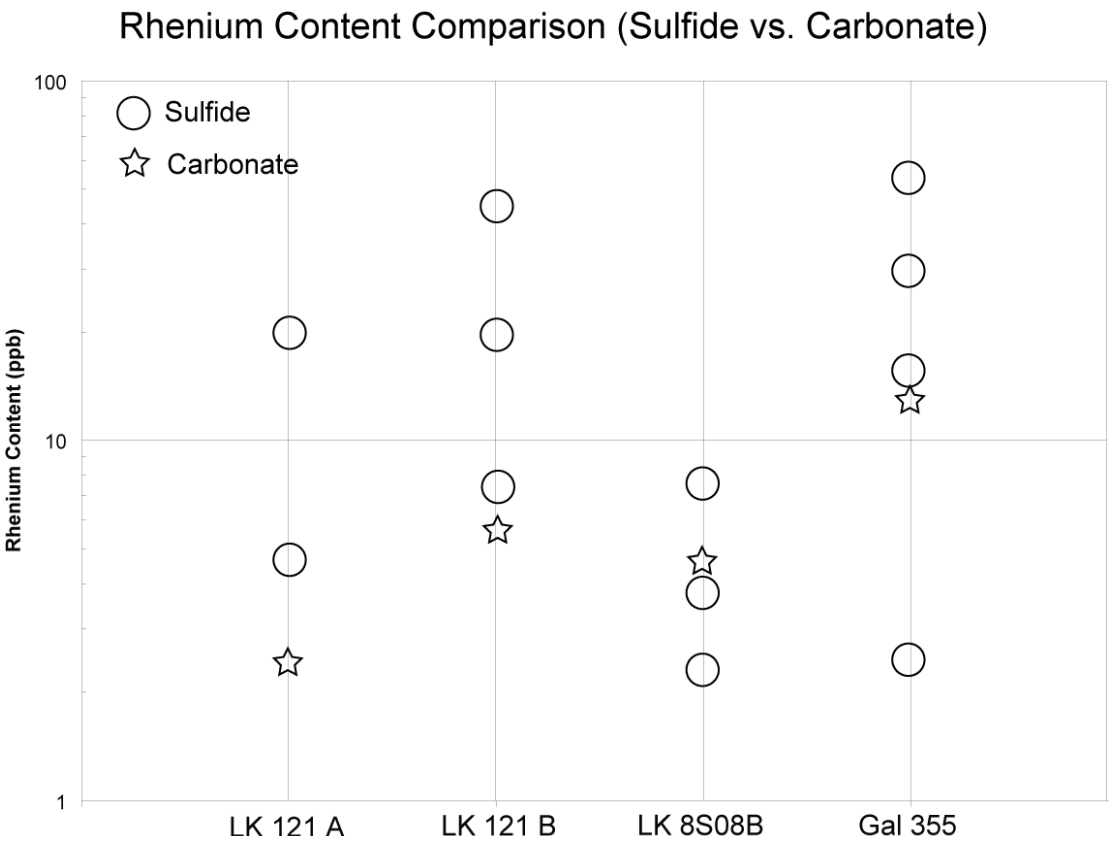

Figure 4.4: A comparison of the rhenium contents between sulfide mineralization and related hydrothermal carbonates.

5.0 Conclusions

This thesis has shown that pyrite Re-Os geochronology has useful application to the problem of dating carbonate-hosted ore deposits. Both case studies demonstrate that useful age information can be extracted from ore stage sulphides, which would have been difficult to obtain using other methods, such as paleomagnetism, or dating of silicate alteration assemblages.

For Nanisivik in particular, the Re-Os results have constrained known economic mineralization in the Borden basin to the Proterozoic at around 1100Ma. This age is important for proper characterization of MVT style deposits through time, as well as for future exploration for MVT deposits in the Borden Basin. An additional discovery is that Hawker Creek mineralization, along with the Sherlock et al. (2004) adularia ages from Nanisivik, supports the idea of active fluid flow in the basin during the Palaeozoic also, as young events of similar ages occur at both location. Ideally future studies in the Borden basin will help clarify the origin and extent of these enigmatic fluids.

Re-Os geochronology of the Lisheen deposit suggests that mineralization occurred over an extended period of time shortly after the deposition of the host Waulsortian limestone. Later stage events associated with the Variscan orogeny have disturbed the paleomagnetic age at Lisheen. This discovery updates our knowledge of the entire Irish ore field, as it puts into question ages that has been reported as Late Carboniferous or Permian, which are more likely due to effects related to the Variscan orogeny, ultimately masking the true Early Carboniferous mineralization event that occurred throughout the Irish ore field.

Beyond answering specific questions about Lisheen and Nanisivik, this thesis has emphasized the need for careful sample selection. Heavy liquid separation, and potentially selective dissolution, is required for all samples due to the discovery of higher than expected Re contents of common gangue minerals such as calcite. Magnetic separation of individual samples may be desired to avoid or minimize the complex zonation and alteration that is frequently present within these deposits. With these caveats, Re-Os geochronology of pyrite in MVT-style deposits supplements our understanding of the history and age associated with the formation of these important class of ore deposits.

6.0 Appendix

6.1-Appendix I: Magnetic Separation of Minerals

Minerals and rocks are characterized by many different attributes, one of the more useful properties that can be used for purification and mineral separation is magnetic susceptibility. Often different minerals are characterized by specific magnetic behaviours (see Section 4.13 for details) that can be used to separate a specific mineral or mineral suite from a particular rock. For this research magnetic separation is needed to purify Re-Os samples and to gather sufficiently diverse samples to create an isochron.

The Frantz isodynamic separator is a specially designed device used to separate minerals that have variable magnetic susceptibility by using the forces of gravity and electromagnetism. A Frantz consists of a vibrating inclined chute that is placed between two electromagnets, which empties into two collection cups, one for "magnetic" minerals and one for "non-magnetic" minerals (Figure 5.1). A non-magnetic separate is defined as the portion of the material where the force of gravity overrides the attractive force created between a mineral and the electromagnet. Adjusting the ratio between the magnetic to gravitational forces allows mineral separation over a large range of magnetic susceptibilities. However, minerals have an extremely wide range of magnetic susceptibilities and as such, there are no well defined criteria for setting the side slope or the electromagnet current. These adjustments must be made by hand during separation to obtain the desired results. Typically, the side slope is held constant (e.g. 5^{o} for this study) while the current of the electromagnet can be increased up to ~2.0 amps. To allow the sample to have enough time to sort into a magnetic and non-magnetic division a forward slope of no greater of 10^{o} is typically used.

Direct measurements of magnetic susceptibility can be made with a Frantz isodynamic separator, but for accurate results proper calibration is needed; see McAndrew (1957) and Nesset and Finch (1980) for details. At low currents (<0.9A) magnetic susceptibility(χ) can be approximated by equation (1):

$$\chi = \frac{19.2x10^{-6}\sin(\theta)}{I^{2}} \qquad (1)$$

Where θ is the side slope and I is the current. At higher currents, direct calibration is required in order to calculated accurate magnetic susceptibility (Nesset and Finch, 1980). Qualitatively, for fixed side slopes, a higher current corresponds to lower magnetic susceptibility, whereas lower currents correspond to higher magnetic susceptibility. The Frantz isodynamic separator therefore has two functions, mineral separation, and the relative measurements of magnetic susceptibility.

5.11 References:

McAndrew, J., 1957, Calibration of a Frantz Isodynamic Separator and its applications to mineral separation: Proceedings The Australian Institute of Metallurgy, No 181, March, 1957.

Nesset, J.E., Finch, J.A., 1980, Determination of magnetic parameters for field-dependent susceptibility minerals by Frantz isodynamic magnetic separator: Transactions/Section C of the Institution of Mining and Metallurgy, v. 89.

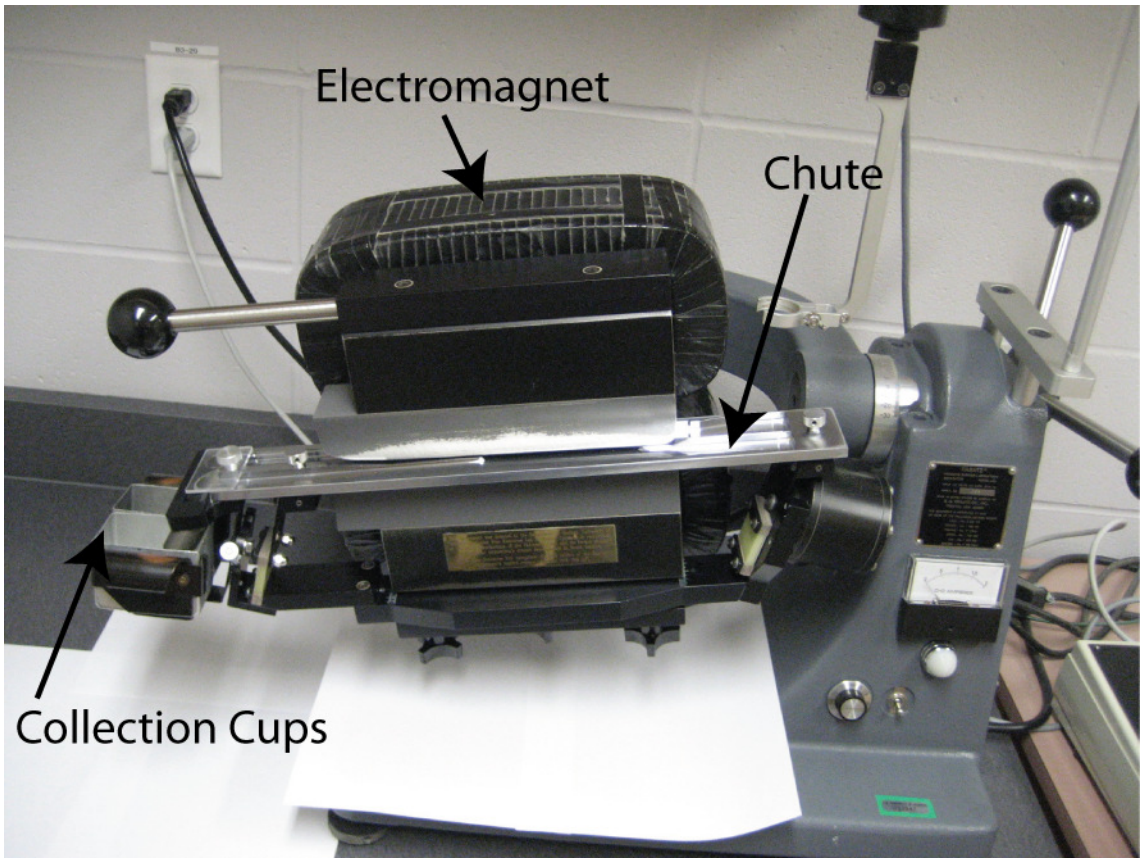

Figure 6.1: Frantz Isodynamic Separator set up. The magnetic force pulls material into the page and gravity forces material out of the page. Non magnetic minerals will be forced out of the page while magnetic minerals are forced into the page.

6.2 Appendix II: Heavy Liquid Separation

6.21 Introduction

Heavy liquid separation is a mineral purification procedure that exploits differences in mineral densities. This particular technique is based on placing a sample in a dense liquid, allowing minerals that are denser than the liquid to sink, whereas minerals that are less dense than the liquid float. The liquid that is used for this procedure is methylene iodide (CH_2I_2) which has a density of 3.32g/cm^3, denser than many common minerals (Table 5.1). A general rule is that oxides and sulphides sink in methylene iodide whereas carbonates and silicates typically float, although mineral impurities may alter the expected behaviour.

Table 6.1: Density Values of Common Values and Subsequent Behaviour in CH_2I_2

Mineral/Compound	Density (g/cm^3)	Behaviour in CH_2I_2
CH_2I_2	3.32	-
Water	1.00	-
Quartz	~2.65	Floats
Calcite	~2.71	Floats
Dolomite	~2.85	Floats
Pyrite	~5.00	Sinks
Sphalerite	~4.1	Sinks
Galena	~7.4	Sinks

6.22 Procedure:

The basic set up for heavy liquid separation is presented in Figure 5.2. Once the glassware is set up, the following steps take place inside a fume hood due to the toxicity of CH_2I_2 (see Figure 5.3 of illustrations for steps 1-4).

Step 1 (Figure 5.3a): With the valve closed a few hundred millilitres of CH_2I_2 is poured into the holding area to the level seen in Figure 5.3a.

Step 2 (Figure 5.3b): Up to a few grams of a sample are carefully funnelled into the CH_2I_2 using a paper funnel.

Step 3 (Figure 5.3c): Once the sample is transferred into the CH_2I_2 it will begin to settle out. The rate at which the minerals sink or float depends on the density and shape of the grains. In general the grains that are the flattest, and have the closest density to that of CH_2I_2, will take the longest to settle out. While the settling occurs, the CH_2I_2 can be swirled occasionally to ensure that surface tension or static doesn't prevent the grains from settling properly.

Step 4 (Figure 5.3d): Once the material has settled out to its preferred location the valve is opened to flush the heavy minerals into a piece of filter paper where they are collected. Ideally only the minimum amount of CH_2I_2 should be released to ensure that only the heavy fraction is collected.

Step 5: Once the dense minerals are collected on the filter paper they must be washed several times with acetone to ensure no CH_2I_2 remains on the grains. Once the acetone dries the heavy mineral separate is transferred into a vial.

Step 6: The light minerals are removed once the dense mineral separate has been extracted from the holding area. Since the filter paper will remove all solid matter from the CH_2I_2, the CH_2I_2 can be stored for future use.

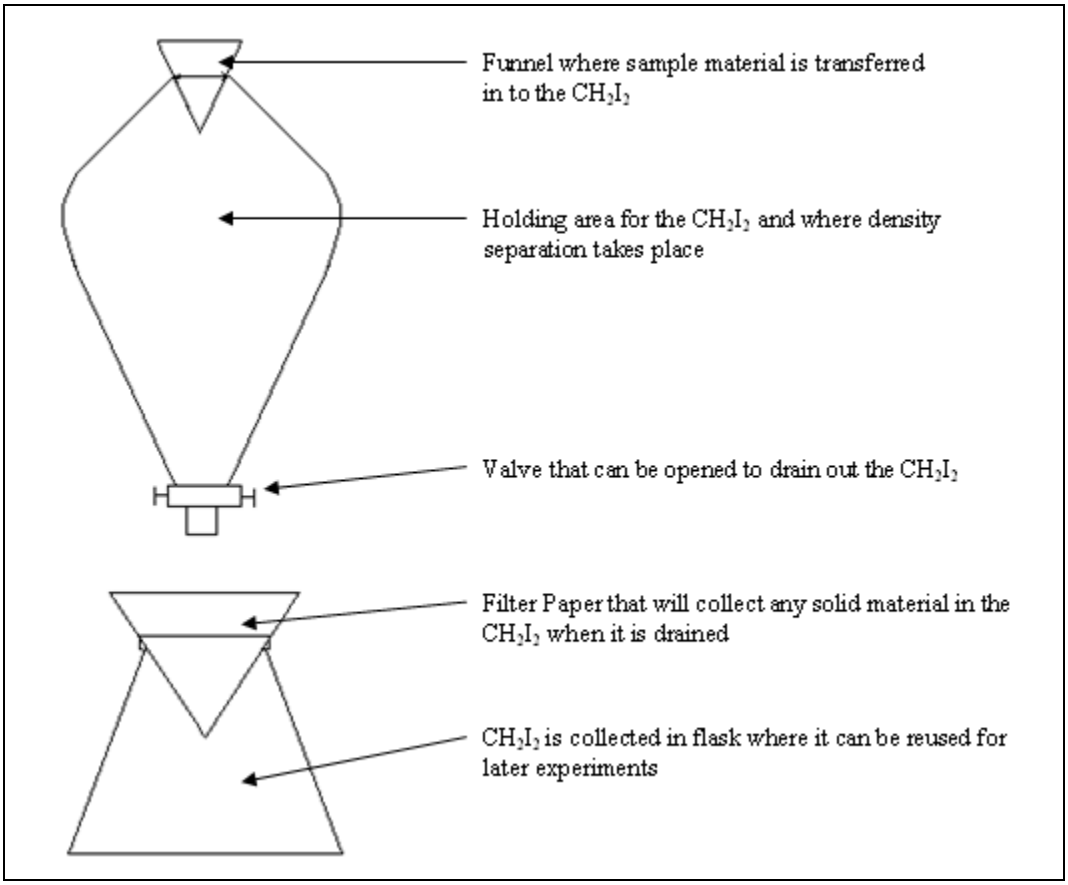

Figure 6.2: Glassware setup for heavy liquid separation

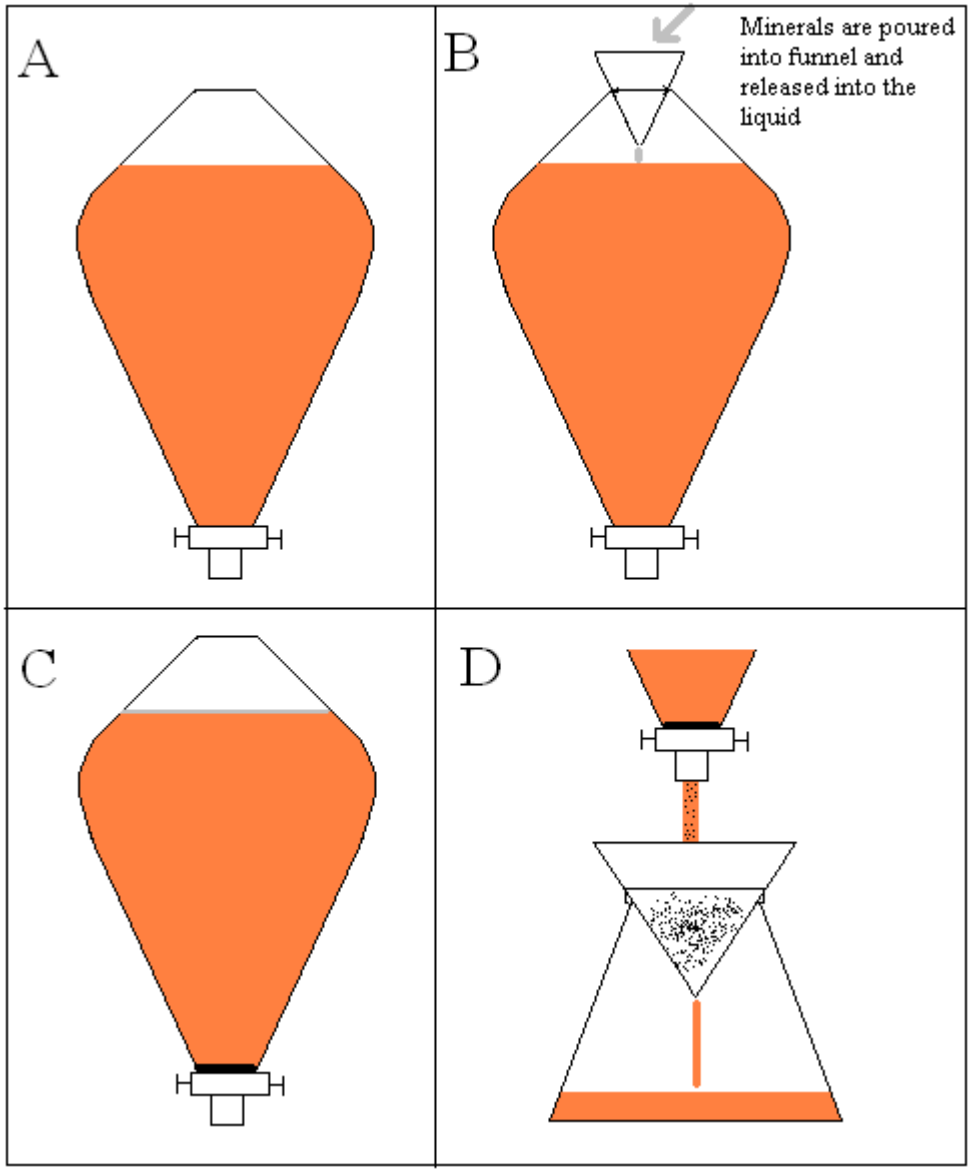

Figure 6.3: Illustration of selected steps in the heavy liquid separation process. (A) Holding area in step 1 filled with CH_2I_2 (Orange). (B) Minerals are released into CH_2I_2 through a funnel. (C) Dense minerals sink to the bottom and form a layer (black) and less dense minerals float to the surface and form a layer (grey). (D) CH_2I_2 is filtered leaving behind a heavy mineral separate on the filter paper.

6.3 Appendix III: Experimental Methods I - Selective Dissolution

In Re-Os geochronology the ideal sample is monomineralic, however, often this condition is extremely difficult to achieve. In these cases, special means may be attempted to purify a sample, such as selective dissolution. The premise of this experimental method is to dissolve unwanted material such as carbonates, sphalerite, and galena. These minerals are known to dissolve in concentrated hydrochloric acid, whereas the mineral pyrite is much more resistant to HCl acid attack. This allows for a potential avenue for purification. However, for this to become a viable purification method the Re and Os must not be leached out of the pyrite during acid dissolution of other mineral phases. Testing whether or not the Re-Os system is affected by such acid treatments is the purpose of this study.

Several very similar experiments were conducted to test for Re-Os disturbance in pyrite when subjected to an HCl acid treatment. Three slightly different methods were attempted to gauge to the behaviour of the sample at different conditions (labelled as Step A, Step B, Step C below). Procedure A is the least intensive procedure, whereas procedure C is deemed the most harsh.

The sample LK 8S08 NM1.5 was selected to be tested for Re-Os leaching when treated in acid. This sample was chosen since it lies on a known, relatively robust, isochron, and contains almost pure pyrite (see Section 2.0 for details). Any significant changes in the Re concentration, Os concentration, and/or the isotope ratios as a result of the acid treatment process would suggest leaching of Re and/or Os occurred.

Step 1A: A sample of up to several hundred milligrams is weighed and transferred into a 22ml glass scintillation vial containing 2.5mL of ~6N HCl per 100mg of sample. The sample is left to dissolve for 4 hours at room temperature.

Step 1B: A sample of up to several hundred milligrams is weighed and transferred into a 22ml glass scintillation vial containing 2.5mL of ~10N HCl per 100mg of sample. The sample is left to dissolve for 4 hours at room temperature.

Step 1C: A sample of up to several hundred milligrams is weighed and transferred into a 22ml glass scintillation vial containing 2.5mL of 10N HCl per 100mg of sample. The sample is left to dissolve for 4 hours on a hot plate at ~100^{o}C. This elevated temperature should enhance dissolution.

Step 2A,B,C: After 4 hours have passed the solution turns yellow and is discarded. The sample is washed with Milli-Q water four times.

Step 3A,B,C: Repeat steps 1A-C only allowing the solution to sit overnight.

Step 4A,B,C: Repeat step 2A,B,C.

Step 5A: Let the sample dry down at room temperature.

Step 5B,C: Let the sample dry down on a hot plate at 100^{o}C for 30-60 minutes.

Step 6: Run all samples through typical Re-Os chemistry and calculate Re-Os concentrations and isotope ratios.

The results of these series of acid treatment experiments are now compared to the results of a untreated sample of LK 8S08 NM1.5, and are reported in Figure 5.4, Figure 5.5, and Table 2.5b.

The results from these experiments show that the Re and Os concentrations of pyrite do not appreciably change during selective dissolution. The Re contents between the different samples differ by less than 0.4 ppb and Os contents by less that 0.7ppt. The isotope ratios ($\frac{^{187}\mathrm{Re}}{^{188}Os}$ and $\frac{^{187}Os}{^{188}Os}$) vary by less than 5% between all samples. These minor variations are negligible and do not change the interpretation of the resulting isochron. This suggests that leaching of Re and Os from pyrite is not an issue for any of the above procedures. All deviations can be explained by either natural variation within a samples or the dissolution of minor minerals (e.g. calcite).

Future research into this experimental technique should focus on making the procedure more efficient by using less acid and dissolving a sample over shorter periods of time.

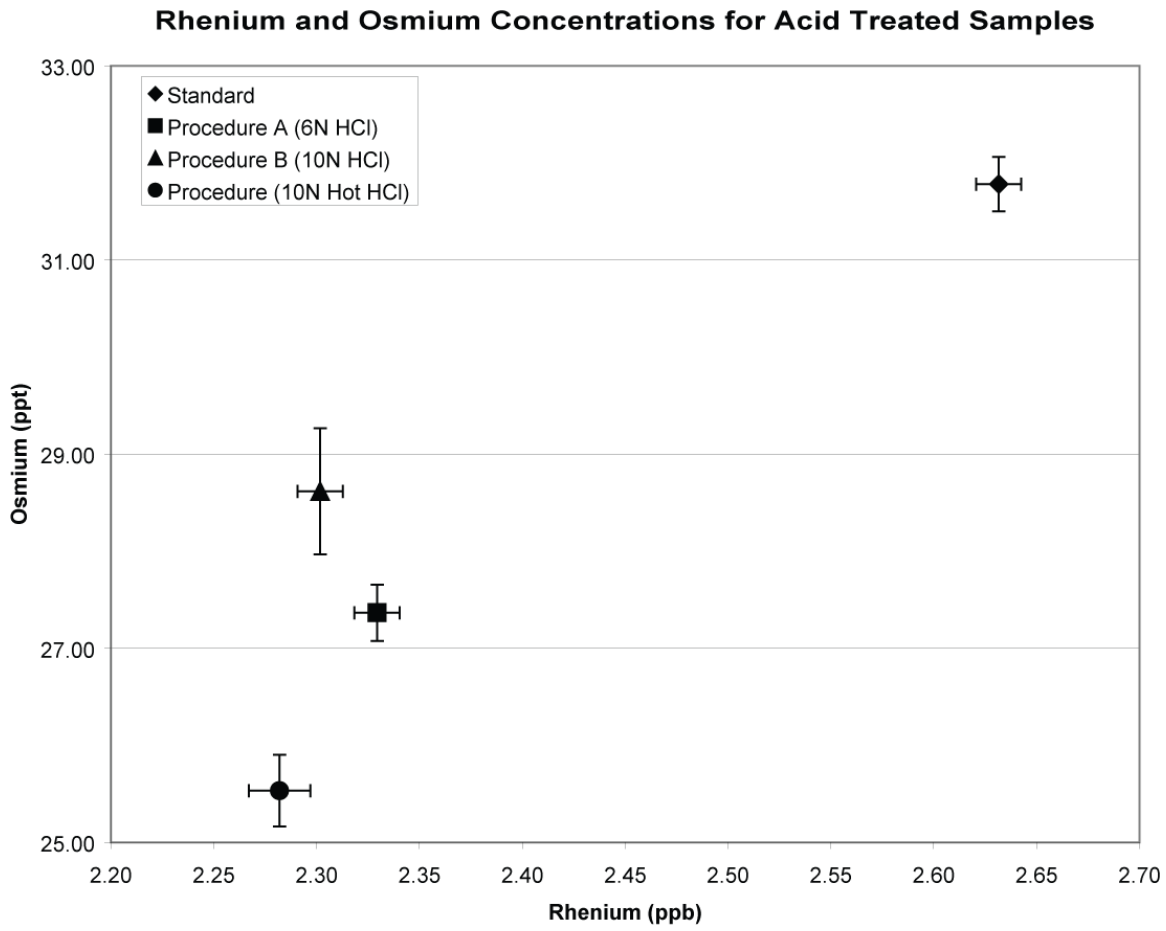

Figure 5.4: Re and Os concentration comparison between different samples of LK 8S08 NM1.5. Error bars are given to 2σ.

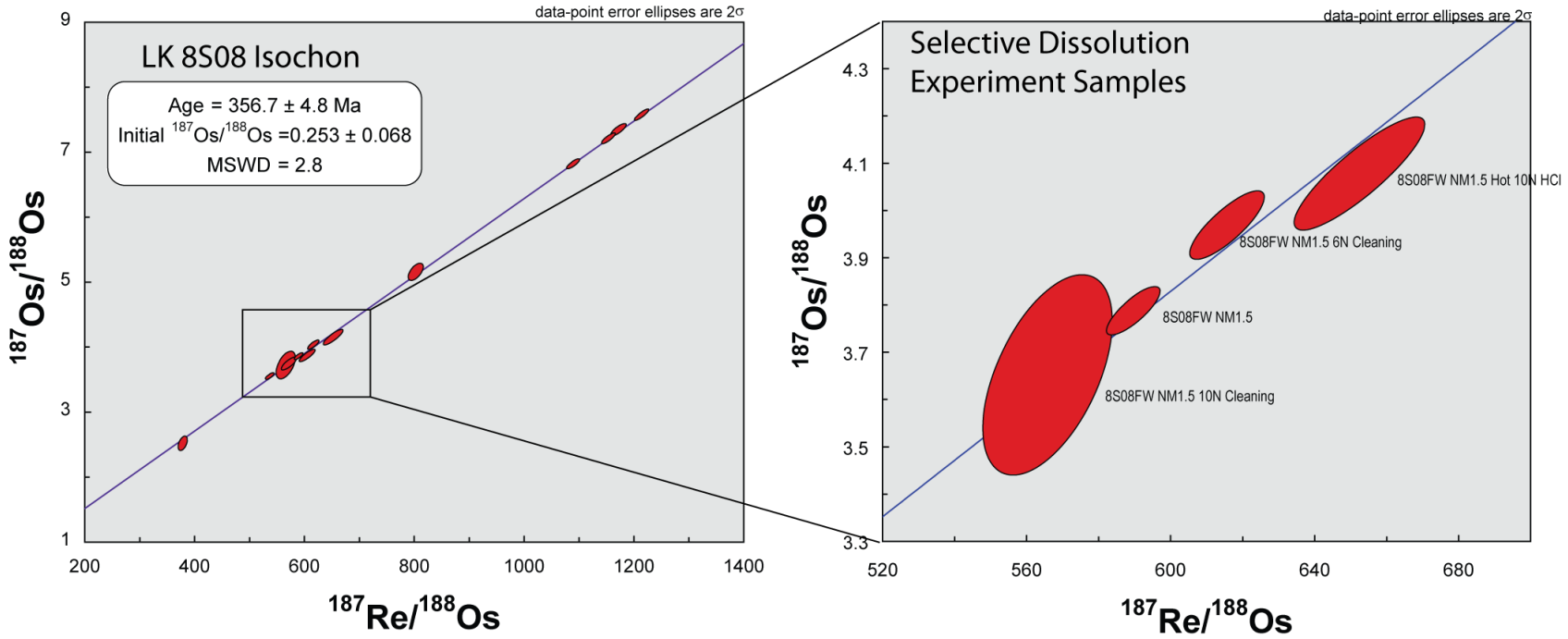

Figure 6.5: Isotope comparison between different samples of LK 8S08 NM1.5 in relation to the LK 8S08 isochron. Error ellipses are given to 2σ.

6.4 Appendix IV: Pyrite Roasting and Magnetic Separation

6.41 Introduction

During typical magnetic separation, a sample division will often contain more than one mineral (see Table 2.3). Sometimes this issue cannot be tackled appropriately with heavy liquid separation, refinements to the magnetic separation, or selective dissolution. Pyrite roasting is a technique that can be applied to extract pyrite. The technique is based on changing the magnetic susceptibility of pyrite through phase transitions. Two important phase transitions that may occur are the conversions to pyrrhotite and/or magnetite via oxidation. Whether the phase transition occurs, and which phase pyrite converts to, depends on the temperature, surface area, and time (Prasad et al., 1985, Lambert et al., 1998). These transitions are useful for magnetic separation because pyrrhotite and magnetite are far more magnetic than original pyrite. Other minerals would be expected to undergo far less dramatic phase changes under similar conditions, at least with respect to their magnetic properties. Applying this technique to Re-Os geochronology requires a feasibility study on how easy it is to cause these transitions, how much does the magnetic susceptibility change, and most importantly whether the Re-Os system becomes disturbed after these transitions. These questions are explored in the few simple experiments discussed below.

6.42 Experimental Procedure

The sample LK 8S08 NM1.5 was selected to be tested for these experiments. This sample was chosen since it lies on a known relatively robust isochron, and contains almost pure pyrite (see Section 2.0 for details). Any changes in Re concentration, Os concentration, and/or the isotope ratios would suggest that the Re-Os has been disturbed during phase transition.

Several similar experiments were conducted to test for Re-Os disturbance in pyrite when subjected to temperatures of 400^{o}C. Since phase transitions are not instantaneous different times of exposure will produce different results. For the purposes of this feasibility study 5min, 15min, 30min, 45min, and 60min were chosen for the exposure times. Samples of approximately 200mg, with grains of~100μm, were

transferred into glass vials and were placed into a furnace. The vials were placed on their side to maximize the surface area exposed to the air. The roasted pyrite had its magnetic susceptibility measured via a Frantz isodynamic separator (see Appendix I) and then subsequently was analyzed for its Re-Os content.

6.43 Results

The results of these experiments are plotted in figures 5.6, 5.7, and 5.8. How the magnetic behaviour of grains changes over time is plotted in Figure 5.6. More specifically, Figure 5.6 shows the percentage of the sample present in the magnetic fraction for a given current on the Frantz isodynamic separator. Figures 5.7 and 5.8 plot how the Re-Os content varies between standard and roasted samples.

6.44 Conclusions

There appears to be no major differences in the Re-Os system between roasted pyrite and standard pyrite suggesting that the kinetics are too slow to lose a substantial amount of Re or Os through roasting. From Figure 5.6 there is an obvious increase in the magnetic susceptibility of pyrite, and after 60 minutes of roasting the pyrite becomes magnetic at a much lower current (~0.5A). Although this is just one sample with a specific magnetic susceptibility it would be expected that all pyrite should behave in a similar fashion. The plotted curves do not follow a perfect trend due the fact the conditions experienced by each sample would be slightly different, especially with respect to the surface area exposed to the atmosphere. A standardize procedure will be needed to address this issue in the future. Future research on this subject should also be directed toward producing more complete transitions of pyrite. This can be accomplished by either lengthening the time the sample is in the furnace, or by increasing the temperature. If such conversions remains viable all the way to magnetite production with respect to the Re-Os systematics, a simple hand magnet may suffice when separating out pyrite. Also the exact magnetic character of other minerals, such as sphalerite or galena, at elevated temperatures is unknown. However, it is expected that any changes in the magnetic character of sphalerite or galena would be on a much smaller scale compared to

pyrite. Overall these experiments suggest that pyrite roasting may be a feasible way to extract pyrite from a rock.

6.5 References

Lambert, J.R., Simkovich, P.L., Walker, J.R., 1998, The Kinetics and Mechanism of the Pyrite-to-Pyrrhotite Transformation: Mettallurgical and Materials Transactions B, V.29B, p. 385-396.

Prasad, A., Singru, R.M., Biswas, A.K., 1985, Study of the Roasting of Pyrite Minerals by Mossbaurer Spectroscopy: Physica Status Solidi (a) Volume 87, Issue 1, p 267–271.

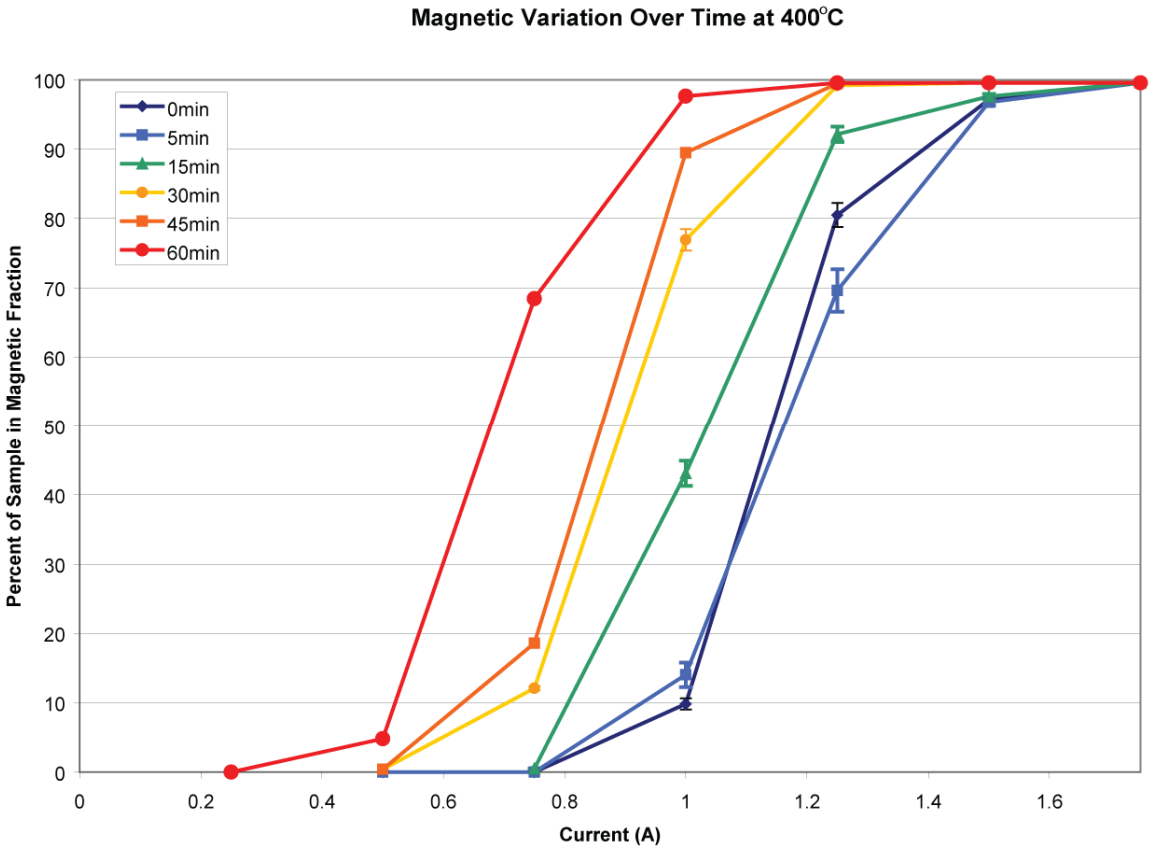

Figure 6.6: The magnetic character of pyrite (LK 8S08 NM1.5) roasted at 400°C as a function of time. All standard deviations are given to 1σ.

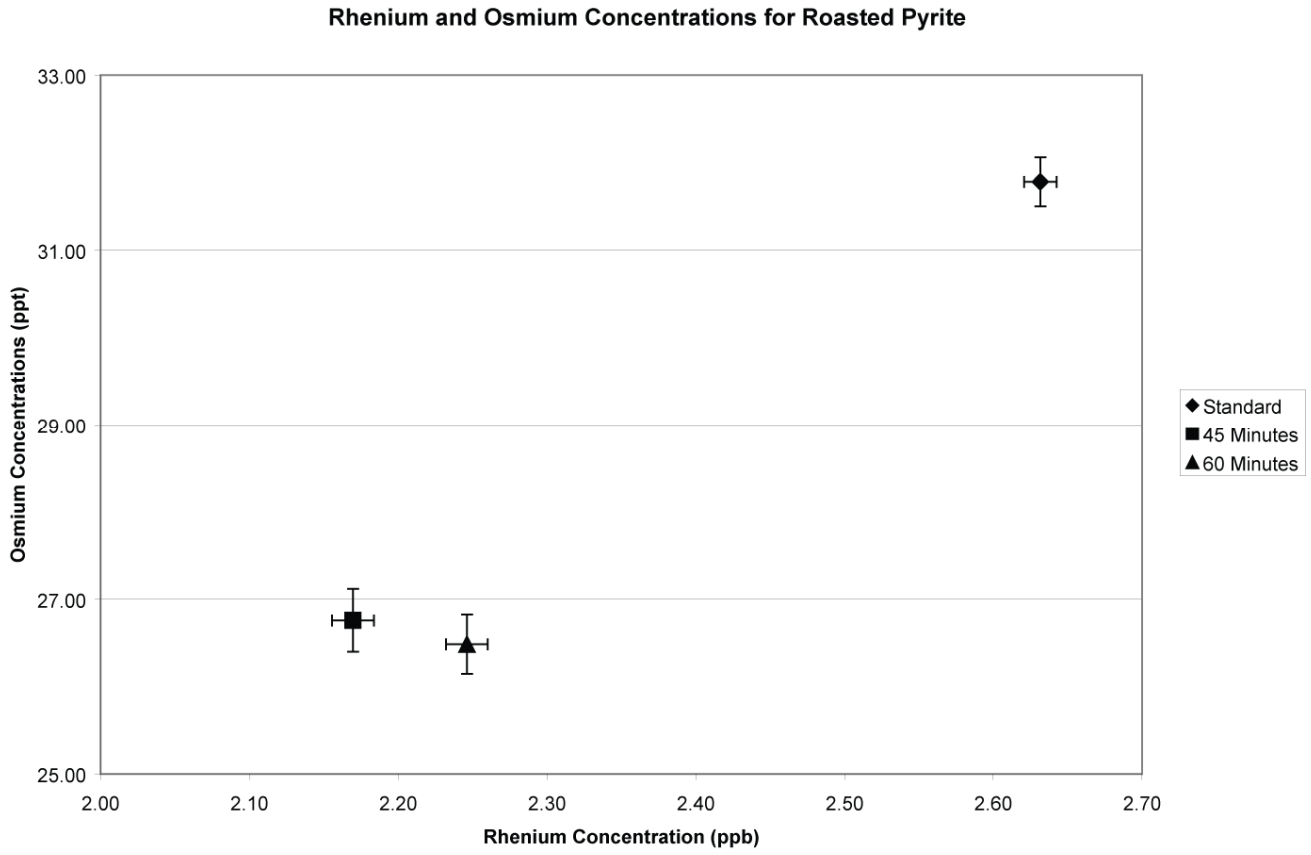

Figure 6.7: The Re and Os concentrations of pyrite (LK 8S08 NM1.5) roasted at 400°C. Error bars are given to 2σ.

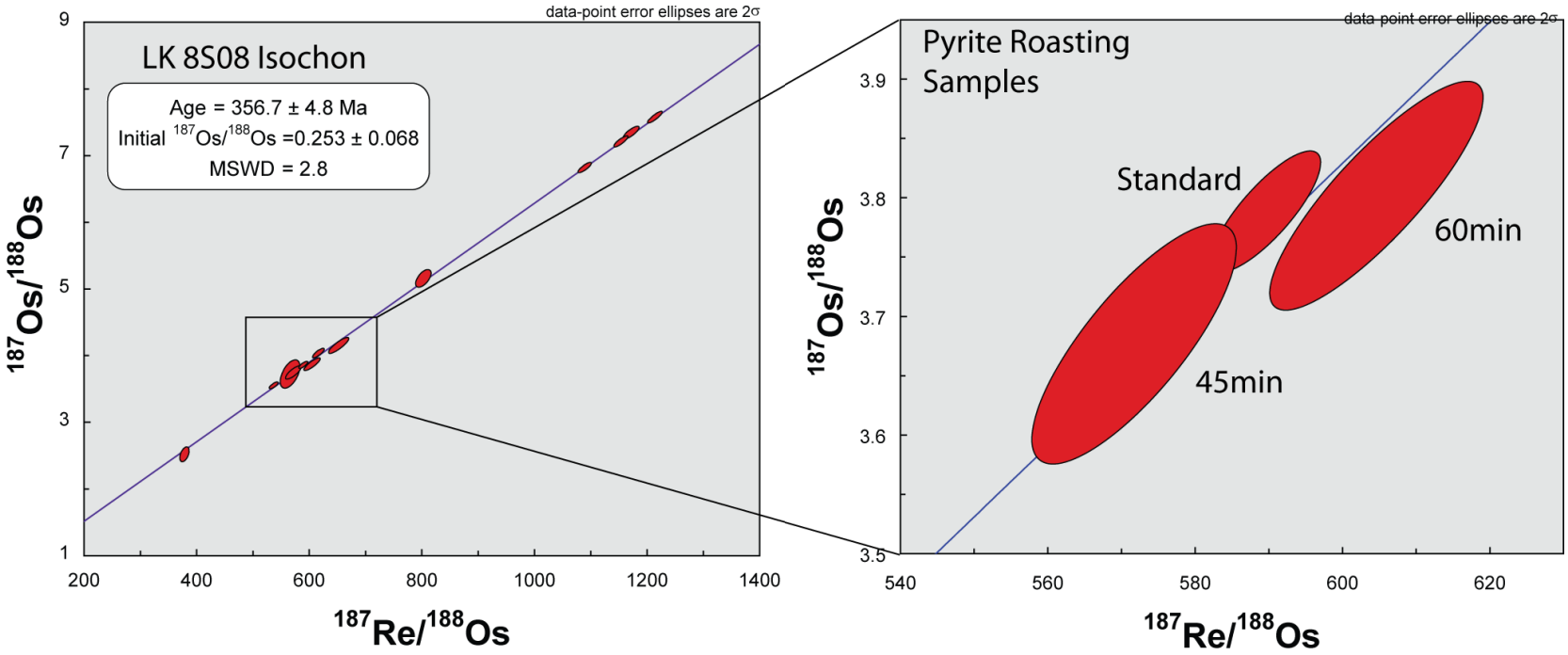

Figure 6.8: Isotope comparison between different samples of 400oC roasted LK 8S08 NM1.5 pyrite in relation to the LK 8S08 isochron. Error ellipses are given to 2σ.

6.5 Appendix V: Modal Abundance Estimation via MATLAB

6.51 Introduction

Modal abundances are an important characteristic in any rock sample, however, estimating these abundances correctly is often tedious. To get around this problem a simple MATLAB code was written that takes backscattered electron images or element maps collected by an electron microprobe, and quantifies modal abundances.

6.52 Procedure and Code

The basic premise behind this technique is that each mineral often has a well defined intensity in both backscattered electron images and elemental maps. The range of intensities that a mineral displays can be used to estimate its abundance by counting what proportion of pixels have the desired intensity. For this study, the main components of a sample consist of pyrite, sphalerite, and galena. These minerals are easy to identify in back scattered images, with galena being the brightest, followed by sphalerite, and then pyrite (Figure 5.9A). The area associated with each mineral in a image can be calculated using the following code:

```
I= imread(359B-18.tif');
level = graythresh(I);
gn = im2bw(I, 0.9);
sph = im2bw(I, 0.3);
py = im2bw(I, 0.1);
bwarea(gn);
bwarea(sph);
bwarea(py);
Area of Galena = bwarea(gn)
Area of Sphalerite = bwarea(sph) - bwarea(gn)
Area of Pyrite = bwarea(py) - bwarea(sph)
Total Area = bwarea(py)
```

By reading a specific image, for example the backscatter image named 359B-18.tif , this code will calculate the associated area with respect to each mineral. This requires the image to first be converted to greyscale using level = graythresh(I) (Figure 5.9A). After proper identification of the mineral's intensity on a scale of 0-100, the results are plugged into the next function. The function im2bw(I, 0.9) will convert the greyscale image to a black and white image where all intensities that are greater than 90 percent of the maximum will be turned white (Figure 5.9B). In this case, that is the domain in which galena is found. Similar conditions apply for the minerals sphalerite and pyrite (Figure 5.9C and Figure 5.9D). The associated area these regions of this image are:

bwarea (gn) = 497
bwarea (sph) = 144200
bwarea (py) = 166000
Total Area = 497 + 144200 + 166000 = 310697

These can converted to the area taken up by individual minerals by the following equations:

Area of Galena = bwarea(gn) = 497
Area of Sphalerite = bwarea(sph) - bwarea(gn)= 144200 - 497 = 143703
Area of Pyrite = bwarea(py) - bwarea(sph) = 166000 - 144200 = 21800
Total Area = bwarea(py) = 166000

These can be converted to modal percent via the following equations:

$$\text{Galena} = \frac{497}{166000} x100 = 0.30\%$$

$$\text{Sphalerite} = \frac{143703}{166000} x100 = 86.57\%$$

$$\text{Pyrite} = \frac{21800}{166000} x100 = 13.13\%$$

This code allows for the quick calculation of modal abundance in a backscattered image. The only caveat is that mineral intensities cannot overlap and that all minerals must be accounted for, otherwise the modal abundances will be inaccurate.

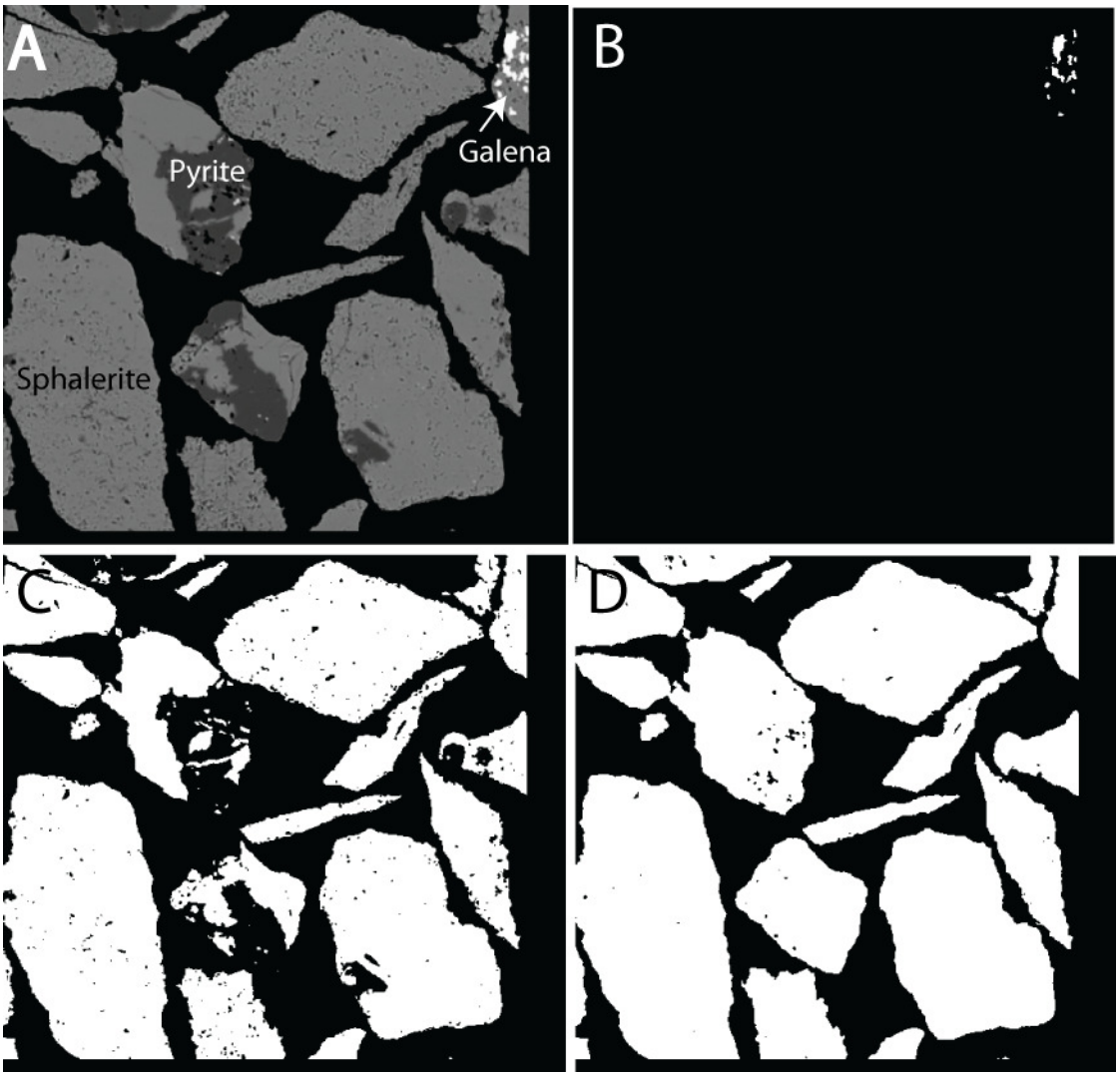

Figure 6.9: (A) Backscattered electron image (B) Black and white image after applying the code gn=im2bw(I, 0.9) (C) Black and white image after applying the code sph = im2bw(I, 0.3) (D) Black and white image after applying the code py = im2bw(I, 0.1).